Finanziato dall'Unione europea NextGenerationEU | Ministero dell'Università e della Ricerca | Italiadomani PIANO NAZIONALE DI RIPRESA E RESILIENZA

multi-Risk sciEnce for resilienT commUnities undeR a changiNgclimate

Codice progetto MUR: **PE00000005** – CUP LEAD PARTNER E13C22001860001

Deliverable title:

Interrelated man-made and natural disasters. Report on the estimation of potential multi-hazard scenarios

Deliverable ID: **DV 5.2.**

Due date: **31-12-2025**

Submission date: **October 2025**

AUTHORS

Antonello Barresi, Micaela Demichela, David J. Castro Rodriguez, Morena Vitale (POLITO), Chiara Vianello, Francesca Da Porto, Marco Donà, Marco Ceresara, Elisa Saler, Carlo Pellegrino, Lorenzo Hofer, Mariano Angelo Zanini (UNIPD), Almerinda Di Benedetto (UNINA), Mara Lombardi (UNIROMA1), Luisa Lavalle (ENEA)

Approved by Carlo Pellegrino (WP Leader)

Technical references

Project Acronym	RETURN
Project Title	multi-Risk sciEnce for resilienT commUnities undeR a changiNg climate
Project Coordinator	Domenico Calcaterra UNIVERSITA DEGLI STUDI DI NAPOLI FEDERICO II domcalca@unina.it
Project Duration	December 2022 – December 2025 (37 months)

Deliverable No.	DV6.5.2
Dissemination level*	PU
Work Package	WP 6.5 - Report outlining main consequences and impacts for CIs
Task	T 6.5.2 - Interrelated man-made and natural disasters
Lead beneficiary	POLITO
Contributing beneficiary/ies	UNIPD, UNINA, UNIROMA1, ENEA.

* PU = Public

PP = Restricted to other programme participants (including the Commission Services)

RE = Restricted to a group specified by the consortium (including the Commission Services)

CO = Confidential, only for members of the consortium (including the Commission Services)

Document history

Version	Date	Lead contributor	Description
0.1	28.07.2025	POLITO	First draft
0.2	15/09/2025		Critical review and proofreading
0.3	30/09/2025		Edits for approval
1.0	9/10/2025		Final version

ABSTRACT

5.2.a – Potential multi-hazard scenarios for transportation infrastructures

The logic of multi hazard for transportation infrastructures has been developed in a framework for the quantitative risk assessment of road and railway infrastructure exposed to both natural and man-made hazards. Based on the analysis and classification of major hazard sources, the methodology focuses on identifying and modelling critical events such as fires in tunnels, exceptional loads on bridges, and extreme natural phenomena capable of damaging the physical infrastructure.

The proposed approach employs the bow-tie model, which integrates fault tree and event tree analyses to reconstruct the logical sequence of events from initiating causes to the Initial Critical Event (IEc). This structure enables a comprehensive understanding of hazard evolution, facilitating the assessment of exposure, the evaluation of asset vulnerability, and the quantification of real-time risk indicators.

Representative multi-hazard scenarios are defined through the identification of IEc, forming the basis for a probabilistic risk analysis aimed at verifying safety conditions against a residual risk acceptability threshold. The model outputs the Individual Risk Indicator, representing the annual probability of damage to exposed assets, thus supporting informed decision-making for infrastructure protection and resilience planning.

Regarding the seismic risk assessment for transportation infrastructures (bridges, in particular), a brief description of the main steps that need to be taken into account by risk practitioners is provided. In particular, the section focuses on how to compute the seismic hazard, on the main methods for computing the structural fragility and how to retrieve consequences for a complete risk assessment. Accordingly, the main references are provided.

5.2.b – Deterministic and dynamic models for the Interrelated Natech Vulnerability with the events of interest and potential multi-hazard scenarios for industrial assets

The Sendai Framework addresses the need to strengthen resilience and adaptive capacity to the interrelation of man-made and natural disasters to reduce losses in lives, livelihoods, health, and the environment. The process industry provides essential services to society that can be harmed by the impact of multiple hazards on these critical infrastructures. Historical record analysis is necessary for evaluating the likelihood of such events, determining the conditional probabilities of hazard impact to industrial structures, and the likelihood of their final scenarios. Modelling is difficult since the features of hazards such as intensity, frequency, and extension are hard to forecast, and their effects on facilities are often unknown. This work aimed to develop a methodology to model vulnerabilities of industrial critical infrastructure to multiple hazards, implementing advanced methods to cope with the lack of or incomplete information available. A historical analysis of events triggered by lightning in the process industry was used as a pilot case study (Case 1), since lightning-triggered events present a critical trade-off between frequency and catastrophic consequences in the process industries. Additionally, the methodology was implemented to analyse a second case focused on material degradation-triggered events in the process industry (Case 2).

As concerns the investigation of the dispersion of flammable gases, this study uses a combination of empirical models, CFD simulations and the PHAST software to investigate the dispersion dynamics and consequences of jet fires associated with the atmospheric release of hydrogen and methane/hydrogen mixtures. Initial analyses employed empirical methods for steady-state consequence estimations and transient CFD simulations for detailed atmospheric dispersion. Additional simulations were then performed using PHAST under equivalent release and environmental conditions to complement these. Key parameters such as the mass flow rate, the extent of the flammable cloud, the flame length and the thermal radiation hazard distances were compared across the different modelling approaches for varying concentrations of hydrogen. This evaluation aims to assess the consistency, strengths and limitations of each modelling approach in predicting the consequences of hydrogen-rich gas releases.

In the context of distribution networks, the interaction between extreme natural events and the structural integrity of pipelines represents a critical area of investigation. Fault Tree Analysis (FTA) and Event Tree Analysis (ETA), complementary methodologies that allow a comprehensive risk assessment from both the perspective of triggering causes and the consequential developments of incident events, are the most effective tools for analysing the causes and consequences of failure.

Steel pallet racks are critical non-structural systems widely used in warehouses and production facilities. Despite their apparent simplicity, their seismic vulnerability can strongly influence the overall risk profile of industrial assets—especially in seismic-prone regions. Past earthquake events have shown that rack collapses not only

endanger worker safety but can also trigger major economic losses due to damage to stored goods, prolonged production downtime, and supply chain disruptions. Yet, their seismic behavior remains largely understudied, and quantitative tools for assessing their seismic fragility are still limited.
This study addresses this gap by proposing a robust and scalable methodology for seismic fragility assessment of industrial pallet racks. A representative stock of 27 unbraced rack configurations was analyzed through advanced 3D nonlinear finite element modelling and cloud-based time-history analysis. Fragility curves were derived with respect to four Engineering Demand Parameters (EDPs) and conditioned on two seismic intensity measures (PGA and S_a), considering both rigid and soft soil conditions. The results show that rack collapse is driven by the combined effects of axial–flexural strain in uprights, nonlinear joint behaviour, and the directionality of seismic input. The proposed fragility models serve as effective tools for risk quantification and mitigation planning, supporting decision-makers in enhancing the seismic resilience of individual facilities and broader industrial districts.

5.2.c– Industrial multi-hazard deployment index

NaTech events involve technological disasters triggered by natural hazards, leading to hazardous material releases. Their multi-risk nature necessitates comprehensive vulnerability assessments to enhance system preparedness. Here a comprehensive NaTech vulnerability assessment for industrial plants is presented. A critical discussion was developed focusing on opportunities to enhance a previous NaTech multi-risk methodology. Based on these opportunities, an adaptation of Quality Function Deployment tool was firstly tailored to enhance multi-risk assessments based on the function-location approach. The resulting Industrial Critical Infrastructure Multi-Risk Deployment (ICI-MRD) framework was tested in an energetic critical infrastructure as a case study, considering multiple hazards and their cascading interactions and assessing their impact on industrial items. The ICI-MRD framework provided a punctual multi-risk warning indicator on NaTech potential, with implications at a primary decision-making level. In addition, the intermediate output of this framework supports decision-makers by raising vulnerability awareness and providing data-driven insights for enhancing industrial and territorial preparedness facing natural challenges. On the other hand, an enhanced index for assessing major industrial accident potential based on hazardous substance criteria was determined for the energetic critical infrastructure under study. The comprehensive decision matrix combined independent evaluations of infrastructure and substance-related factors in a multidimensional risk assessment supporting preparedness strategies for industrial systems.

5.2.d– Potential multi-hazard scenarios for civil infrastructures

Water distribution network (WDN) are lifeline infrastructures whose disruption can have severe consequences for households, industries, and critical services. Natural hazards are of particular concern because they can affect multiple components simultaneously, and their impacts are often compounded by interdependencies with other critical infrastructures such as power supply, telecommunications, and transportation. The loss of key services can critically escalate emergencies. The research introduces a quantitative, simulation-based approach developed within the RETURN framework to model WDN performance under multi-hazard conditions and able to support both operator-defined and automatically generated scenarios, enabling large-scale simulation campaigns at high speed and low data cost. This capability makes it possible to explore unprecedented “unthinkable” events, replicate past incidents, and reverse-engineer the sequences of events that could lead to critical system failures.

3. Table of contents

Technical references 2

Document history 3

ABSTRACT 4

3. Table of contents 6

List of Tables 7

List of Figures 7

4. Potential multi-hazard scenarios for transportation infrastructures 9

4.1 Quantitative probabilistic risk assessment: fault tree and event tree analysis, multi hazard scenarios analysis (fire, seismic and landslide simulation) for road and railway tunnel 9

4.1.1 Overview of multi hazard concepts for transportation infrastructure 9

4.1.2 Methodological framework for multi-hazard assessment 10

4.1.3 Example of the application of multi hazard methodology for road tunnel 16

4.2 Seismic risk assessment for transportation infrastructures 22

5. Deterministic and dynamic models for the Interrelated NaTech Vulnerability with the events of interest/Potential multi-hazard scenarios for industrial assets 26

5.1 Methodological procedure to characterize industrial vulnerabilities facing NaTech events 26

5.1.1 Case 1: Past lightning-triggered NaTech events in process industry 28

5.1.2 Case 2: Historical analysis of material degradation in the process industry 34

5.2 Interaction between H_2 and H_2/CH_4 mixture release consequences and natural events 41

5.2.1 CFD vs. PHAST: atmospheric dispersion 42

5.2.2 Empirical Point Source Model vs. PHAST: Jet fire consequence 43

5.2.3 Assessment of the probability of occurrence of natural events in pipeline ruptures using Fault Tree Analysis (FTA) and Event Tree Analysis (ETA) 45

5.3 Parametric framework for seismic fragility assessment of industrial steel pallet racks 48

5.3.1 Seismic vulnerability of industrial racks: Literature gap 48

5.3.2 Parametric analysis framework and selected rack stock 49

5.3.3 Seismic fragility models for pallet racks on rigid and soft soils 53

6. Industrial multi-hazard deployment index 57

6.1 Multi-risk simplified NaTech indicator for local planners 57

6.2 Opportunities to enhance the multi-risk simplified NaTech indicator for local planners 59

6.3 Comprehensive evaluation of the NaTech potential in Industrial Critical Infrastructures 59

6.3.1 The Industrial Critical Infrastructure Multi-Risk Deployment framework (ICI-MRD) 59

6.3.2 Major industrial accident potential based on dangerous substance criteria 61

6.3.3 Multi-risk NaTech decision matrix 64

7. Potential multi-hazard scenarios for civil infrastructures 66

7.1 Multi-hazard scenarios approach for water distribution networks 66

7.1.1 Introduction 66

7.1.2 Hazard categories, interrelations, and interdependencies in Water Distribution Networks 66

7.1.3 Quantitative simulation-based approach for multi-hazard scenarios in WDS 68

8. Conclusions 69

9. References 72

List of Tables

Table 5.1: Probabilities from Event Tree Analysis 32
Table 5.2: CPTs for the ignition scenarios given "damage states" and "source of damages" for a) refined dataset including S?; b) refined dataset treating uncertainty; c) extended NaTech-driven dataset treating uncertainty. 33
Table 5.3: Conditional Probability Table (CPT) of Cause and Final Scenario 40
Table 5.4: Conditional Probability Table (CPT) of Equipment involved and Final Scenario 40
Table 5.5: Input parameters for PHAST simulations 41
Table 5.6: Chocked mass flow rate and PHAST evaluated mass flow rate 42
Table 5.7: Results obtained from CFD and PHAST simulations, varying the composition of the released gas 43
Table 5.8: Flame Length varying the composition of the released gas 45
Table 5.9: Effect Zone Radius varying the composition of the released gas 45
Table 5.10: OpenSees objects and material laws employed in the pallet rack modelling 51
Table 5.11: Damage state thresholds associated with the adopted EDPs 52
Table 5.12: Median values (μ) and logarithmic standard deviations (β) for fragility models on rigid soils .. 55
Table 5.13: Median values (μ) and logarithmic standard deviations (β) for fragility models on soft soils 55

Table 6.1 - Rating of Factors B1 and B2, and thresholds for NI(HH) and NI(Env) 58
Table 6.2 - Characterization of hazardous substances stored in the case study plant 63

List of Figures

Figure 4.1: Methodological framework for multi hazard risk assessment for road and rail tunnels.
Figure 4.2: Description of the hazards taken into account for the multi hazard analysis of road and rail tunnels.
Figure 4.3: Venn Diagram of Fires, Structural Collapse and Earthquake.
Figure 4.4: ALARP in the Italian Legislative Decree 264/2006 (Decree 264/2006)
Figure 4.5: An example of back cumulated risk distribution following the Italian rail tunnel ALARP criteria. Guarascio et al. (2007).
Figure 4.6: Historical Earthquakes surrounded by the San Benedetto tunnel
Figure 4.7: Results of geostatistical analysis.
Figure 4.8: Back cumulative curve that represents at least one event with equal acceleration will occur or higher than a given PGA threshold using probability.
Figure 4.9: Fragility curves.
Figure 4.10: Comparative analysis of these three curves
Figure 4.11: Failure due to a) earthquake, b) flooding, c) landslide and d) windstorm (Deng et al., 2016).
Figure 4.12: Failure due to a) an overloaded truck, b) vessel impact (Deng et al., 2016) and c) explosion.
Figure 4.13: Basics of PSHA: a) earthquake zones, b) distribution of earthquake magnitudes, c) distribution of source-to-site distances, d) distribution of ground motion intensity (Baker et al., 2021).
Figure 4.14: Example of hazard curve.
Figure 4.15: Example fragility courves computed with the cloud analysis.

Figure 5.1: Two-phase procedure to model functional vulnerabilities to NaTech in the process industry
Figure 5.2: Lightning-triggered NaTech-driven dataset structure
Figure 5.3: Lifespan of the retrieved records

Figure 5.4: Frequency for the type of industrial event
Figure 5.5: Bar graph for the different industrial macro-sectors affected by lightning strikes
Figure 5.6: Vulnerable industrial equipment to lightning strikes
Figure 5.7: Technological scenarios triggered by lightning vs. classification of substances involved
Figure 5.8: Event tree for the records reporting ignition scenarios
Figure 5.9: a) Bayesian Network structure for the ignition scenarios in the refined dataset, mapped from the event tree. b) Bayesian Network model learned with NPC algorithm with a 10% significance level
Figure 5.10: Database structure built to collect material degradation events in process industry
Figure 5.11: Trend over the years in the number of records collected. Green bars indicate the number of reports retrieved from the NRC database, yellow bars from other sources
Figure 5.12: Number of events for each category of degradation cause
Figure 5.13: Number of events for each macro-sector analyzed
Figure 5.14: Number of events for each macro-sector analyzed
Figure 5.15: Number of events for each outcome
Figure 5.16: Frequency of the final scenario in relation to the degradation mechanism. A) Final scenario for corrosion-triggered events. B) Final scenario for all other deterioration mechanisms
Figure 5.17: Age of the plants for which it was possible to report the data.
Figure 5.18: Event tree for records reporting corrosion of equipment in industrial plants
Figure 5.19: Bayesian network for material degradation
Figure 5.20: Molar fraction profile of the gas released (left) and Molar fraction profile of the gas released within the flammability limits (right) in the plane *z-x* at *y*=50 m
Figure 5.21: Molar fraction profile of the gas released within the flammability limits using PHAST software
Figure 5.22: Radiation heat flux received, varying the composition of the gas released: pure methane (a), 10% H_2 (b), 20% H_2 (c), pure hydrogen (d)
Figure 5.23: Radiation vs. distance for Jet Fire using PHAST software
Figure 5.24: Radiation Ellipse for Jet fire using PHAST software
Figure 5.25 Example of event tree for pipelines
Figure 5.26 ETA hydrogen release
Figure 5.27: a) Common plan layout. b) Rack configurations showing pallet load (in tonnes) per level, span, and frame for each upright type (U1, U2, U3).
Figure 5.28: a) View of the 3D FE model for the intermediate case study rack. b) Main cross-sections.
Figure 5.29: Main non-linear hysteretic laws used in the FE rack modelling.
Figure 5.30: Information on ground motion dataset for rigid and soft soils: (a) PGA and (b) S_a values.
Figure 5.31. Fragility curves of the rack stock on rigid soils in PGA: (a) ε^*, (b) θ_X, (c) φ_{btc}, (d) φ_{base}.
Figure 5.32. Fragility curves of the rack stock on rigid soils in S_a: (a) ε^*, (b) θ_X, (c) φ_{btc}, (d) φ_{base}.
Figure 5.33. Comparison of median ($\mu_{DS,i}$) and logarithmic standard deviation ($\beta_{DS,i}$) values of the fragility curves based on ε* for different soil conditions.

Figure 6.1: Theoretical conception of the multi-risk NaTech vulnerability indicator
Figure 6.2 : Framework Industrial Critical Infrastructure Multi-Risk Deployment (ICI-MRD) numbering the steps for its implementation
Figure 6.3: Output of ICI-MRD framework tested on the energetic critical infrastructure
Figure 6.4: Pareto diagram for individual items multi-vulnerability (IAW)
Figure 6.5: Pareto diagram for items individual function-location multi-vulnerability (IRW)
Figure 6.6: Dangerousness of each hazard against the critical infrastructure is a punctual element
Figure 6.7: a) Framework representation for assessing the potentiality to cause major industrial accidents based on the dangerous substance criteria. b) Decisional scale for Q_{Cs} in function of $Q_{Ux(s)}$
Figure 6.8: Different views for the reference scale of the Index of compliance $Q_{S(ref)}$ including each dimension of substance classification
Figure 6.9: Multi-risk NaTech decision matrix

Figure 7.1: Interdependencies between hazards, infrastructures, and the Water Distribution Network (WDN)

4. Potential multi-hazard scenarios for transportation infrastructures

4.1 Quantitative probabilistic risk assessment: fault tree and event tree analysis, multi hazard scenarios analysis (fire, seismic and landslide simulation) for road and railway tunnel

Transport infrastructures, such as roads, bridges, and tunnels, constitute critical elements of the national emergency management system, ensuring continuity of mobility, accessibility to affected areas, and support to rescue and relief operations. However, these assets are increasingly exposed to a wide spectrum of natural and man-made hazards, including extreme weather events, fires, structural failures, and technological incidents, all of which may trigger cascading effects during emergencies.
In a country like Italy, the management of multi-hazard risks must be considered a structural component of infrastructure governance, due to the convergence of several vulnerability factors: elevated seismic risk, a widespread presence of subterranean road assets (notably tunnels), and a high density of heavy-duty transport within an overall congested mobility framework. These conditions increase the probability and potential impact of compound emergency scenarios, requiring integrated risk anticipation and preparedness.
To ensure effective emergency preparedness and response, it is essential to maintain an accurate and continuously updated knowledge base concerning hazard sources, exposure levels, and critical interdependencies across infrastructure systems. Such data supports the pre-identification of critical nodes, the activation of contingency plans, and the prioritization of protective measures.
This study presents a quantitative probabilistic risk assessment (QRA) framework tailored for application in road and railway infrastructure management, with a specific focus on emergency risk governance. The methodology adopts a bow-tie analysis structure, integrating fault tree analysis (FTA) to model initiating failures and event tree analysis (ETA) to map potential evolution paths. This approach facilitates the identification of Initial Critical Events (IEc) and the construction of multi-hazard emergency scenarios.
By combining static parameters (exposure, vulnerability) with real-time operational risk indicators, the model supports the estimation of residual risk and provides a robust tool for emergency decision support, enabling risk-informed activation of response protocols, infrastructure safeguarding strategies, and cross-sectoral coordination mechanisms.

4.1.1 Overview of multi hazard concepts for transportation infrastructure

Modern infrastructure systems are increasingly exposed to a wide spectrum of threats arising from both natural and anthropogenic sources. In underground settings such as tunnels, subways, and utility corridors, risks are not isolated. Instead, they frequently emerge in interconnected or cascading forms, where one hazardous event can trigger or amplify others. This dynamic interplay gives rise to what is known as multi-hazard scenarios, which pose a more complex and often more severe risk profile than individual hazards considered in isolation (Liu et al., 2016).
A multi-hazard condition is defined as the combination of two or more potentially harmful events that may occur simultaneously, in sequence, or with compound interdependencies. These include both independent hazards (with no probabilistic influence on each other) and non-independent hazards (where the occurrence of one affects the probability of another). In underground environments, examples include seismic shocks followed by structural collapse, fires induced by infrastructure damage, or toxic gas propagation impairing evacuation procedures. Understanding and managing such scenarios is critical for maintaining operational safety and ensuring life protection, especially in confined spaces where evacuation options are limited and event progression may be rapid and nonlinear.
Studies conducted by Badr et al. (2024) had led to the possibility of introducing the link between multi hazard risk assessment and resilience evaluation applied to an hydropower plants. The analysis of the man-made related risks is supported by previous case studies conducted by the same authors.
The exposure of critical infrastructure to multiple, interconnected natural and anthropogenic hazards could have severe repercussions on global economies and societies. Therefore, the assessment of the resilience of such infrastructure is of fundamental importance for maintaining its functionality (Argyroudis et al., 2020)

Currently, there are evident gaps in the evaluation of the resilience of such infrastructures, and as already highlighted, these are represented by the fact that single hazards tend to be considered as independent from each other when, instead, a more reliable assessment must take into account the occurrence of multiple related hazardous events.
Ouyang (2014) presented an overview of the CIs interferences of the different infrastructures. It is evident that the functionality of the infrastructure is dependent on the single components. For example, a road considered as a critical infrastructure, is composed of viaduct, tunnel, and road itself.
A study conducted by Wisetjindawat et al. (2017) proposes an analysis procedure that made it possible to evaluate the resilience of a transportation system with reference to a pair of extreme events. The logic of the analysis is based, specifically, on the fact that there are two general families of approaches to quantitatively evaluate the resilience of a system: vulnerability analysis and network reliability analysis. Vulnerability analysis focuses on identifying the weak points of a system and estimating the consequences of system failure. Therefore, the ability to identify vulnerabilities in transportation systems is essential to make them more resilient.
Another quantitative probabilistic method for analyzing the multi-hazard resilience of an infrastructure system is presented by Kong et al. (2019), which considers the resilience approaches of infrastructure systems under critical conditions. In particular, the innovative aspect of this method is that it is applied considering that multiple hazards refer to a situation where hazards of different types or magnitudes occur simultaneously or, more often, successively with damaging force.
Chen et al. (2002) introduced "capacity reliability" as a measure to evaluate the performance of a road system. In this context, reliability is defined as the probability that the maximum capacity of the network is greater than or equal to a required demand level, considering the random variations in link capacities. This approach involves comparing travel times under degraded and non-degraded capacity states and is particularly useful for extreme event simulations, as the network may experience substantial degradation, leading to significant increases in travel time between an origin-destination (OD) pair.

4.1.2 Methodological framework for multi-hazard assessment

The traditional approach to risk assessment has largely relied on the independent analysis of distinct hazards, evaluating each through its probability of occurrence and associated consequences. However, multi-hazard assessment necessitates a more comprehensive framework that can simultaneously capture complex interactions between hazards and incorporate temporal, spatial, and structural dependencies.

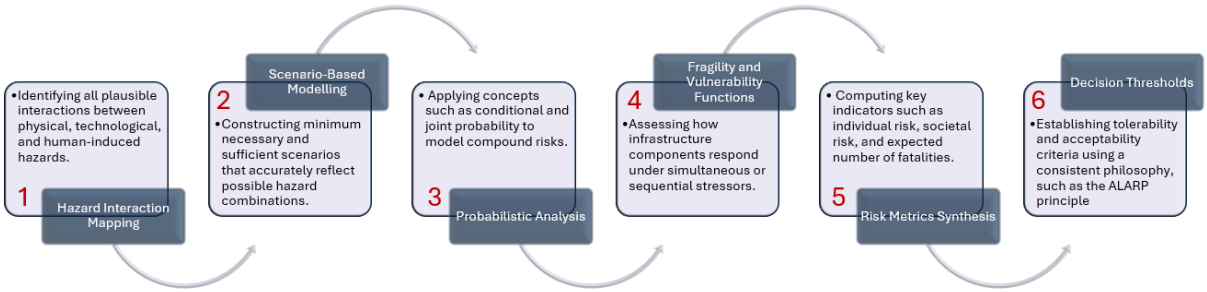

Figure 4.1: Methodological framework for multi hazard risk assessment for road and rail tunnels.

To address this, a multi-hazard risk assessment framework should include the following core components (see **Figure 4.1**):

- **STEP 1 – hazard interaction mapping**: identifying all plausible interactions between physical, technological, and human-induced hazards.
- **STEP 2 – scenario-based modelling**: constructing minimum necessary and sufficient scenarios, exhibiting a group structure according to algebraic principles, that accurately reflect possible hazard combinations.

- **STEP 3 – probabilistic analysis**: applying concepts such as conditional and joint probability to model compound risks.
- **STEP 4 – fragility and vulnerability functions**: assessing how infrastructure components respond under simultaneous or sequential stressors.
- **STEP 5 – risk metrics synthesis**: computing key indicators such as individual risk, societal risk, and expected number of fatalities.
- **STEP 6 – decision thresholds**: establishing tolerability and acceptability criteria using a consistent philosophy, such as the ALARP principle.

This framework adopts a systemic risk perspective, shifting the focus from individual hazard events to an integrated approach in which hazards are treated as interdependent components within a complex system. The underlying multi-hazard methodology, along with the associated probabilistic assumptions, is presented in the following section.

Scenario modelling and role of interdependencies

Scenario identification and modelling constitute the essential foundation of any multi-hazard assessment. An inaccurate or partial representation of the scenario may undermine the reliability of the entire risk analysis, regardless of the complexity or precision of the analytical methods employed. For this reason, scenario development should not be limited to estimating event probabilities and consequences, but must also incorporate considerations of event sequencing, potential simultaneity, and interdependencies arising from conditional or cascading effects.
Events can be classified into:

- Mutually exclusive (only one occurs)
- Not mutually exclusive (multiple can occur together)
- Independent (no probabilistic influence)
- Dependent (one affects the probability of others)

Once the fixed characteristics of the tunnel, such as its geometry, structural configuration, and construction materials, have been defined, the following key parameters form the basis for the development of the **Event Tree Analysis (ETA)**:

- **Fire incidence rate and P(EI):** estimation of the probability of the initiating event (P(EI)) based on predefined fire size classes and historical occurrence rates.
- **Temporal and seasonal traffic characteristics:** analysis of time-dependent traffic profiles, including daily, weekly, and seasonal fluctuations in vehicle type, volume, and occupancy.
- **Spatial parameters:** determination of the likely fire location and distribution of occupants within the tunnel at the time of the initiating event.
- **Definition of intermediate events:** identification of sequential events that may occur following the initiating fire event. These may include fire development, activation of detection and suppression systems, and initiation of evacuation protocols.
- **Definition of final outcomes (End Branch Scenarios):** characterization of the terminal consequences arising from the combination of intermediate events. Examples include complete or partial evacuation, successful fire suppression, and various degrees of structural damage to the tunnel.
- **Assignment of probabilities:** quantitative estimation of the likelihood associated with each event in the tree structure. These probabilities, informed by historical data, expert judgment, or engineering models, must satisfy the condition that the sum of probabilities of all mutually exclusive outcomes at each branching point equals one.
- **Computation of final event probabilities:** the probability of each end branch scenario is obtained by multiplying the conditional probabilities along the corresponding path of the event tree.
- **Damage quantification for each final scenario:** each end branch is associated with a predefined damage metric, typically expressed in terms of **expected fatalities** or **structural impact indices**.
- **Calculation of the Expected Fatalities (Damage) Value (EFV):** the EFV is computed as the sum of the products of each end branch probability and its corresponding damage value. This scalar output serves as a risk indicator that can be used for comparison against **risk acceptability thresholds**, such as those defined by ALARP-based criteria or regulatory standards.

The ETA modelling framework incorporates a series of quantitative estimations, among which the computation of joint probabilities plays a central role. Specifically, the joint probability of two events, A and B, occurring concurrently is defined by the following expression:

$$P(A \cap B) = P(A) * P(B|A) \tag{4.1}$$

where P(A) denotes the probability of the initiating event A, and P(B|A) represents the **conditional probability** of event B occurring, given that event A has already taken place. This formulation allows for the representation of sequential dependencies within the event tree structure and is fundamental for the probabilistic propagation of scenarios leading to end-event outcomes.

The concept of conditional probability is introduced to quantify the likelihood of an event occurring given the prior occurrence of another.

Formally, the conditional probability of event B occurring, given that event A has already occurred, is defined by the expression:

$$P(B|A) = P(A \cap B) / P(A) \tag{4.2}$$

provided that $P(A)>0$.

This relationship is fundamental in probabilistic modelling, particularly within ETA, as it enables the evaluation of sequential dependencies between interconnected events.

A three-set Venn diagram is utilized to represent all possible logical intersections and unions among the selected hazard categories. This graphical representation enables the systematic visualization of multi-hazard interactions and their potential co-occurrence within a shared spatial and temporal framework.

Prior to addressing the probabilistic modelling of hazard interactions and the estimation of the joint occurrence of interconnected events, **Figure 4.2** provides an overview of the primary events that may affect tunnel infrastructure, whether road or rail, serving as the foundational basis for subsequent scenario construction.

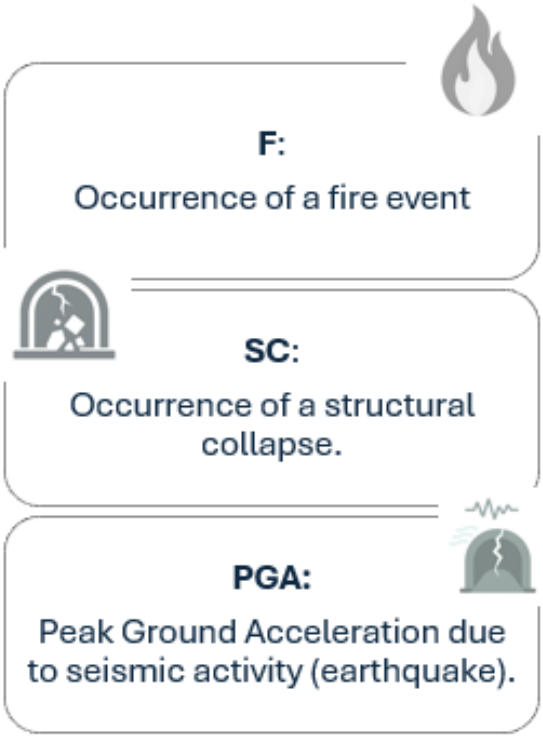

Figure 4.2: Description of the hazards taken into account for the multi hazard analysis of road and rail tunnels.

The figure illustrates three key hazardous events that may compromise the safety of infrastructures, particularly in contexts such as tunnels or confined environments exposed to multi-hazard scenarios:

- F – Occurrence of a **fire event**: this refers to the potential for a fire to occur, which can be triggered by various factors such as electrical faults, vehicle accidents, or the release of flammable substances. The flame icon visually emphasizes the thermal hazard associated with fire events.
- SC – Occurrence of a **structural collapse**: this indicates the risk of structural failure, which may result from overloading, material degradation, design flaws, or the cascading effects of other hazards

like earthquakes or fires. The icon depicts a damaged structure, highlighting the direct threat to physical integrity.

- PGA – Peak Ground Acceleration due to **seismic** activity (**earthquake**): PGA is a seismic parameter measuring the maximum ground acceleration during an earthquake. It is a critical input for evaluating the seismic demand on infrastructure.

Subsequently, the **Venn diagram** is employed to support the representation and interpretation of a **multi-hazard evaluation framework**. Specifically, **Figure 4.3** illustrates all possible probability configurations associated with the individual hazard events. These configurations are then analytically described in the subsequent sections, with reference to the different conditions of occurrence and interaction among the hazards considered.

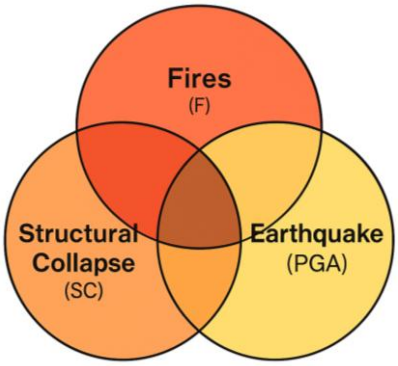

Figure 4.3: Venn Diagram of Fires, Structural Collapse and Earthquake.

Each area of the diagram represents a unique combination of presence or absence of the above-described hazards. (see section scenario classification)

Scenario classification

Following, a description of the possible combination in terms of scenarios occurring.

Single-Hazard Scenarios

- $\boldsymbol{F} \cap \overline{\boldsymbol{SC}} \cap \overline{\boldsymbol{PGA}}$: Fire without structural collapse or earthquake.
- $\overline{\boldsymbol{F}} \cap \boldsymbol{SC} \cap \overline{\boldsymbol{PGA}}$: Structural collapse not triggered by fire or seismic events.
- $\overline{\boldsymbol{F}} \cap \overline{\boldsymbol{SC}} \cap \boldsymbol{PGA}$: Earthquake occurs, but no secondary fire or collapse.

Dual-Hazard Scenarios

- $\boldsymbol{F} \cap \boldsymbol{SC} \cap \overline{\boldsymbol{PGA}}$: Fire induces or coincides with structural collapse, independent of seismic excitation.
- $\boldsymbol{F} \cap \overline{\boldsymbol{SC}} \cap \boldsymbol{PGA}$: Earthquake and fire occur, but structural integrity is maintained.
- $\overline{\boldsymbol{F}} \cap \boldsymbol{SC} \cap \boldsymbol{PGA}$: Seismic activity causes structural collapse, but without fire.

Triple-Hazard Scenario

- $\boldsymbol{F} \cap \boldsymbol{SC} \cap \boldsymbol{PGA}$: Simultaneous occurrence of all three hazards. This represents the worst case, potentially involving synergistic effects and posing maximum threat to life safety and structural integrity.

Null Event

- $\overline{\boldsymbol{F}} \cap \overline{\boldsymbol{SC}} \cap \overline{\boldsymbol{PGA}}$: No event occurs. While not visually included in the Venn diagram, this scenario represents the base state or control condition for probabilistic assessments.

The classification scheme aids in distinguishing between isolated and compound hazard scenarios, which is relevant for:

- **Risk prioritization**: allocating resources based on the frequency and severity of combined events.
- Design of **mitigation strategies**: ensuring that emergency systems are robust under multiple stressors.
- Development of **simulation models**: improving the accuracy of dynamic risk evaluations in built environments.

The identification of interdependencies among hazards and system responses enables the structured development of event trees, where each branch delineates the progression of a hazard scenario and the terminal nodes represent distinct outcome states.

Furthermore, scenario modelling must account for the non-linear and emergent dynamics that characterize infrastructure behavior under compound hazard conditions. For example, a moderate seismic event may pose

limited threat in isolation, yet it can trigger disproportionately severe consequences if it results in the ignition of flammable materials under conditions of limited evacuation preparedness.

To accurately capture such complex interactions, it is essential to adopt modelling approaches capable of representing emergent phenomena, such as agent-based models for simulating occupant evacuation dynamics or coupled fluid–structure interaction models for analyzing fire-induced collapse mechanisms. These methodologies enhance the fidelity of risk assessments by incorporating both physical and behavioral dimensions of system response under multi-hazard stressors.

A fundamental aspect of multi-hazard risk governance and tunnel resilience is the ALARP (As Low As Reasonably Practicable) principle, which mandates risk reduction to levels at which further mitigation measures become either technically unfeasible or economically unjustifiable. In the framework of multi-hazard assessment, the application of ALARP is further complicated by:

- the inherent difficulty in quantifying the probabilities of compound events;
- the ambiguous delineation of risk tolerability thresholds under interacting hazard scenarios;
- the complexities involved in prioritizing mitigation measures across heterogeneous hazard domains.

To effectively address these challenges, the ALARP principle is frequently operationalized through risk quantification models. Such models integrate ethical criteria for risk acceptability with semantically and mathematically rigorous evaluation methodologies, synthesizing both deterministic and probabilistic data inputs. Within these frameworks, risk is characterized by multiple quantitative and qualitative indicators, including but not limited to:

- Risk Quantum – A composite measure of expected losses across multiple hazards.
- Individual Risk – The probability that a specific person will be harmed in a given timeframe.
- Societal Risk – Aggregate probability of multiple fatalities, often visualized through FN-curves.
- Expected Number of Fatalities – The statistical average of deaths per year for a given system configuration.

These indicators serve both analytical and normative purposes, enabling rights-holders (e.g., the public) and duty-holders (e.g., operators and designers) to negotiate acceptable levels of residual risk.

Effective multi-hazard risk assessment frequently necessitates the integration of heterogeneous modeling platforms tailored to distinct hazard typologies and corresponding system responses. These platforms may encompass:

- Seismic geostatistical tools for spatial and temporal analysis of ground motion.
- Structural fragility models for assessing collapse probability.
- Fire dynamics simulators (e.g., FDS) for modelling heat, smoke, and gas propagation.
- Evacuation simulators based on Performance-Based Design (PBD) to account for human behavior.

The integration of these tools within a unified modeling framework enables scenario-specific analyses wherein hazard initiation, propagation, and mitigation responses are simulated concurrently.

In multi-hazard contexts, establishing criteria for acceptable risk levels presents a multidimensional challenge. Unlike single-hazard scenarios—where risk thresholds are often clearly defined through deterministic regulations or empirical historical data—multi-hazard environments are characterized by simultaneous or sequential risk interactions exhibiting variable probabilities, interdependencies, and severities. Such complexity amplifies epistemic uncertainty and limits the adequacy of conventional risk tolerability frameworks.

Consequently, risk acceptability in these contexts must be grounded in a structured, transparent, and ethically informed methodology that encompasses not only technical feasibility and economic considerations but also societal perception, social equity, and long-term sustainability. Risk acceptance thereby transcends a purely scientific judgment, constituting a socio-technical deliberation that integrates engineering standards, legal frameworks, philosophical principles, and stakeholder values.

The ALARP Principle: A foundational ethic

The principle of ALARP – As Low As Reasonably Practicable – is a widely accepted doctrine in safety of tunnels (both road and rail) and forms the ethical foundation for risk governance in multi-hazard assessment. It posits that risk should be reduced to the lowest level that is reasonably achievable, considering the costs and effort required to mitigate it further (**Figure 4.4**).

This principle introduces a three-tiered structure for risk decision-making:

- Unacceptable Region – Where risk is intolerable regardless of the benefits or cost of mitigation. Immediate intervention is mandatory.

- Tolerable (ALARP) Region – Where risk may be tolerated only if further risk reduction is impractical or the costs grossly outweigh the benefits.
- Broadly Acceptable Region – Where risk is so low that no specific risk-reduction measures are typically required.

However, within multi-hazard frameworks, this structure requires reinterpretation in terms of scenario interactions, compounded probabilities, and cascading failure mechanisms. The conventional linear cost-risk-benefit paradigm is challenged by nonlinear system dynamics and the inherent complexity of quantifying joint probabilities associated with rare, interdependent events.

Safety objectives and risk acceptability criteria—previously outlined for road tunnels and applicable to each individual bore in the case of multi-bore tunnel configurations—are depicted by the threshold lines illustrated in the following **Figure 4.5**.

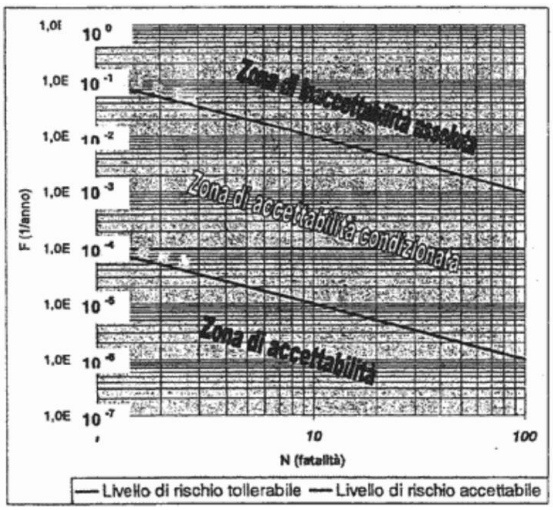

Figure 4.4: ALARP in the Italian Legislative Decree 264/2006 (Decree 264/2006)

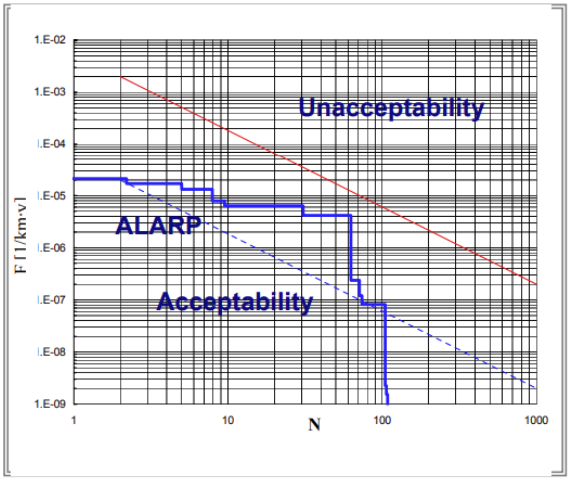

Figure 4.5: An example of back cumulated risk distribution following the Italian rail tunnel ALARP criteria. Guarascio et al. (2007).

These two curves, if compared, leave some necessary considerations. The slope (α) of the risk curve, typically ranging between 1 and 2, serves as an indicator of risk aversion. In a log-log plot, a steeper negative slope (−α) reflects a higher degree of risk aversion, meaning that the acceptability of risk decreases more rapidly as the severity of consequences increases. A slope of $\alpha = 1$ corresponds to a risk-neutral position, where the decrease in acceptability is directly proportional to the severity of the outcome. In contrast, a slope $\alpha > 1$ signifies a risk-averse approach, where more severe events are accepted only at significantly lower probabilities. As α increases within this range, the level of aversion to high-consequence events becomes progressively stronger.

For example, in Italy, specific tolerability limits are defined for road and rail systems:

- road tunnel tolerability limit: for road tunnels the reference values is α = 1, starting from N = 1 fatality. This represents a neutral decay rate, where the exceedance probability decreases in direct inverse proportion to the number of fatalities, indicating a moderate level of risk tolerance.
- railway tunnel tolerability limit: for railway tunnels the reference values is α = 1.4168, starting from N = 2 fatalities. This reflects a stricter risk acceptance criterion, where the exceedance probability declines more rapidly with increasing severity, consistent with a lower tolerance for high-fatality incidents.

The railway tolerability curve begins at N = 2, implicitly excluding single-fatality scenarios. This may indicate an assumption of inherent control over such events or that they are considered too unlikely to be explicitly addressed. While this reflects a higher baseline safety expectation in the railway sector, it may risk underestimating the relevance of lower-severity events, which, if left unaddressed, could still pose significant operational or reputational consequences.

After defining the background ethical and mathematical consideration about ALARP principle and curve to apply it meaningfully in multi-hazard environments, the following methodological adjustments are proposed (Guarascio, 2021).

In fact, rather than assigning acceptability thresholds based solely on aggregated metrics (e.g., average fatalities per year), each minimum necessary and sufficient scenario should be evaluated in terms of:

- Triggering mechanisms (e.g., earthquake-induced collapse leading to fire)
- Propagation potential (e.g., blockage of exits, toxic gas accumulation)
- Human-system interaction (e.g., confusion during evacuation, decision delay)

This scenario-based stratification ensures that unacceptable risks are not hidden within averaged data.

The decision to accept or mitigate a risk should be informed by multiple indicators, including:

- **Risk quantum**: this represents a comprehensive measure integrating likelihood, exposure, and severity across cascading events.
- **Individual risk**: this metric represents the annual probability of fatality for a single exposed individual.
- **Societal risk**: this parameter is represented by FN-curves (back cumulated probability versus number of fatalities), which illustrate collective risk acceptability thresholds.
- **Expected number of fatalities**: This metric is instrumental in evaluating and comparing the cost-effectiveness of various risk mitigation strategies.

The application of multiple metrics mitigates reliance on a single potentially biased indicator and facilitates a more refined prioritization process.

In multi-hazard contexts characterized by limited data availability and elevated uncertainties, exclusive dependence on quantitative cost-benefit analyses may be ethically tenuous. Accordingly:

- The application of precautionary principles is recommended to complement probabilistic assessments.
- Worst-case scenario analyses should be incorporated, regardless of the low or uncertain probability estimates.

Stakeholder consultation is vital, especially where public exposure or irreversible consequences are involved.

This expanded interpretation of the ALARP principle emphasizes that risk tolerability constitutes not merely a technical threshold but a boundary shaped through social negotiation. In jurisdictions where ALARP holds legal significance (e.g., the United Kingdom, European Union member states), case law and regulatory precedents establish that the responsibility lies with the duty-holder to demonstrate that all reasonably practicable measures have been implemented to mitigate risk. The reasonableness of such measures must be evaluated not solely on direct costs but also considering systemic effects and cross-hazard interactions—for instance, the potential for an automated suppression system to inadvertently delay evacuation.

Residual risks must be communicated with transparency, and the rationale underpinning risk management decisions must be thoroughly documented to withstand ethical and legal scrutiny (ISO, 2018). Consequently, multi-hazard contexts necessitate a more dynamic, auditable, and participatory application of the ALARP framework.

4.1.3 Example of the application of multi hazard methodology for road tunnel

Italy, characterized by a high density of tunnels and significant seismic hazard, necessitates the incorporation of multi-hazard scenarios in infrastructure design processes. Geostatistical modeling is indispensable for accurately characterizing localized seismic effects and assessing their influence on structural elements. The integration of seismic risk considerations into fire safety analyses is particularly critical for bidirectional tunnels permitting heavy traffic volumes with stable percentage compositions.

Case Study: The San Benedetto Tunnel event (Italy, 2016)

Following the systemic framework outlined, the San Benedetto tunnel provides a concrete application of multi-hazard assessment in road infrastructure. Italy, characterized by both extensive underground transport assets and high seismic vulnerability, is a crucial context for exploring how natural and anthropogenic hazards can interact, triggering cascading effects and amplifying risk (Lombardi et al., 2021).
The San Benedetto tunnel, located in Umbria (Central Italy), was significantly affected by the seismic sequence of 2016, particularly during the October 30 earthquake of magnitude 6.6 (see **Figure 4.6**). This case study illustrates a multi-hazard scenario involving seismic activity, structural damage, traffic-related accidents, and fire risk. It is a bidirectional tunnel with a single tube approximately 4400 meters in length. The eastern entrance is at 1014 m a.s.l. and the western entrance is at 1001 m a.s.l. with a maximum coverage of about 600 meters. The tunnel was excavated through the geological formations of "Calcare Massiccio" and "Corniola", a grey-brown limestone containing varying fractions of flint, intensely fractured without a clear fracture orientation.

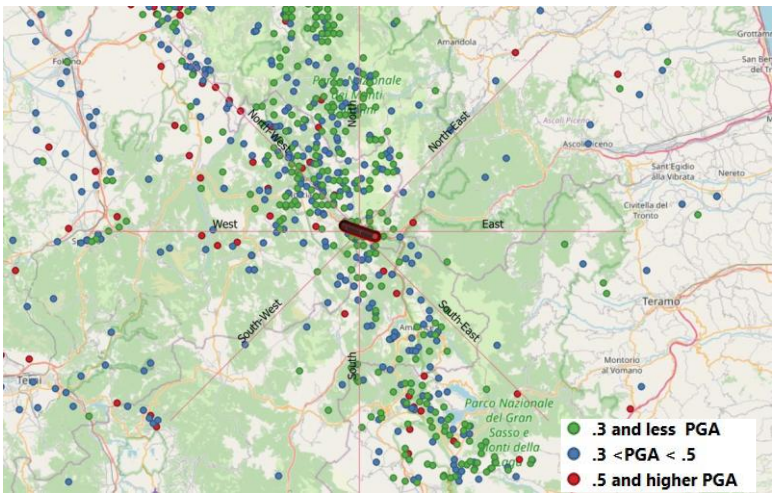

Figure 4.6: Historical Earthquakes in the surrounding of the San Benedetto tunnel.

The concept of multi-hazard refers to the occurrence of two or more hazardous events which can be independent (co-existing by coincidence), concurrent (originating from the same source), or successive (where one event triggers another). In this study, the multi-hazard concept is applied specifically to road tunnels, investigating the cascading effects of seismic events that could trigger secondary hazards, including accidents and fires.
In particular, the project focused on earthquake-induced traffic accidents within the tunnel, caused by abrupt swerving due to intense ground shaking or structural damage to the pavement. These incidents may evolve into fire events, representing a compound risk scenario. Central Italy, and especially the Norcia region, is known for high seismicity, and in 2016 a sequence of strong earthquakes occurred across the borders of Marche, Umbria, Lazio, and Abruzzo: 24 August with M 6.2, 26 October with M 6.1, and 30 October with M 6.6.
The Norcia area has a long seismic history, with major earthquakes recorded over 400 years. The 2016 events were particularly impactful due to their high intensity and short succession. During the October 30 event, unusually strong vertical ground accelerations were recorded and caused extensive damage to the San Benedetto tunnel, particularly around 920 meters from the western portal. Concrete cracking and spalling were predominantly concentrated along the southern sidewall of the tunnel, in some cases extending up to the crown. Major vertical cracks delineate a severely damaged portion of the sidewall, while the remaining fissures indicate a combined failure mechanism involving bending (excessive compressive stresses) and shear in the transverse section. Post-event surveys revealed a reduction in the tunnel's cross-sectional width, with maximum contraction of approximately 0.15 meters in the most affected segment.
A geostatistical analysis (**Figure 4.7**) was applied to estimate the Peak Ground Acceleration (PGA) across the tunnel alignment. Data sources included historical epicenters, seismic stations, and Digital Elevation Models (DEMs). Both horizontal and vertical PGA distributions peaked in the area of maximum damage, with vertical acceleration arriving approximately 0.5 seconds earlier than horizontal components. This vertical impulse is considered a primary factor in the damage mechanism. Looking at the profile and cross sections, the components of the seismic action at the site of the structural break reached approximately 900 cm/s^2. From the hazard curve,

the estimated probability of a seismic action of this intensity was determined, closely aligning with the 30 October 2016 event.

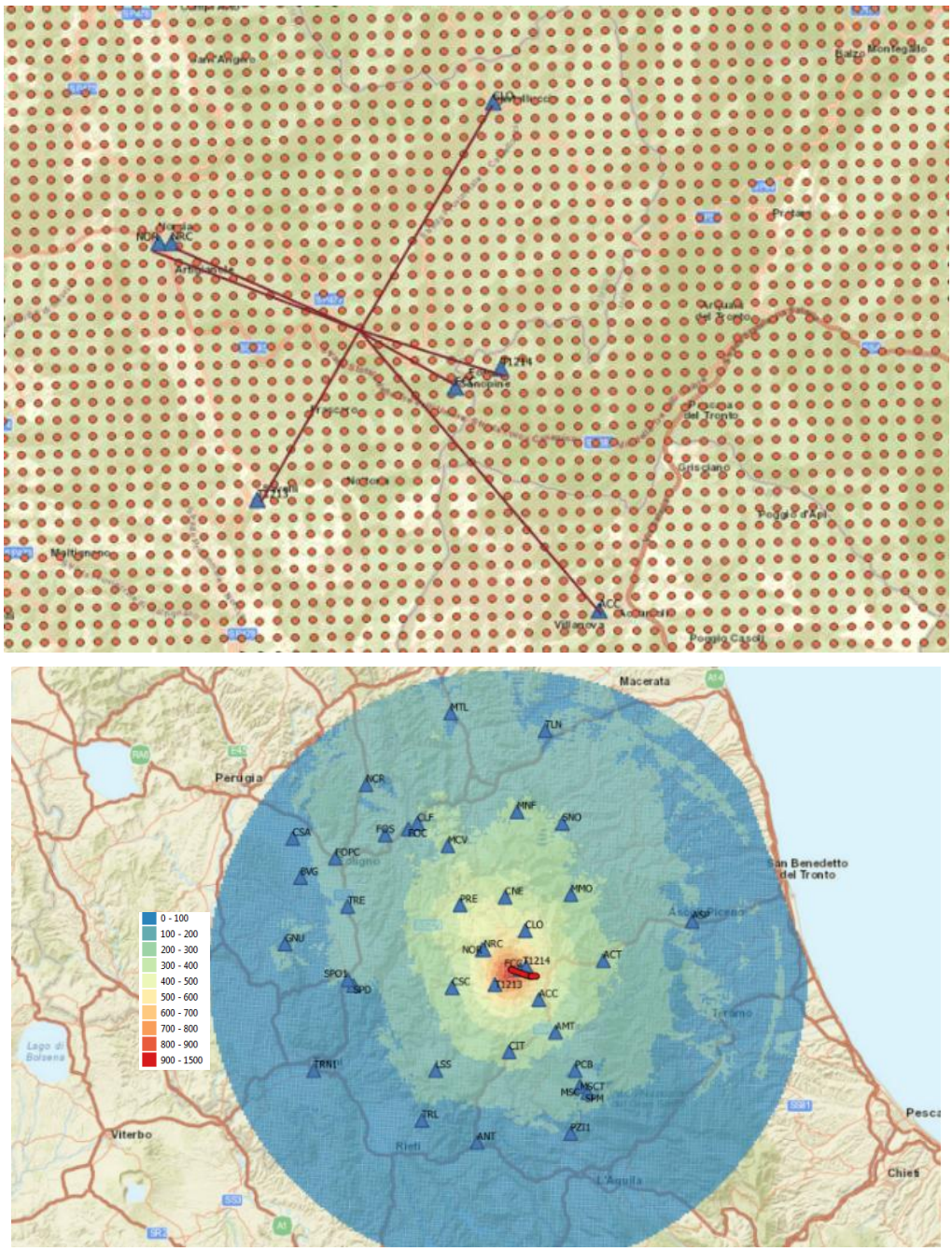

Figure 4.7: (a) Grid points of the digital terrain model used for the geostatistical estimation of the seismic action component – (b) - Contour maps of vertical PGA.

Hazard curves were developed (see **Figure 4.8**) to estimate the probability of experiencing seismic events of varying intensities at different points along the tunnel, focusing particularly on epicentral activity from the south-east azimuthal sector. Based on these curves, fragility curves were derived to assess the likelihood of structural damage levels. These fragility curves reflect the probability of exceeding slight, moderate, or heavy damage states as a function of PGA.

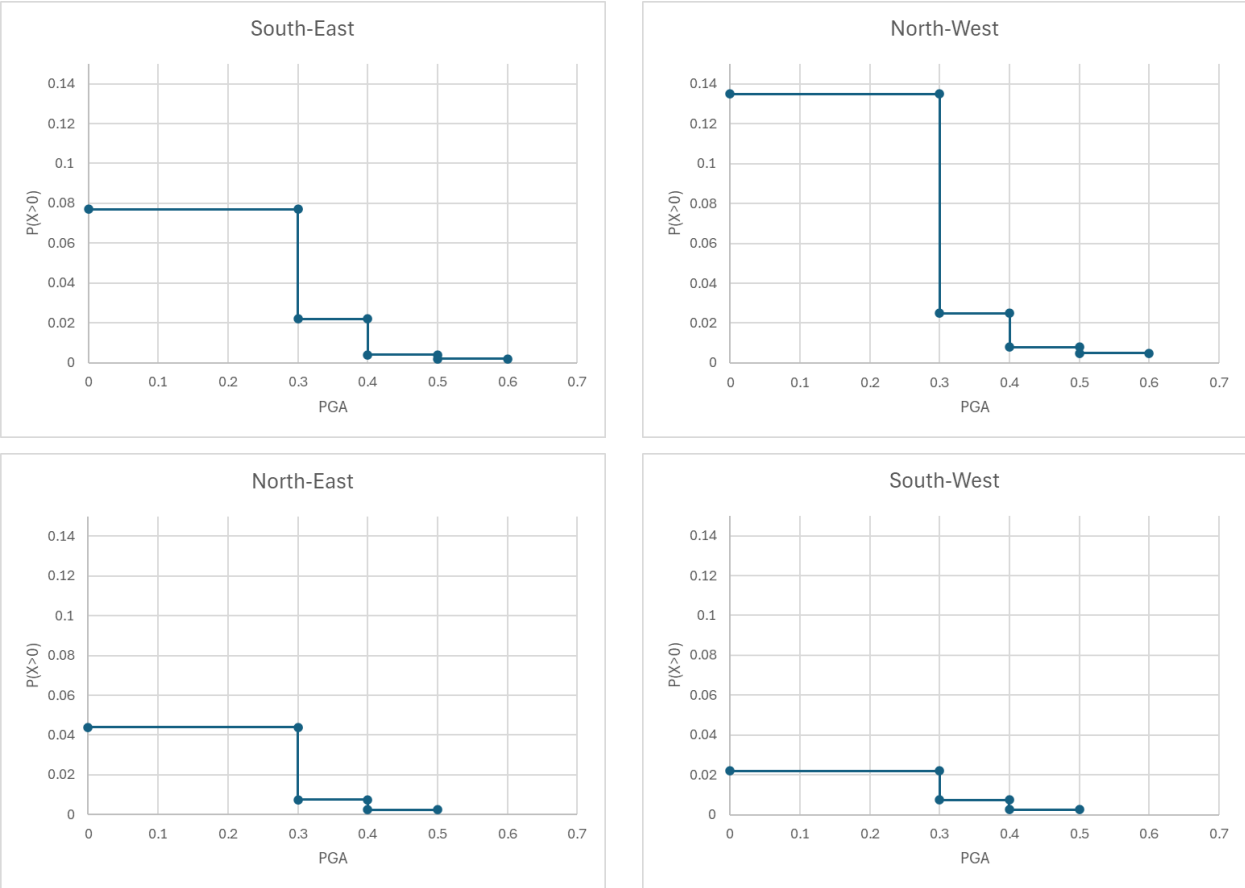

Figure 4.8: Back cumulative curve that represents at least one event with equal acceleration will occur or higher than a given PGA threshold using probability.

The multi-hazard scenario, as seen in this case, highlights the interaction of non-mutually exclusive events, seismic shaking, structural degradation, vehicular accident, and fire, each with probabilistic conditioning and physical cause-effect relationships. An appropriate correlation analysis between the value of seismic actions and the cracking state produced allows us to estimate the so-called fragility curves (**Figure 4.9**) that provide an estimate of the corresponding damage level probability.

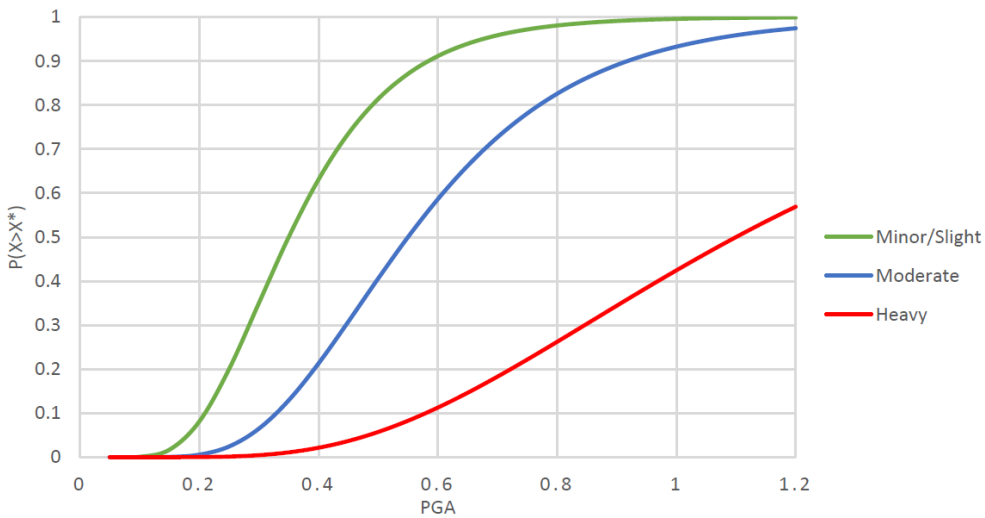

Figure 4.9: Fragility curves.

The San Benedetto tunnel is a bidirectional tunnel that accommodates also heavy goods traffic. In the event of a strong earthquake ground displacement can cause loss of vehicle control and resulting head-on collisions may lead to fire incidents. This cascading scenario underscores the tunnel's vulnerability to compound hazard effects. A hazard curve was developed for vertical and horizontal PGAs, and back-cumulative probability curves were used to assess the likelihood of exceeding threshold accelerations. Return time analysis indicates that damaging events may occur within the tunnel's design life, emphasizing the need for mitigation.

Italian Legislative Decree 264/2006, based on EU Directive 2004/54/EU, require that safety in tunnels be guaranteed by quantitatively assessing the risk through the use of F(N)-N curves to evaluate the acceptability of fire-induced fatalities, also taking into account a cost-benefit analysis. These diagrams are an effective tool for representing the societal risk associated with hazardous scenarios. This graphical representation, typically plotted on logarithmic scales, relates the number of fatalities (N) on the x-axis to the annual cumulative probability (F(N) on the y-axis that an event causes at least N fatalities.

The resulting curve describes the likelihood that, in any given year, the system or infrastructure under consideration could be involved in an event resulting in N or more fatalities. The function is typically decreasing, as high-fatality events are, by their nature, less probable than those with minor consequences.

The F(N)-N curve enables comparative evaluations across different risk scenarios or system configurations, including the presence or absence of mitigation measures. Moreover, it allows the results of the analysis to be benchmarked against predefined reference curves that establish thresholds of risk acceptability and tolerability. Specifically, three main regions are typically distinguished in the F(N)-N space:

- the unacceptable risk region, above the tolerability curve, where mitigation actions are mandatory regardless of cost;
- the ALARP region (As Low As Reasonably Practicable), between the tolerability and acceptability curves, where risk may be tolerated only if further reductions are not reasonably practicable;
- the acceptable risk region, below the acceptability curve, where the risk is considered fully compatible with safety criteria.

By using this approach, analysts can perform a structured and transparent assessment of societal risk, providing valuable support for design decisions, operational management, and prioritization of safety interventions.

When it is possible to compare three F(N)-N curves, each referring to the same initiating event but with different mitigation strategies applied, meaningful insights can be drawn regarding the effectiveness of the implemented safety measures. The curves clearly show how the implemented safety measures influence the cumulative probability of events involving an increasing number of fatalities (see **Figure 4.10**):

- the light blue curve, positioned slightly above the acceptability threshold, represents a scenario in which the risk is just beyond the limits considered fully acceptable. This may reflect a situation where safety measures are in place but not fully effective or sufficiently integrated. Although the risk does not fall within the unacceptable region, further mitigation should be considered, particularly if it is economically viable or easily implementable.
- the blue curve, located just below the acceptability threshold, corresponds to a scenario that is technically compliant with safety criteria. In this case, the system demonstrates adequate protection, and the associated risk remains within acceptable boundaries. No additional action is required, although optimizations could be evaluated to ensure a greater safety margin.
- the orange curve, positioned significantly below the acceptability limit, represents a highly secure scenario achieved through the implementation of advanced mitigation measures. The probability of events with a high number of fatalities is very low, and the risk profile remains well within the acceptable zone. This scenario can be considered a benchmark for best practice in risk management.

The comparative analysis of these three curves clearly demonstrates how collective risk can be substantially influenced by acting on the effectiveness of safety system. Even minor design or operational improvements can prove decisive in shifting a scenario from marginal acceptability to full compliance with established safety criteria.

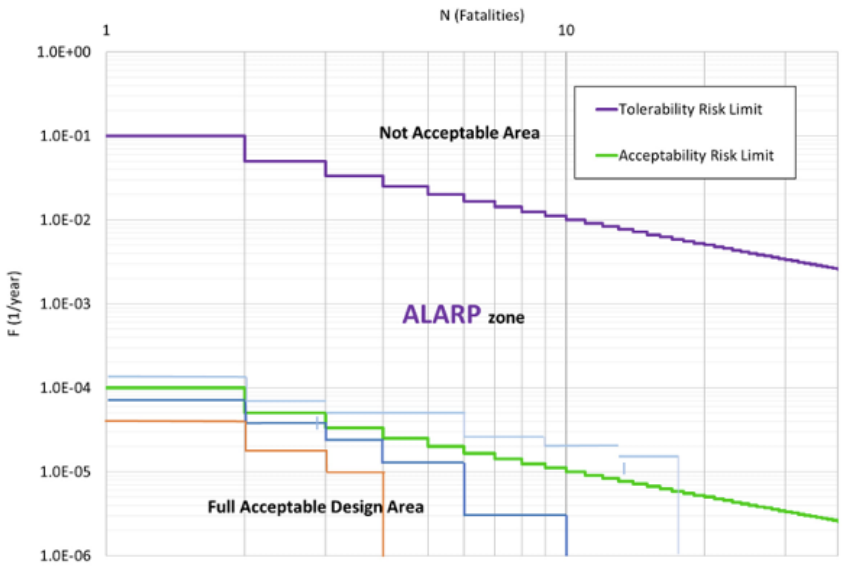

Figure 4.10: Comparative analysis of these three curves.

The presented case study investigates three alternative design configurations, evaluated in terms of their compliance with established fire risk acceptability criteria. Within a multi-hazard framework, it is essential to account for how certain triggering events, such as seismic activity, influence the probability of the initiating event, thereby determining the position of the initial point on the F(N)-N back-cumulative risk curve. In contrast, the fire scenario affects the entire event tree, shaping both the number of potential fatalities and the magnitude of the overall damage.

The event that occurred in the San Benedetto tunnel constitutes a representative multi-hazard scenario, in which a single natural trigger, seismic excitation, activated a cascade of interdependent events with significant compound effects. The structural damage detected in the central section of the tunnel, particularly at approximately 920 meters from the western portal, increased the likelihood of traffic-related incidents, including collisions involving heavy vehicles and subsequent fire outbreaks. This case highlights the critical importance of integrating seismic hazard assessment with traffic flow modeling and fire dynamics simulations, in order to properly evaluate risk acceptability in accordance with the ALARP (As Low As Reasonably Practicable) principle.

To support such evaluations, the use of coupled simulation tools, such as the Fire Dynamics Simulator (FDS) for modeling fire propagation, and performance-based evacuation models, is fundamental. These tools enable a more accurate representation of complex interactions among structural vibrations, tunnel geometry, and user behavior under emergency conditions. In the context of multi-hazard configurations, resilience assessment must address both active safety systems (e.g., mechanical ventilation, fire detection, protected escape routes) and passive protection measures (e.g., fire-resistant linings, structural compartmentalization).

The definition of critical thresholds for the conditional probability of combined hazard scenarios, such as structural damage induced by Peak Ground Acceleration (PGA) followed by fire ignition, should be informed by historical incident data and supported through the development of hazard-specific fragility curves for tunnel linings and associated equipment. In this context, Bayesian probabilistic frameworks offer a robust methodological approach to model interdependent event sequences, allowing for the integration of empirical evidence with numerical simulations.

This case study reinforces the need for proactive maintenance strategies and continuous structural health monitoring, particularly in tunnel sections exposed to high seismicity and characterized by high traffic volumes. The adoption of a comprehensive multi-hazard perspective in tunnel design, operation, and risk governance contributes to more realistic risk quantification and significantly enhances both preparedness and response capabilities under critical operating conditions.

4.2 Seismic risk assessment for transportation infrastructures

Bridges and infrastructural systems form the backbone of transportation networks across every country. Their structural integrity and functional reliability are essential for the mobility of people and goods, economic development, and the overall resilience of modern societies. Over time, however, these critical assets are increasingly exposed to a combination of natural hazards, anthropogenic threats, and gradual material degradation. In such a context, understanding and managing the risks associated with infrastructure failure has become a central concern for engineers, planners, and policymakers alike.

Risk assessment provides a structured methodology to anticipate potential failures, evaluate their likelihood, and quantify their consequences. It does not only enhance safety but also supports sustainable asset management and informed decision-making in the face of uncertainty. As such, it has evolved into a multidisciplinary practice that integrates structural engineering, statistical modelling, economics, and public policy (Frangopol and Liu, 2007). Thus, the primary objective of infrastructure risk assessment is to ensure the safety and reliability of existing structures while optimizing the use of available resources. By systematically evaluating the probability of structural failure in conjunction with the potential consequences, risk assessment enables stakeholders to prioritize maintenance efforts, schedule interventions strategically, and justify investments.

Moreover, risk assessment serves as a decision-support tool in broader planning frameworks. It allows authorities to identify vulnerable infrastructure components, assess the impact of disruptive events on transportation networks, and evaluate the cost-effectiveness of mitigation strategies. By shifting the focus from reactive to preventive management, it promotes long-term sustainability and enhances public trust in the safety of critical systems (Ellingwood, 2001).

Commonly risk assessments involve the definitions of the hazards that can hit the structure, and their expected occurrence, the computation of the structural fragility (i.e., the probabilistic behavior of the structure) and finally the associated losses.

Regarding the hazards, bridges are exposed to a wide spectrum of hazards, each presenting unique challenges to structural integrity and performance. According to Deng et al. (2016), natural hazards include seismic events, flooding, landslides, and windstorms (**Figure 4.11**).

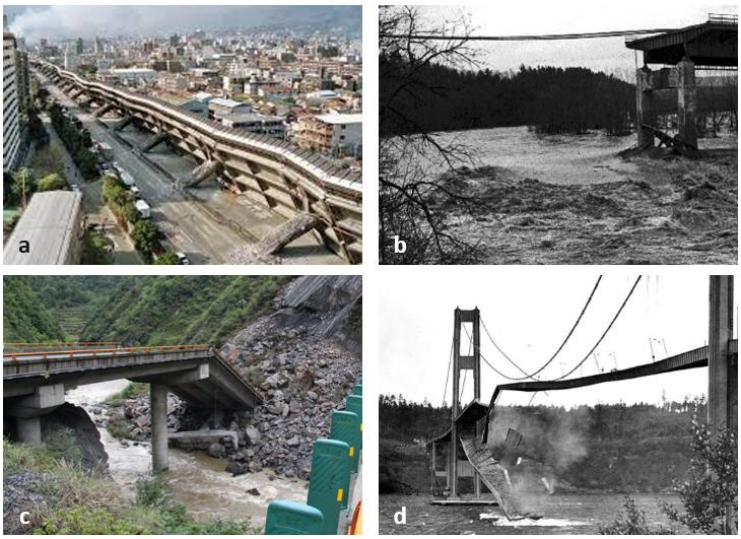

Figure 4.11: Failure due to a) earthquake, b) flooding, c) landslide and d) windstorm (Deng et al., 2016).

Anthropogenic hazards, on the other hand, stem from human activity and may include vehicular collisions, overloading due to increased traffic demand, fire, accidental explosions, or acts of sabotage. These threats may be unpredictable or result from systemic issues such as deferred maintenance or flawed design practices (**Figure 4.12**).

Figure 4.12: Failure due to a) an overloaded truck, b) vessel impact (Deng et al., 2016) and c) explosion.

In addition, all bridges are subject to time-dependent deterioration. Material degradation processes such as corrosion of steel elements, fatigue cracking, concrete spalling, and chemical attacks like alkali-silica reaction can silently compromise structural integrity. In particular, this chapter will focus on the state of the art regarding seismic risk for bridges.

Nowadays, the Probabilistic Seismic Hazard Analysis (Cornell, 1968; McGuire, 1995; Baker et al., 2021) is the most diffused approach for computing the hazard curve that associates to each level of ground motion intensity measure im the corresponding annual exceedance rate λ_{im} for a specific site of interest. The PSHA integral is given by:

$$\lambda(IM > im) = \sum_{j=1}^{n_{sources}} \lambda(EQ_j) \left(\int_R \int_M P(IM > im|m,r) f_{M,R}(m,r) dm dr \right)_j \tag{4.3}$$

where $\lambda(IM > im)$ is the occurrence rate of ground motions with IM grater than im, $P(IM > im|m,r)$ comes from the ground motion model (GMM), $f_{M,R}(m,r)$ is the joint probability distribution of the magnitude M and the site-to-source distance R and finally $\lambda(EQ_j)$ is the rate of earthquakes on source j (**Figure 4.13**).

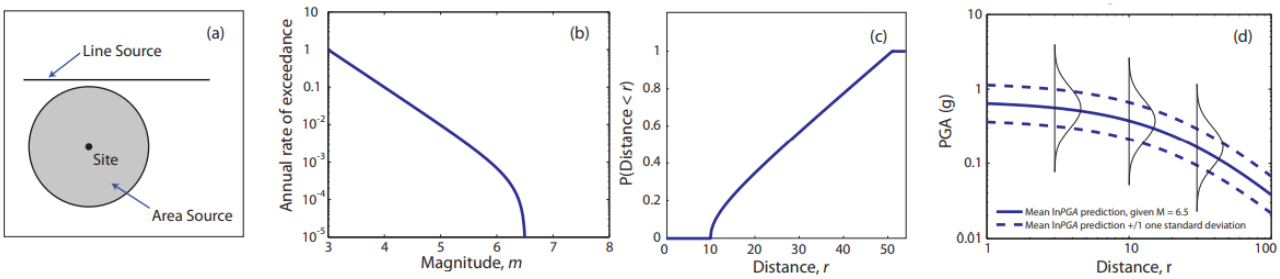

Figure 4.13: Basics of PSHA: a) earthquake zones, b) distribution of earthquake magnitudes, c) distribution of source-to-site distances, d) distribution of ground motion intensity (Baker et al., 2021).

Usually the Peak Ground Acceleration (PGA) is adopted as intensity measure, but depending on the specific case, many other quantities, as the spectral acceleration can be adopted. **Figure 4.14** shows the results of Eq. (4.3).

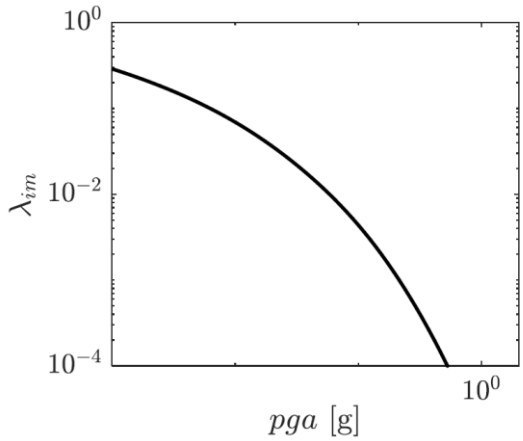

Figure 4.14: Example of hazard curve.

The probabilistic structural behaviour of a bridge is commonly summarized by fragility functions that represent the probability of reaching and exceeding a specific damage state for a given value of intensity measure im. Many approaches are available in scientific literature for computing the structural fragility, such as field observations of damage, static structural analyses, or expert judgment (Kim and Shinozuka, 2004; Calvi et al., 2006; Villaverde, 2007; Porter et al. 2007; Shafei et al., 2011; Baker 2015). Nowadays, current engineering practice relies on the execution of a series of non-linear time-history analysis (NLTHAs) that are needed to withdraw a series of samples of the structural behaviour of the investigated structure. Commonly, the structural response is recorded in terms of a suitable engineering demand parameter (EDP, e.g. inter-storey drift ratio for framed buildings or top-displacement for cantilever structures) that can be assumed to be a relevant metric for quantifying the damage to structural (and/or non-structural) elements. Once numerical analyses are performed, EDP and IM values are coupled for deriving fragility functions. Even in this case, different methodologies are available in scientific literature: one common approach is *incremental dynamic analysis* (IDA), where a set of accelerograms are scaled in order to find the IM level at which each ground motion causes collapse (Vamvatsikos and Cornell, 2002). A second approach is the so-called multi-stripes analysis (Jalayer, 2003). Finally, also the *cloud analysis* represents a widely diffused method for the derivation of fragility functions, based on a regression between n values of $[edp_1, edp_2 \dots edp_n]$ and $[im_1, im_2 \dots im_n]$. For a better description of the progressive damage, usually fragility functions for different damage states are computed. **Figure 4.15**: shows an example of cloud analysis and associated fragility curves.

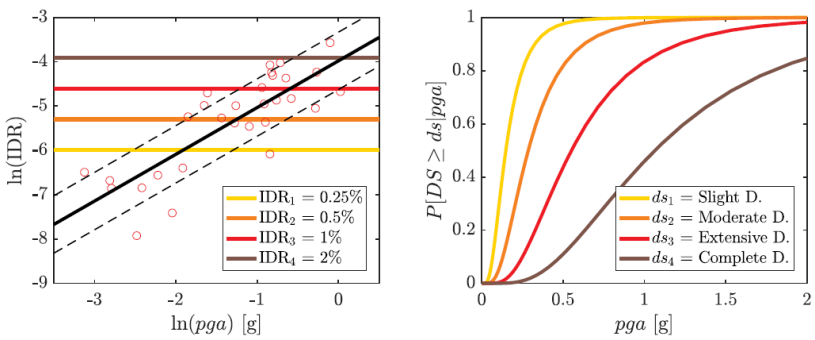

Figure 4.15: Example fragility curves computed with the cloud analysis.

A first seismic risk metric associated to a specific structure is the so-called *failure rate*. This value is computed by combining the hazard curve, that quantifies the likelihood of different im values, with the fragility function:

$$\lambda(F) = \int_0^\infty P(F|IM = x) \left|\frac{d\lambda(IM>x)}{dx}\right| dx \tag{4.4}$$

Usually, many uncertainty sources are involved in both the seismic hazard and structural vulnerability; the effect of epistemic and aleatoric uncertainties on the seismic reliability is shown in Zanini and Hofer (2019) and Hofer et al. (2023).

Then, a potential consequence C (or loss) can be associated to each damage state, whose probability is retrieved directly from the fragility curves. Thus, the mean consequence, conditioned on a specific level of IM, can be computed as

$$E[C|IM = x] = \sum_{i=0}^{n} E[C|DS = ds_i]P(DS = ds_i|IM = x) \tag{4.5}$$

where C may represent a direct consequence of seismic damage, such as reconstruction costs (usually expressed in terms of loss ratio, i.e., the cost to repair a structure hit by a quake divided by the total replacement cost) or as an indirect consequence, commonly expressed by specific traffic indicators (e.g., drivers' total delay) in the case of analysis of transport networks (Zhou et al., 2011). Finally, it is possible to compute the so-called *loss exceedance curve* that provides the rate of exceeding various levels of losses. A particularly meaningful indicator, especially for insurance purposes, is the so called average annual loss (AAL) that represents the yearly expected amount of loss, and can be computed as

$$E[C] = \int_0^{\infty} E(C|IM = x)|d\lambda(IM > x)| \tag{4.6}$$

This summary indicator is also used for cost-benefit analysis.

When dealing with a spatially distributed systems, usually synthetic shaking scenarios need to be generated for computing IM values at multiple locations and thus the related losses and consequences on the network, following a Monte Carlo approach. Once component consequences have been simulated, they can be used to evaluate an aggregate system consequence, either a summation of component consequences (Grossi et al., 2005; Sokolov and Wezel, 2011), or some other more complex relationships. An example of this latter case is the computation of impacts to an infrastructure system, where component damage at specific locations relates to the ability of the system to provide services (Lee and Kiremidjan, 2007; Baker et al., 2021). Finally, a risk analysis considering aging in infrastructure can be found in Zanini et al. (2017).

5. Deterministic and dynamic models for the Interrelated NaTech Vulnerability with the events of interest/Potential multi-hazard scenarios for industrial assets

5.1 Methodological procedure to characterize industrial vulnerabilities facing NaTech events

A methodological procedure was designed to model functional vulnerabilities to multiple hazards on industrial critical infrastructures (ICIs) (**Figure 5.1**).

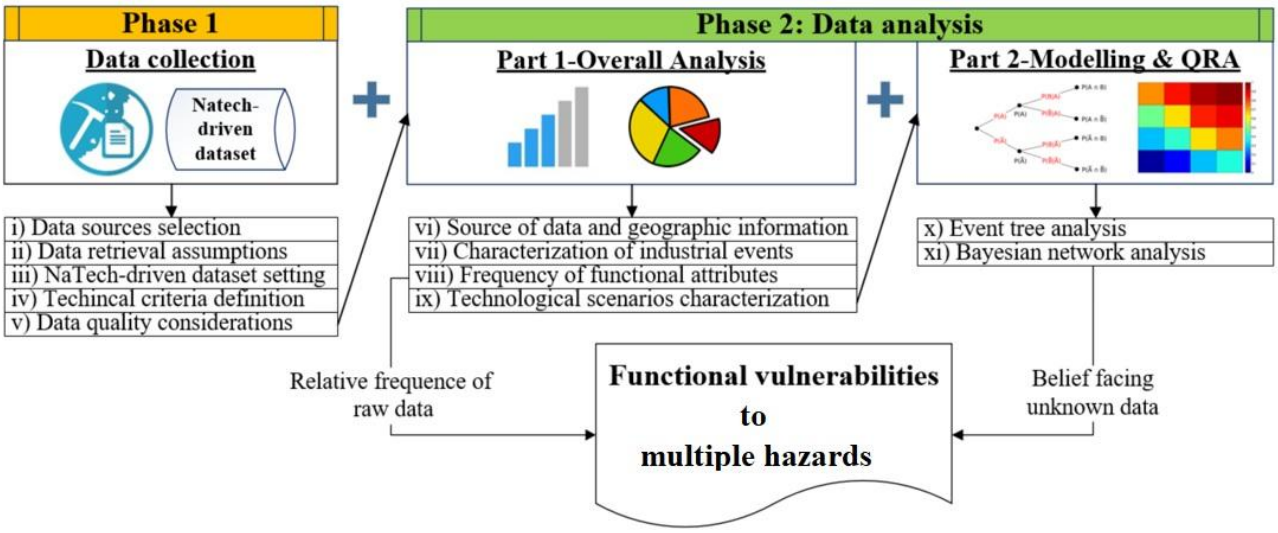

Figure 5.1: Two-phase procedure to model functional vulnerabilities to multiple hazards in the process industry. Source: modified from Castro Rodriguez et al. (2025).

Phase 1–Data collection

Phase 1 involves i) the source selection, ii) the data retrieval assumptions, iii) the NaTech-driven dataset setting, iv) the technical criteria definition for the variables of interest, and finally, v) the data quality considerations. Phase 1 constitutes the cornerstone of the methodological procedure, and it is focused on data collection from open sources industrial accident databases, about historical records that happened within the process industry, caused directly or indirectly by the natural hazards of concern. A brief description of step i to step v can be found below:

i) Data sources selection

For the compilation of the raw data, several currently available open-source databases on industrial accidents were consulted (ARIA, eMARS, TAD IChemE, eNATECH, NRC, CSB). An overall description of each database used and the data characteristics that they contain can be found in Castro Rodriguez et al. (2024).

ii) Data retrieval assumptions

To identify vulnerabilities to different hazardous events which can impact the industrial infrastructures, then, the following necessary inclusion criteria were adopted to consider the records:

- The type of industrial event should be classified in one of the four categories according to the definitions in Castro Rodriguez et al. (2024): 1) Accident, 2) Incident, 3) Loss of containment, 4) Near miss,
- To ensure relevant criteria from the chemical and process industry, the registered technological events must have occurred in the process industry or eventually in an industrial sector of interest that handles a significant number of hazardous substances. They should be clustered within the eight industrial macro-sectors used by Ricci et al. (2021), which resulted in a slightly modified from the original proposal (Casson Moreno et al., 2018). They are: 1) Chemical and petrochemical, 2) Storage and warehousing, 3) Power production, 4) Bioprocesses, 5) Water treatment, 6) Transportation, 7) Pipeline, 8) Manufacturing.

- The technological event should involve the release (or the potential release) of hazardous substances, triggered by the hazard of concern, using definitions for these specific hazards.

Once the necessary inclusion criteria are established, the data retrieval process started by querying open-source databases with single keywords related to the hazard under consideration, in line with prior research (Krausmann et al., 2011; Renni et al., 2010; Ricci et al., 2021). Retrieving data involves an iterative approach for each consulted database, sometimes needing translation of keywords into the database original languages

Subsequently, the most time-consuming phase involves meticulously reviewing each retrieved record summary, to verify remaining criteria, ensuring relevance to the process industry. Particular attention was given to avoiding duplicate entries across databases. To address this, a double-check process was implemented post-data collection, filtering records by date and location. In those cases where the couple date─location appears in more than one case, it is necessary to control the kind of plant, the address, and/or the commercial name of the facility to ensure a unique registration, avoiding duplications or treating events in neighboring facilities as such. In cases of events duplicated, preference is given to the most precise and detailed record complementing the information.

iii) NaTech-driven dataset setting

Once the assumptions are clear for the scope of the research, then the data retrieved from the different open-source industrial-accident databases previously described is structured in a new general dataset structuring all the technical criteria.

iv) Technical criteria definition for the variables of interest

According to the available information in open-source industrial-accident databases, there are labels to classify the retrieved information which are mainly categorical. Many labels are free entrance such as record code ID, date, continent, country, location/city, and substances involved, which correspond to specific descriptive data of the associated record. On the other hand, some labels such as the above-described assumptions (macro-sectors and type of industrial events), or other variables of interest for the classification, require technical definitions for its categorization. The diverse criteria adopted in each case can be consulted in Castro Rodriguez et al. (2024) and Vitale et al. (2024).

v) Data quality considerations

Often, the information in the open-source industrial-accident databases is not homogeneous or not precise in describing the events, the failure mode, the structural damage, the presence of barriers, or the severity of the final scenario. Consequently, the possibility of learning from historical records is limited by the quality of the data which often is uncertain. Aiming to face this uncertainty by implementing further advanced methods, during the data collection phase, some considerations were made. For instance, the subcategory "others" was inserted for records in which the information available does not match the predefined technical criteria. In addition, when the lack of information did not allow for the classification of a category, the "unknown" subcategory was added for all labels in the NaTech database, aiming to underscore the information uncertainty

Phase 2–Data analysis

Moving to Phase 2, the data analysis is split into two parts. Phase 2–Part 1 is presented as an overall analysis, addressing qualitative and semiquantitative risk analysis. Part 1 addresses the records from diverse points of view, providing a clearer characterization of the historical records, through a combination of tabular and graphical analyses which were undertaken to explore the diverse labels and subcategories such as vi) source of data and geographic information, vii) characterization of industrial events, viii) determination of frequency for categories of functional attributes to the natural hazard of concern, and ix) technological scenarios characterization. On the other hand, Phase 2–Part 2 introduces modelling techniques in line with the quantitative risk assessment (QRA) techniques. For the sake of clarity, step x) stresses the logic pathways of the NaTech events through event tree analysis, while step xi) analyzes the hidden signals that denote conditional causality and frequency among the technological scenarios triggered, and their complex relationships with functional attributes within the dataset. It is important to remark that this last step is open to any inclusion of quantitative risk assessment tools that improve data learning, and uncertainty reduction.

Phase 2 -Part 1 Overall analysis

In a nutshell, step vi (source of data and geographic information) identifies the origin of records concerning the original data source and its geographical provenance. This step clarifies elements of the data, given the known heterogeneity in the information recorded depending on the different origins of the sources. Subsequently, step vii (characterization of industrial events) involves analyzing together the collected information to identify crucial aspects such as trend, variability, and seasonality as well as the identification of type of industrial events.

After that, step viii (Frequency of functional attributes) involves analyzing the frequency of the different functional attributes within the general dataset to have a first estimation of the vulnerability of industrial critical infrastructure to natural hazards. Then, technological scenarios are characterized in step ix. These scenarios are tailored to subsets within the general dataset with enough information to ensure the final scenario association with relevant functional attributes. Furthermore, the analysis about the associated losses is carried out based on the available information of the selected subset of data.

Phase 2 –Part 2 Modelling

x) Event tree analysis

After the characterization of technological scenarios, it is necessary to understand the complexity of the logic events pathways from the triggering natural factor and branches that lead to increasingly specific potential consequences. To this aim, step **Errore. L'origine riferimento non è stata trovata.** implements the event tree analysis which presented several applications for natural hazard modeling (Molinari and Handmer, 2011; Newhall and Hoblitt, 2002; Renni et al., 2010). Furthermore, the inclusion of the new paradigm in the pathway –direct or indirect– of NaTech (Misuri and Cozzani, 2021), associated with both the different lightning sources of damage and the structural damages classifications, between the initiating factor and the final scenarios, undoubtedly strengthens the identification of infrastructural vulnerabilities. For the sake of precision, this technique may be tailored to refined datasets, which means subsets of interest derived from previous steps or with more accurate information within the general dataset.

xi) Bayesian network analysis

While event tree analysis effectively identifies and organizes possible outcomes, it has limitations in capturing the interdependence between events, updating probabilities with new information, and managing the uncertainty inherent in NaTech events. Bayesian networks (BNs), which have been shown to work well in NaTech analysis (Cheng and Luo, 2021; Hao et al., 2023; Khakzad and Van Gelder, 2018; Moriguchi et al., 2023), are a great way to solve these problems because they allow for predictive modelling and probabilistic reasoning when there is uncertainty.

BNs are particularly well-suited to handle uncertainty, a common challenge in NaTech risk assessment related to the data quality, as previously discussed. Using BNs in step xi, after event tree analysis (Bearfield and Marsh, 2005), improves the modelling process by offering a better look at the functional vulnerability that is controlled by how attributes depend on each other in certain situations. Moreover, more variables can be added as BNs are flexible, allowing to scale the model by accommodating more variables and integrating various data types (numerical or categorical) (Margaritis, 2003), typical of NaTech-driven datasets where interactions are often non-linear and involve multiple expert categorizations.

Specifically, the Necessary Path Condition (NPC) algorithm was implemented to define the structural framework in the BNs model (Steck and Tresp, 2000). The NPC algorithm can estimate parameters even when the data is missing or incomplete. This is particularly useful for the research scope, given the uncertainty that comes with data from open-source databases for industrial accidents. The model parameterization was achieved through the utilization of the Expectation-Maximization (EM) algorithm (Lauritzen, 1995). The NPC is based on the Peter-Clark (PC) algorithm (Strobl, 2021), which uses conditional independent tests to find the structure of the model. The Bayesian Information Criterion (BIC) was also used to show the trade-off between model complexity and how well the model fits the data when BN models were expanded from reduced datasets to larger ones; a higher BIC value is better (Neath and Cavanaugh, 2012). Comprehensive details of the algorithms here mentioned can be found in the specific literature (Kjærulff and Madsen, 2013), while the professional software Hugin 9.3 was used to implement them (Hugin Expert A/S, 2023).

5.1.1 Case 1: Past lightning-triggered NaTech events in process industry

As the pilot case to implement this procedure, NaTech triggered by the lightning factor in the process industry was analyzed since this phenomenon presents a critical trade-off between frequency (Ricci et al., 2021) and catastrophic consequences in general (Krausmann et al., 2011; Renni et al., 2010).

Since the research scope of Case 1 is focused on identifying vulnerabilities against lightning strokes able to trigger a NaTech event within the process industry, then, the technological event should involve the release (or the potential release) of hazardous substances, triggered by a lightning impact, which is defined as a single electrical discharge of atmospheric origin between cloud and earth consisting of one or more strokes (British Standards Institution, 2017). In this instance, keywords such as "lightning," "thunderstorm," or "flash" were employed to meet the initial criteria.

The main result of the data collection phase was a new dataset of 689 records, saved in a public repository (Castro Rodriguez et al., 2023), including records that span until 2022. The dataset architecture followed the structure shown in **Figure 5.2**.

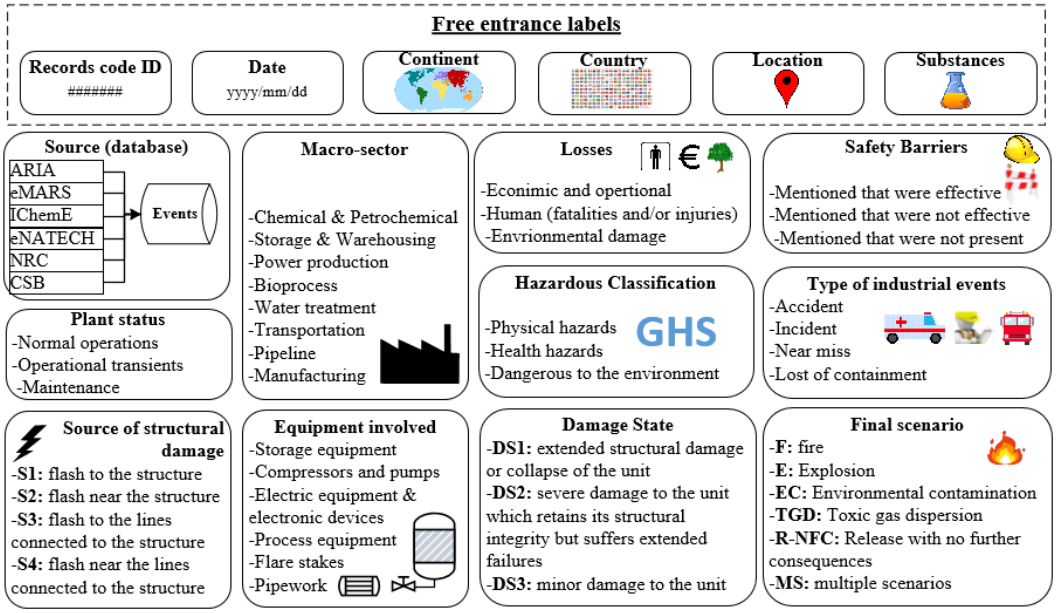

Figure 5.2: Lightning-triggered NaTech-driven dataset structure. Castro Rodriguez et al. (2024).

The principal results of Phase 2–Part 1 are discussed below:

Errore. L'origine riferimento non è stata trovata. **5.3** provides a representation of the record frequency over the years, illustrating the life span of events.

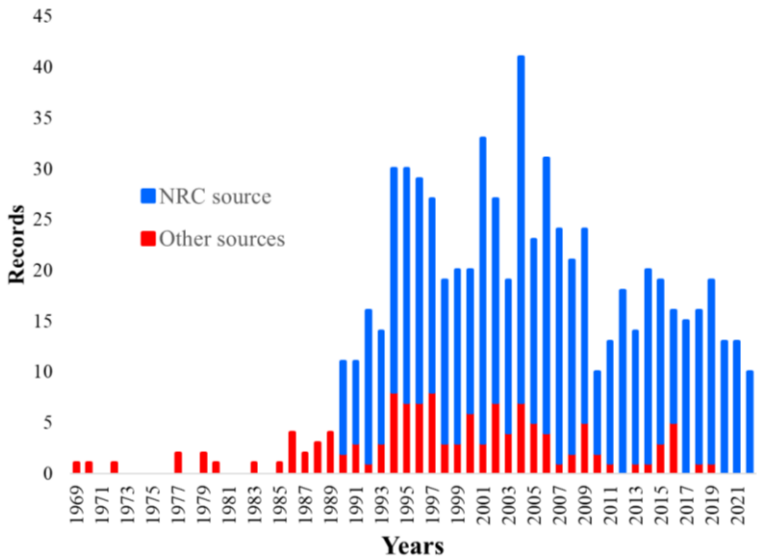

Figure 5.3: Lifespan of the retrieved records.

The study focuses on industrial events, with NRC (National Response Center) managed by the U.S. Coast Guard, being the primary source of observations. The data illustrated by the red bars aligns with a span from the mid-1960s to the 1970s, highlighting the growth of the European process industry (Jain et al., 2017). On the other hand, blue bars started in 1990 which corresponds with the date that NRC started to record events.

Figure 5.4 clearly illustrates the categories for the event classification.

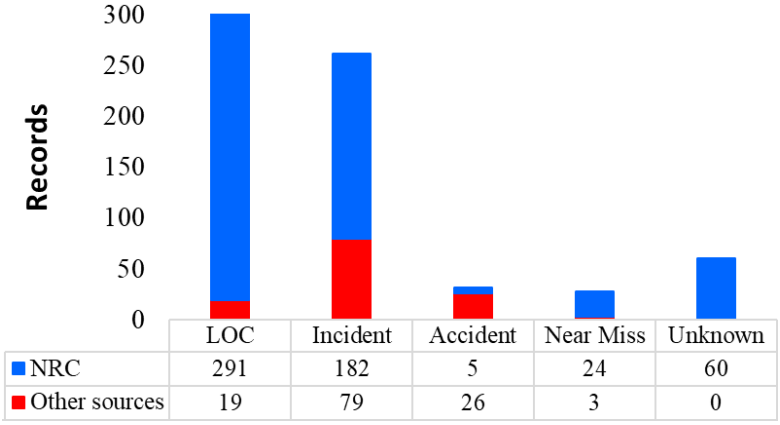

Figure 5.4: Frequency for the type of industrial event.

The majority of NaTech events reported across all sources are incident and loss of containment (LOC) events, accounting for over 80% of the total. Accidents and near misses make up a smaller proportion, with only 4% of the total. Most events occur during normal plant operations. significant 92% of total events lack reference to safety barriers, with only 40% of events from other sources addressing these issues. The category labeled "unknown" comprises 60 records from the NRC source, suggesting a NaTech scenario triggered by a lightning strike in the process industry. However, the available information is insufficient to identify key details, such as fatalities, injuries, material releases, or hazardous situations without notable consequences.
More details about the implementation of data analysis for the lightning case (Part 1 and Part 2) can be found in previous work (Castro Rodriguez et al., 2024). Further research is highly encouraged to implement this procedure and focus on other natural factors.
Figure 5.5 illustrates the vulnerability of the different industrial macro-sectors to lightning-triggered NaTech.

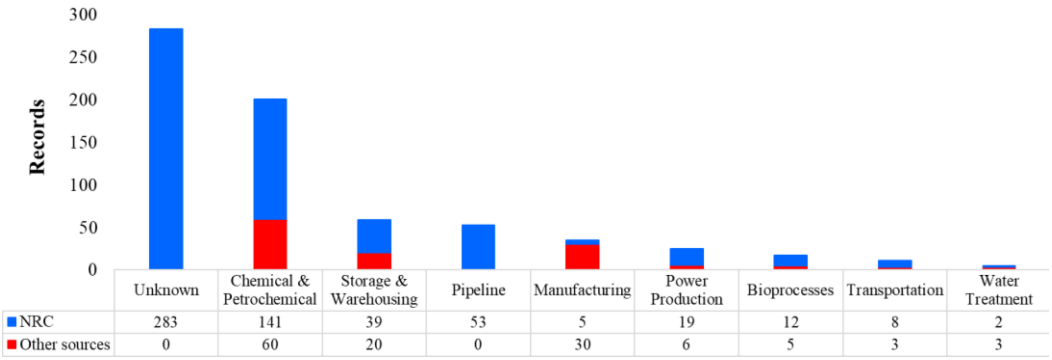

Figure 5.5: Bar graph for the different industrial macro-sectors impacted by lightning strikes.

Setting aside the fact that a significant portion of the events, 41% (283 events), were categorized as "unknown" due to the information gap in the NRC database, highly valuable insights into the vulnerability of various industrial macro-sectors could be gleaned from the remaining 406 events. The "chemical and petrochemical" sector was the most vulnerable to lightning impacts, accounting for 50% of known records. Additionally, the "storage and warehousing" contributed 15%, while pipelines and manufacturing sectors made up 13% and 9% respectively. However, disparities in reported events between NRC and other sources can be appreciated in **Figure 5.5** for all the macro-sectors.
Figure 5.6 displays a set of eight bars representing six distinct categories of industrial items together with the categories of other and unknown.
The data shows a pattern with storage equipment and electric and electronic devices accounting for 62% of all data (278 and 150 records respectively). The pipework category ranks next with 59 recorded events. The remaining categories show heterogeneity in event proportions between NRC and other source components. Compressors and pumps present 40 to 42 records primarily from the NRC source, while the flare stakes category reports 4 to 5 events from other sources.

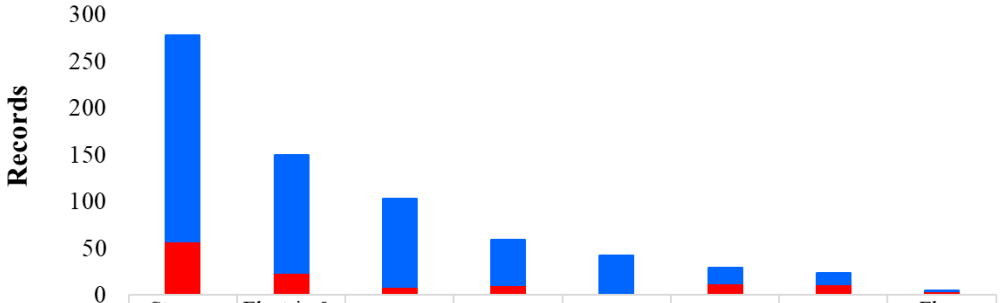

	Storage equipment	Electric & Electronic	Unknown	Pipework	Machinery	Process	Others	Flare Stakes
NRC	221	127	95	49	40	17	12	1
Other sources	57	23	8	10	2	12	11	4

Figure 5.6: Vulnerable industrial equipment to lightning strikes.

Figure 5.7 associates the distribution of technological scenarios within the principal hazardous categories of physical hazards, health hazards, and dangers to the environment according to the Global Harmonized System (GHS) using a reduced subset containing the 127 observations from other sources.

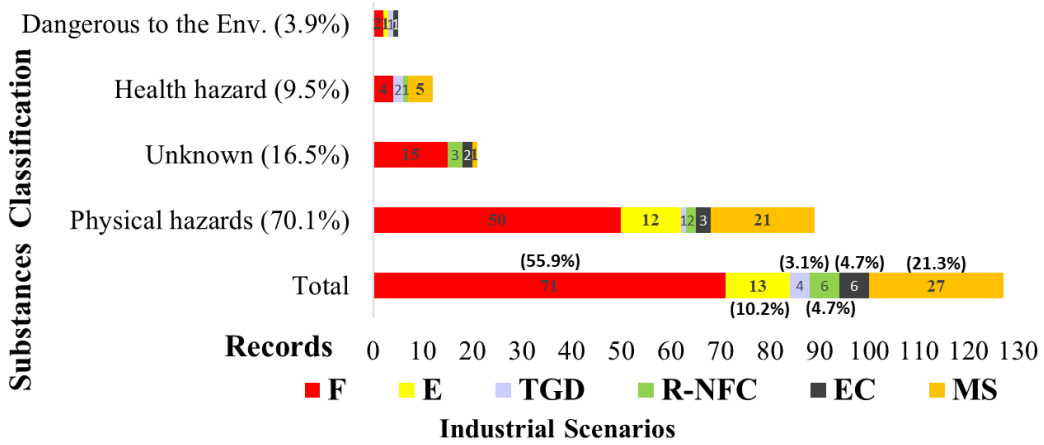

Figure 5.7: Technological scenarios triggered by lightning vs. classification of substances involved. [F, fire; E, explosion; TGD, dispersion of toxic gases; R-NFC, release without further consequences; EC, environmental contamination; MS, multiple scenario]

The study reveals a significant prevalence of red bars across all substance categories, with fire accounting for 56% of total records. Multiple scenarios followed, with ignition being a common theme. The explosion category was the third most frequent, accounting for 10% of records. The physical hazards category, accounting for 70% of total triggered scenarios, is prominent, with 92% attributed to flammable substances. The unknown substances category, representing 16.5%, is the second most observed, with a dominance of fire scenarios.
Additional overall analysis such as the variability of the records concerning the source of data, the seasonality of the events, and the categories of involved losses, as well as deeper discussions of the analysis here presented, can be found in Castro Rodriguez et al. (2024).
The principal results of Phase 2–Part 2 are discussed below:
A refined dataset of 107 records corresponding just to those scenarios finalized with ignition were considered for modelling the event tree. It was built including the labels "sources of structural damage" (Si) and "damage state" (DSj). These labels serve as intermediate attributes from the initiating event lightning strikes (LS) to the final ignition scenarios (ISk).
Figure 5.8 shows the event tree for the sequence (LS)→ (Si)→(DSj)→(ISk), from the initiating event, passing through both intermedial events, the "i" sources of damage (S1, S2, S3, S4, and S? ─unknown records), and the "j" damage states (DS1, DS2, and DS3), finally leading to the considered "k" ignition scenarios (F, E, and MS). The probabilities estimated for the considered events within the refined dataset are shown in the connecting arrows of the event tree. Each branch of the tree represents a distinct sequence of events that could occur.

Table 5.1 offers the probabilities from the even tree analysis, for the different ignition scenarios pathways, focusing on the damage states or the sources of damage. Probabilities hereinafter are rounded by 10^{-2} which may result in a sum that does not exactly equal one.

Table 5.1 - Probabilities from event tree analysis

Labels	Category	F	E	MS
Damage State	DS1	0.15	0.08	0.17
	DS2	0.29	0.03	0.06
	DS3	0.21	0	0.01
Source of Damage	S1	0.22	0.02	0.12
	S2	0.02	0	0.01
	S3	0.05	0.02	0.01
	S4	0.01	0	0
	Unknown	0.35	0.07	0.1

The study reveals that the S1 pathway is the most common source of structural damage, accounting for 36% of occurrences where lightning directly strikes industrial assets. Indirect pathways make up 12% of the dataset but disregarding these could trigger severe consequences. 52% of the time, the source of structural damage cannot be classified due to uncertainty. The predominant scenarios involve fire, with categories S1 and Unknown contributing most significantly.

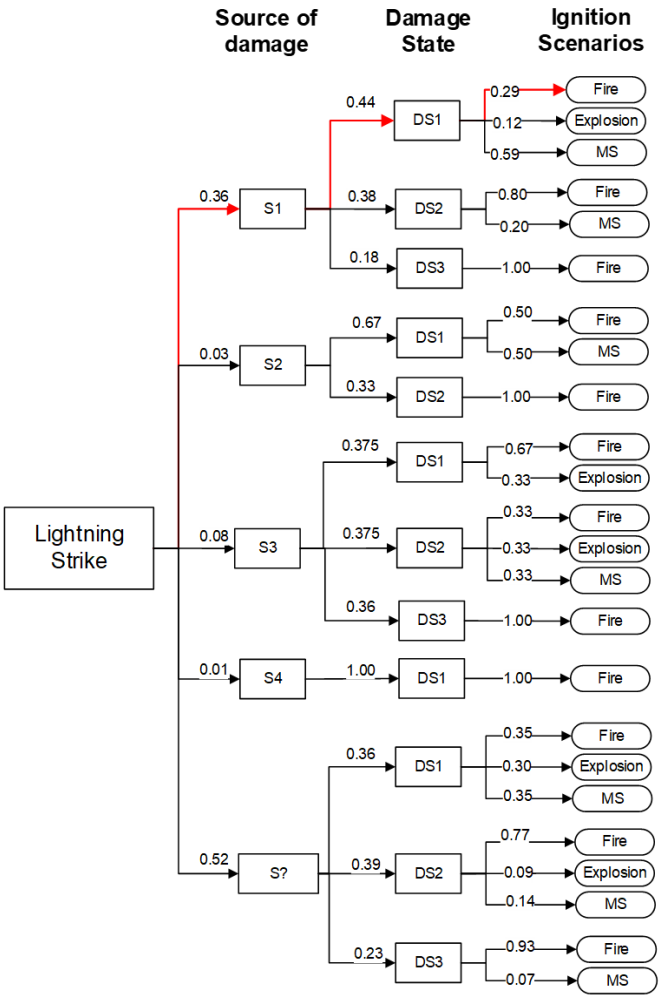

Figure 5.8: Event tree for the records reporting ignition scenarios.

The damage state is balanced across three categories: unit collapse (DS1), severe unit damage (DS2), and minor damage (DS3). The damage state is reasonably balanced across three categories of final scenarios. Specifically,

unit collapse (DS1) accounts for 40%, severe unit damage (DS2) comprises 38%, and minor damage (DS3) represents 22%. Moreover, from **Figure 5.8** it can be elucidated that S1 is responsible for over 70% of collapses and severe damage to industrial units (DS1 + DS2).
Additional passages about how calculate the probabilities in each branch and further discussions from the event tree analysis can be found in Castro Rodriguez et al. (2024).
The event tree in **Figure 5.8** was mapped into the Bayesian network shown in **Figure 5.9a** and further enhanced to the structure in **Figure 5.9b** adding more variables. The direction of the arrows determines the causal relationship between the nodes.

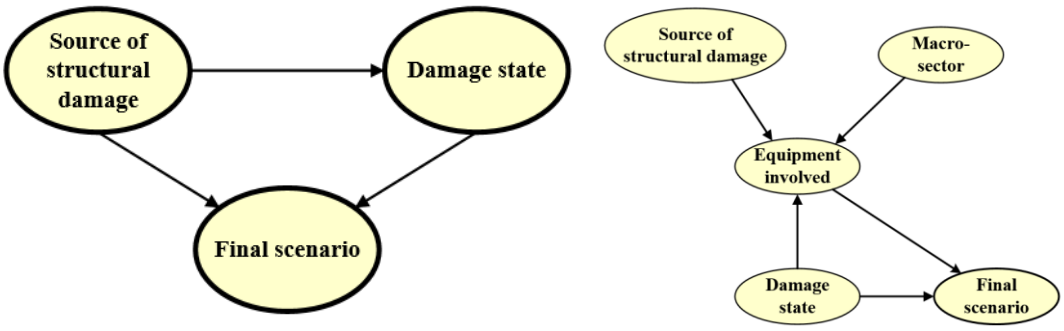

a) b)

Figure 5.9: a) Bayesian Network structure for the ignition scenarios in the refined dataset, mapped from the event tree. b) Bayesian Network model learned with NPC algorithm with a level of significance of 10%.

First, conditional probabilities for each node of the model were calculated. Second, using the same refined dataset, the conditional probabilities were recalculated by applying the NPC algorithm, treating the "unknown" categories within the "source of structural damage" as missing values. Third, this algorithm to cope with the uncertainty was iteratively applied to the extended dataset of 689 records. The conditional probability tables (CPT), comprising both the refined and the extended dataset, are presented in **Table 5.2**, including the Bayesian Information Criterion (BIC) corresponding in any case.

Table 5.2 - CPTs for the ignition scenarios given "damage states" and "source of damages" for a) refined dataset including S?; b) refined dataset treating uncertainty; c) extended NaTech-driven dataset treating uncertainty.

Records in the dataset (BIC)		a) 107(-396)			b) 107 (-303)			c) 689 (-665)		
Labels	**Category**	**F**	**E**	**MS**	**F**	**E**	**MS**	**F**	**E**	**MS**
Damage state (DSj)	**DS1**	0.35	0.23	0.42	0.35	0.23	0.42	0.32	0.24	0.44
	DS2	0.76	0.07	0.17	0.76	0.07	0.17	0.76	0.02	0.20
	DS3	0.96	0	0.04	0.96	0	0.04	0.90	0.02	0.08
Source of structural damage (Si)	**S1**	0.62	0.05	0.33	0.67	0.06	0.27	0.70	0.05	0.25
	S2	0.67	0	0.33	0.64	0	0.36	0.84	0.06	0.1
	S3	0.50	0.38	0.13	0.47	0.42	0.1	0.69	0.24	0.07
	S4	1	0	0	0.93	0	0.06	0.97	0.03	0.01
	S? (unknown)	0.66	0.14	0.20	---------					

The present discussion focuses on the utility of techniques to deal with data uncertainty, rather than delving into the specifics of the most probable conditional scenarios. Starting the discussion on the refined dataset (107 records), for the *DSj* variable, since there was no missing data (unknown), the conditional probabilities remained unchanged before and after addressing the uncertainty. Moving on to the *Si* variable, the conditional probabilities for its categories were numerically consistent with those in the presence of uncertainty. Additionally, the BIC value for the second model was found to demonstrate a better fit in comparison with the initial model, which included unknown values (-396<-303).

Therefore, the expected relative frequencies of NaTech for *Si* after addressing the uncertainties were recalculated: P(S1) = 0.74, P(S2) = 0.06, P(S3) = 0.18, and P(S4) = 0.02. It is evident that the probabilities nearly double in every scenario. In particular, the direct pathway for lightning damage to the structure (S1) goes from 36 to 74% of events, which fits with the subtle insights we talked about earlier and suggests that unknown records might mostly come from direct pathway events.
The outputs of the second model using the refined dataset were compared with those of the model using all the records in the NaTech-driven dataset. As can be observed, the BIC value for the extended model shows a lower fit compared with the reduced dataset (-665<-303). Previous sessions extensively discussed the high number of unknown records related to information reporting in different geographic zones, which may contribute to the extended dataset complexity. The higher complexity of the dataset may need the inclusion of more variables into the model to increase the fit goodness.
Despite the issue with the BIC value, the conditional probabilities for the same categories in both datasets are largely consistent. In general, fire emerges as the most likely scenario across various damage sources. The most notable variations pertain to the increase in fire probability in the extended dataset for S2 and S3, which change from 0.64 to 0.84 for S2 and from 0.47 to 0.69 for S3, respectively. Consequently, variations in E and MS for the same categories take place. The limited occurrences of S4 in the extended NaTech-driven dataset contribute to the certainty associated with S4.
Similarly, the expected relative frequencies for *Si* were recalculated: P(S1) = 0.88, P(S2) = 0.05, P(S3) = 0.06, and P(S4) = 0.01. The direct pathway predominates here even more than for the reduced dataset. On the other hand, within the categories associated with the indirect pathway, S2 and S4 remain almost identical in percentiles for both datasets, while S3 experiences a notable reduction in percentile from 0.18 in the reduced dataset to 0.06 in the extended dataset.
Additional passages about the BNs applied algorithms and further discussions of the results can be found in Castro Rodriguez et al. (2024).

5.1.2 Case 2: Historical analysis of material degradation in the process industry

Another application of the procedure outlined above is in the study of material degradation within the process industry. According to previous research, this phenomenon accounts for 30% of containment losses in process plants, which are one of the main causes of accidents (Casal (2008); Candreva and Houari, 2013).
The database built has a structure in line with the study on lightning, the main differences are in the characteristics of the phenomenon studied. Therefore, there are no categories regarding the source of structural damage and the state of the damage, which strictly concern lightning, but there is the category of the cause that triggered the event. This category is divided into 1) corrosion 2) fatigue 2) vibrations 3) erosion 4) hydrogen embrittlement and 5) multiple causes, when more than one listed cause contributes to the event, with the addition of undefined material degradation for all events in which the type of deterioration occurred is unknown (Davis, 2000; Horrocks et al., 2010; Li et al, 2019). To study the link between material degradation and plant age, the category relating to the years of plant operation was introduced, using the subdivision of Hansler et al. (2022). Then, if the plant has been operating for more than 25 years it is defined as old, between 5 and 25 years as medium, below 5 years as new. Another difference lies in the classification of the equipment involved in the event; in this second case study the classification of the equipment was taken from the study on the ageing of the material by Horrocks et al. (2010): 1) Primary containment system (PCS), 2) Control & mitigation system 3) Electrical, control, and instrumentation (EC&I) and 4) Structures. The category of actions taken post-event has also been added (Marrazzo and Vazzana, 2021), divided into 1) inspections, when after the event the inspection plan is reviewed and improved, 2) treatments, when treatments are implemented on the materials after the event in order to make them less vulnerable to degradation and 3) inspections already taken when the inspection plan was already adequate with a high frequency but the event occurred anyway.
Therefore, case two concerns material degradation and what it generates in the process industry; for this case the keywords used to build the database are " degradation", "fatigue", "corrosion", "erosion", "wear", "embrittlement", "creep", "vibration" and "ageing", combined with words such as "plant", "industry" and "establishment".
The data collection phase returned a new publicly available dataset of 3772 events (Vitale et al., 2025a), with records from 1966 to 2023. The structure of the material degradation database is shown in **Figure 5.10**:

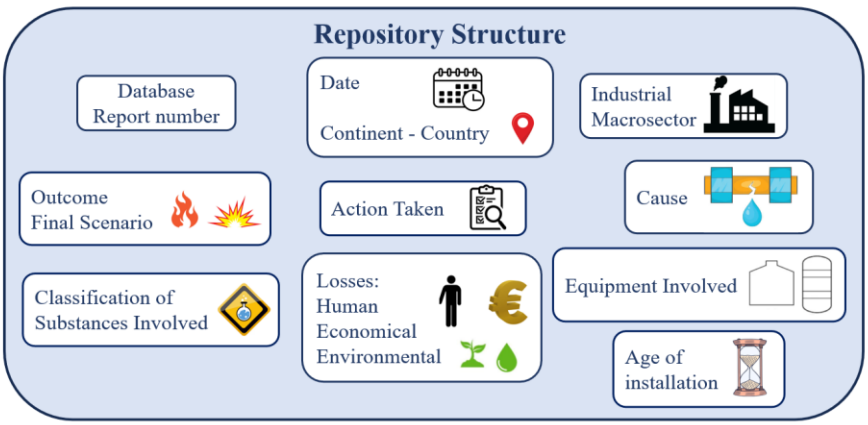

Figure 5.10: Database structure built to collect material degradation events in process industry.

The main results obtained from Phase 2–Part 1 of the analysis are discussed below:
The databases examined in this case study are ARIA, CSB, eMars and NRC. 84.7% of the data comes from the NRC database, 15% from ARIA, 3% from eMars and only 0.3% from CSB. Given the high number of reports from the NRC, the results are presented separately for: 1) NRC and 2) other sources, such as ARIA, CSB and eMars, in line with the case study presented above. It is important to note that the NRC data are events that occurred in North America, while the other sources are 95% of reports from Europe, and only 5% from America. The variation in number of the reports from 1966 to 2023 is shown in **Figure 5.11**:

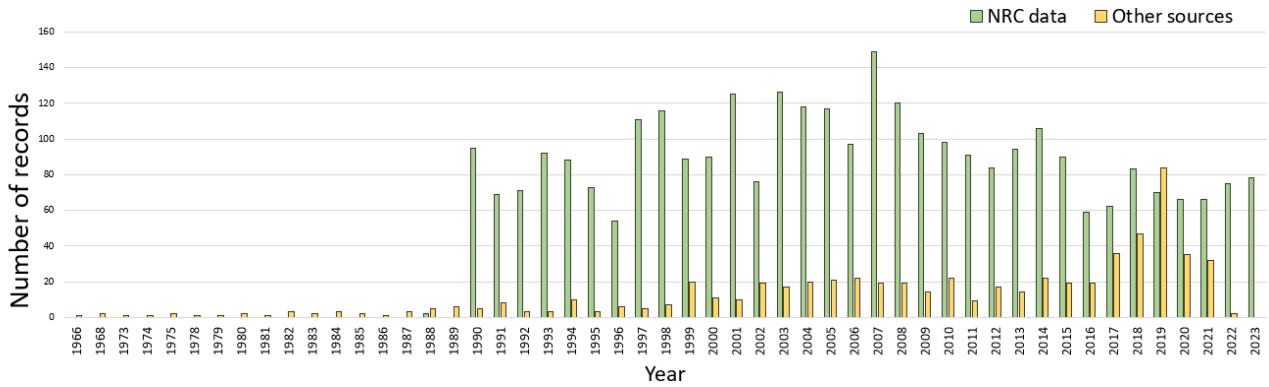

Figure 5.11: Trend over the years in the number of records collected. Green bars indicate the number of reports retrieved from the NRC database, yellow bars from other sources.

From 1966 to 1990, the trend of recorded events remained stable. In terms of NRC data, the trend has generally remained stable, with a slight decrease in incidents between 2016 and 2023. This decline in material degradation incidents in the United States since 2016 can be attributed to factors such as improved regulations, and technological advances. In particular, the Pipeline and Hazardous Materials Safety Administration (PHMSA) has introduced more stringent inspection and maintenance requirements, while the ASME has updated its Boiler and Pressure Vessel Code to better address corrosion (Fehring and Reynolds, 2021; Cazenave et al., 2024). Other sources show an increase since 2000. This increase could be related to the fourth industrial revolution, which facilitated documentation via the Internet, and to the ageing of structures built after World War II. The COVID-19 pandemic in 2020 led to a temporary decrease in ageing-related incidents. Furthermore, guidelines introduced since 2016, such as those of Milazzo and Bragatto (2019), could have further contributed to the reduction of recorded events.
The cause of the analyzed events, that is the type of material degradation that triggered the event, is reported in **Figure 5.12**. Corrosion is the most recurrent mechanism, followed by vibration and fatigue.
The most affected sectors, shown in **Figure 5.13**, are chemical and petrochemical, pipelines and storage and warehousing. In the chemical and petrochemical sectors, process conditions such as temperature and pressure gradients can cause mechanical stress, while pipelines are mainly affected by environmental conditions such as extreme weather conditions.

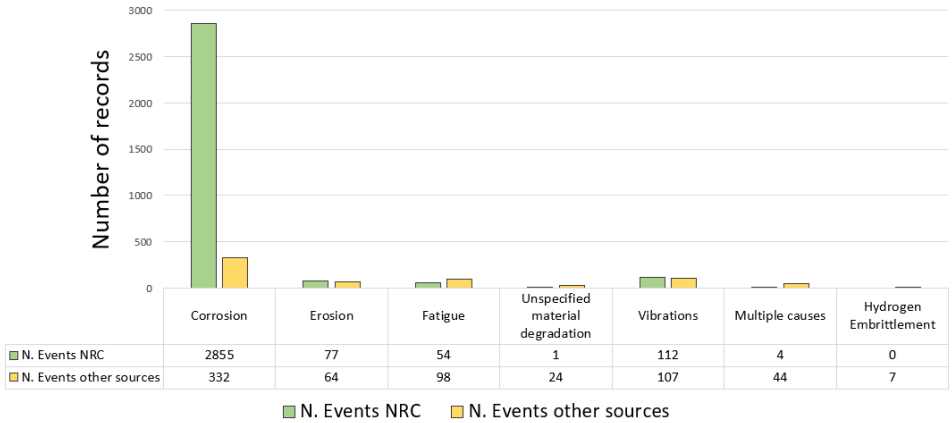

Figure 5.12: Number of events for each category of degradation cause.

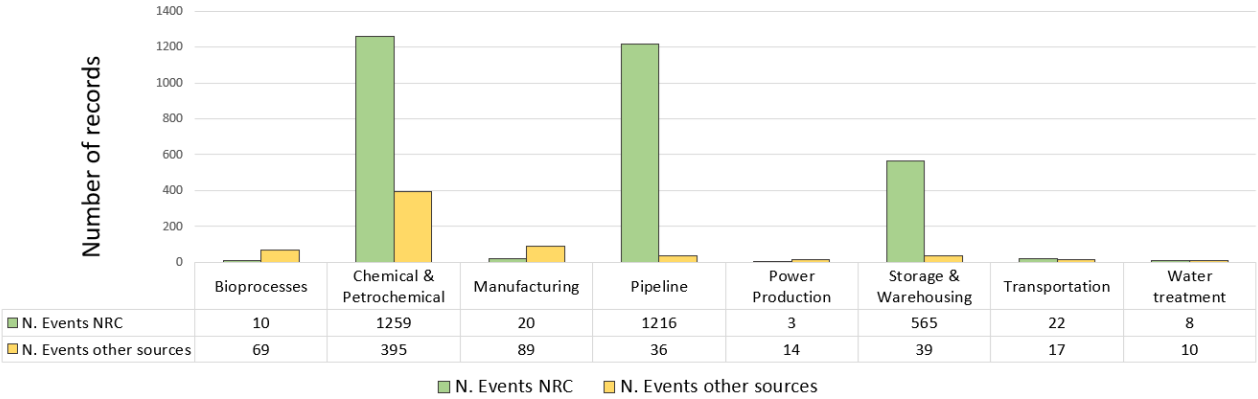

Figure 5.13: Number of events for each macro-sector analyzed.

Trends vary depending on the continent. The analysis shows that in America, pipeline transport is more frequently involved in material degradation events, emerging as the second affected macro-sector, compared to Europe, where the second affected macro-sector is manufacturing.
As regards the equipment most affected, the trend of the reports studied is shown in **Figure 5.14**, and it is evident that the primary containment systems are those most affected by the degradation of the material, probably because they are in contact with aggressive substances and for the operating conditions that can stress the materials.

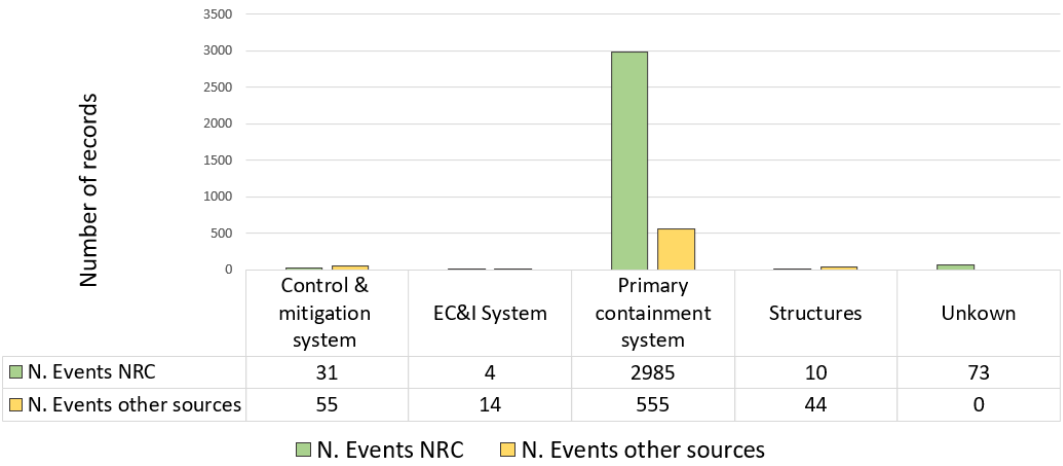

Figure 5.14: Number of events for each macro-sector analyzed.

The frequency of outcomes is illustrated in **Figure 5.15**; it is observed that over 90% of the events result in LOC, while 2% and 3% in accidents and incidents respectively, 1% in cases of near misses.

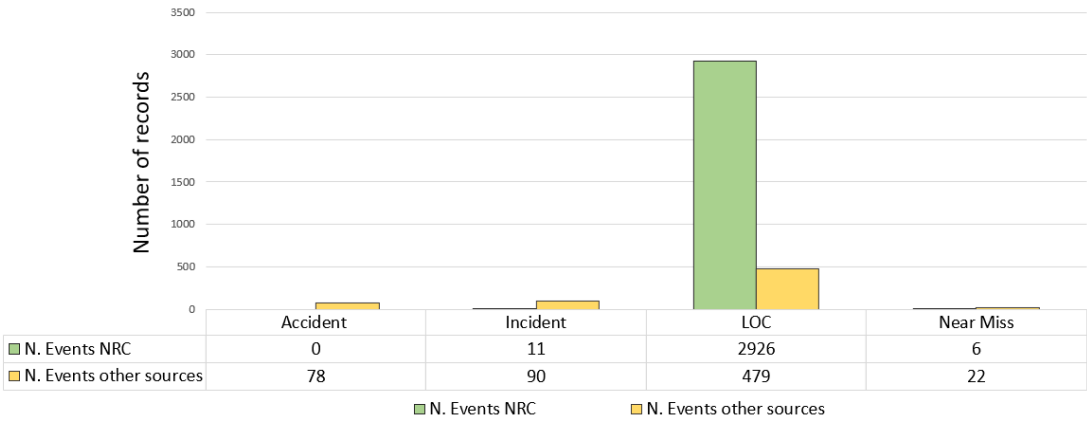

Figure 5.15: Number of events for each outcome.

Figures 5.16a and **5.16b** present the different final scenarios related to failure mechanisms.

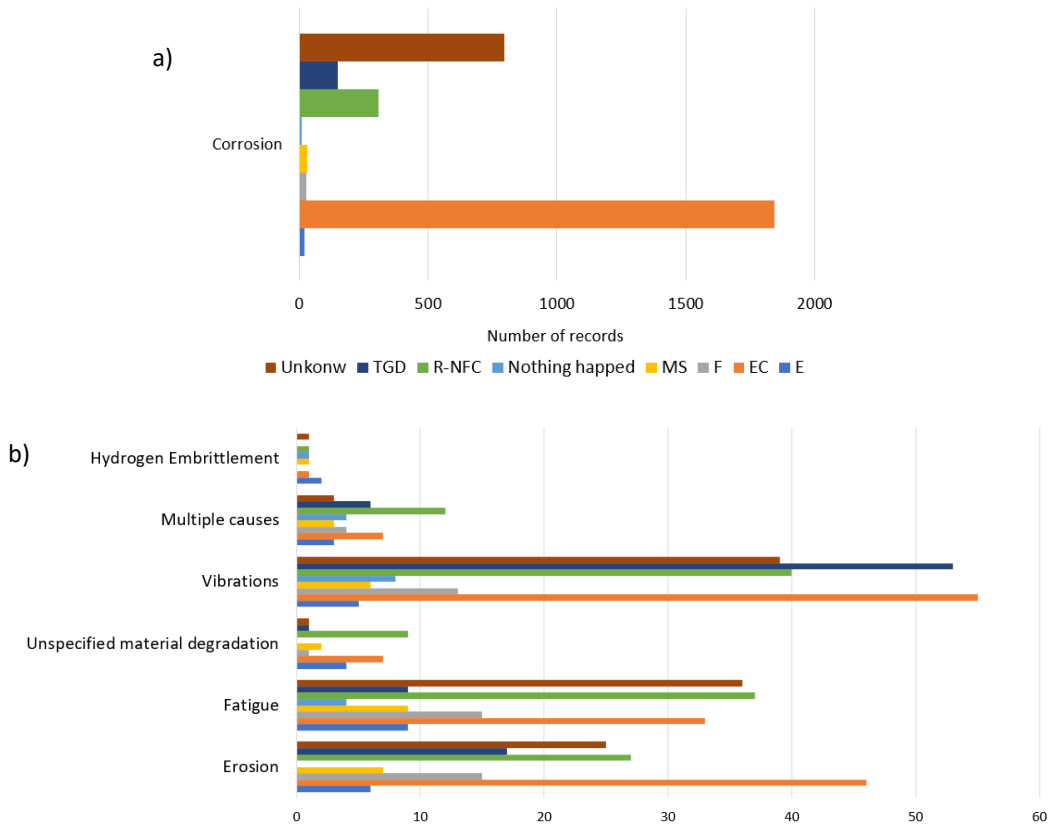

Figure 5.16: Frequency of the final scenario in relation to the degradation mechanism. a) Final scenario for corrosion-triggered events. b) Final scenario for all other deterioration mechanisms. [see Caption of **Figure 5.7** for legenda of industrial scenarios]

The results are shown in two separate figures for the significantly higher number of corrosion events. Separating the data allows for clearer visualization and easier understanding of the results. Corrosion mainly leads to environmental contamination, EC (58%) due to substances that damage materials and accelerate the deterioration of equipment. Second, with 10% of the events, is the release without further consequences (R-NFC), often due to effective management of the release or the presence of non-hazardous substances. This highlights the need for better management, frequent inspections and specific treatments. Vibrations also cause environmental contamination (25%) but are significantly linked to the dispersion of toxic gases, TGD, (24%). Fatigue and

erosion are both mechanical phenomena. Fatigue mainly causes release without significant consequences (24%), while erosion causes the final scenario with the highest frequency, environmental contamination (32%). About 40% of the events leading to fires (F) or explosions (E) involve fatigue and erosion. Hydrogen embrittlement (HE) leads to explosions in 29% of cases but not to fires, indicating that hydrogen release during a structural failure is more likely to cause explosions than fires. A significant amount of data is missing, especially for corrosion, where the second most frequent scenario is classified as "Unknown".
As regards the age of the plants, it was not always possible to trace the data, in particular for the records of the NRC database which reported an insufficient amount of data to track the data. The available results are shown in **Figure 5.17**:

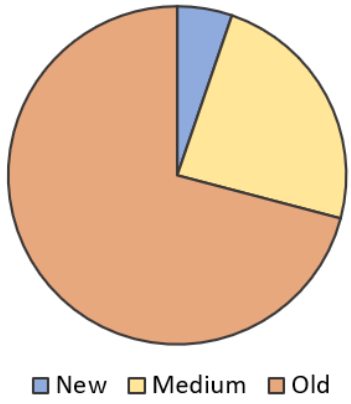

Figure 5.17: Age of the plants for which it was possible to report the data.

Over 70% of incidents involve old plants, those over 25 years old; indeed in Europe many plants were built after the Second World War and are still in operation. However, about 5% of plants are less than 5 years old, suggesting that operating time alone is not the only factor in preventing material degradation.
The analysis concerning actions taken showed that after the event in 90% of the cases the inspection plan was revised, highlighting that in most of the events the inspection plan was not sufficient, resulting in the need for a more effective management and control system.
Further results regarding the substances involved in the analyzed events, and the human, economic and environmental losses are reported in the study by Vitale et al (2025b).
The principal results of Phase 2–Part 2 are discussed below:
From the analysis just discussed, it emerged that corrosion has a frequency of 85%, so the event tree was developed on this degradation mechanism, illustrated in **Figure 5.18**. If equipment in an industrial plant corrodes, this can lead to a loss of containment, which can be triggered and the ignition can be instantaneous or delayed (Vílchez et al., 2011). From the event tree analysis, it is possible to calculate the probability of a final scenario by multiplying the frequencies of the branches that lead to that scenario. The analysis reveals that the most common final scenario in the event of equipment corrosion in a process plant is the loss of containment without ignition, evidenced in green in **Figure 5.18**, with subsequent environmental contamination, with a probability of approximately 50%.
A Bayesian Network model was built to explore the relationships between various variables in the NRC database, selecting “Equipment involved,” “Cause,” “Outcome,” “Macro-sector,” “Substance involved,” and “Final scenario” as key variables. This method provides an estimate of failure frequencies and improves understanding of risk factors and their interactions.
As said before, the Peter-Clark algorithm was used to explore the structure of the BN model. The skeleton was derived from conditional independence tests, with edge directions learned via random rules and expert knowledge. For this application, the database was split into training and validation sets using K-fold cross-validation (K=5), with performance evaluated over 5 iterations.
The results, shown in **Figure 5.19**, reveal that the cause of an event is influenced by the macro-industry, the equipment involved, and the substances and operating conditions to which they are exposed. The event scenario is influenced by the macro-sector, equipment, degradation mechanism, and nature of the substance. Although

many Bayesian Network configurations were identified, only the most obvious dependencies were retained, simplifying the analysis and interpretation of the system.
Initially, the conditional probabilities were evaluated for each model node. After analysis with the Peter-Clark algorithm, these probabilities were recalculated. This allowed assigning values to the scenarios previously defined as "Unknown". **Tables 5.3** and **5.4** present the results of the analysis, providing a probabilistic estimate of the risk scenarios and probability distributions for the functional attributes. **Table 5.3** includes conditional probability tables for the cause of occurrence and the final scenario, while **Table 5.4** shows the probability for the equipment involved and the final scenario. The frequencies of the previous data are shown in brackets for comparison. Some probabilities are rounded to zero due to their negligible value.

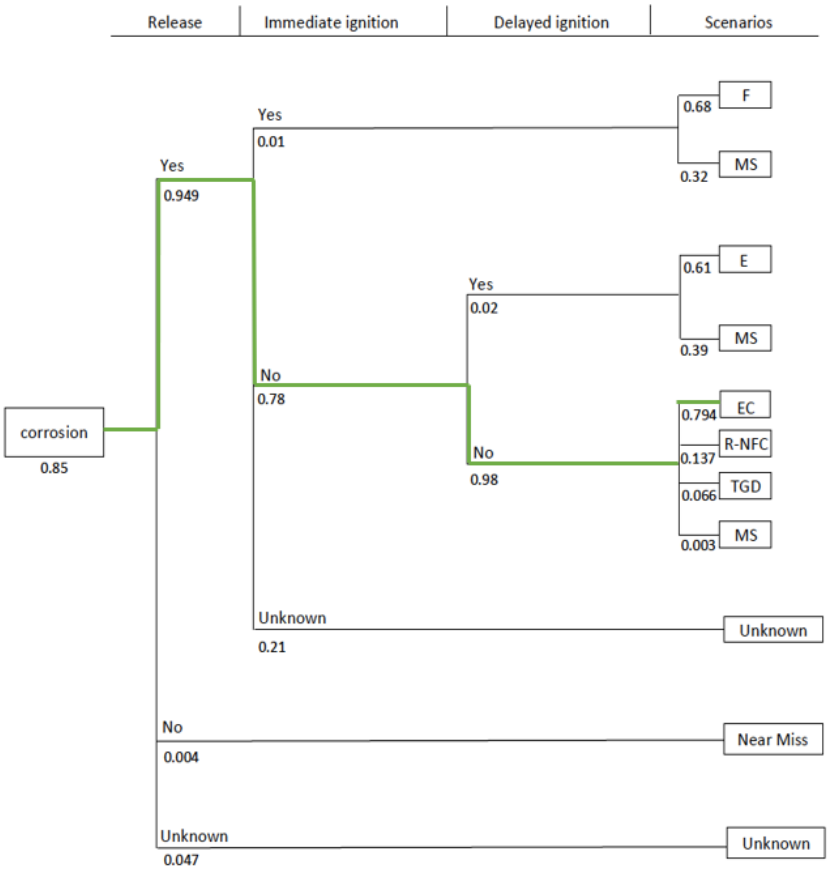

Figure 5.18: Event tree for records reporting corrosion of equipment in industrial plants.

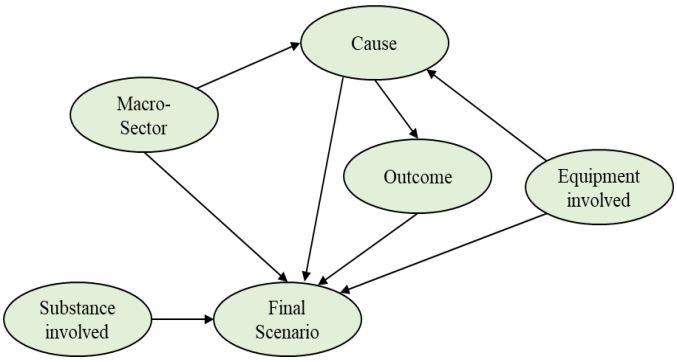

Figure 5.19: Bayesian network for material degradation.

Table 5.3 Conditional Probability Table (CPT) of Cause and Final Scenario.

Cause/final Scenario	Corrosion	Erosion	Fatigue	Vibrations
Near miss	0.002 (0.004)	0 (0)	0 (0.037)	0.005 (0.046)
EC	0.875 (0.782)	0.644 (0.414)	0.675 (0.308)	0.511 (0.316)
F	0 (0.011)	0 (0.135)	0 (0.14)	0 (0.075)
R-NFC	0.055 (0.131)	0.104 (0.243)	0.036 (0.346)	0.103 (0.23)
TGD	0.067 (0.064)	0.252 (0.153)	0.289 (0.084)	0.380 (0.305)
E	0 (0.008)	0 (0.054)	0 (0.084)	0 (0.029)

Table 5.4. Conditional Probability Table (CPT) of Equipment involved and Final Scenario.

Equipment/final Scenario	Control & mitigation system	EC&I system	Primary containment system	Structures
Near miss	0 (0.030)	0 (0)	0.002 (0.008)	0.091 (0.077)
EC	0.304 (0.348)	1 (0.267)	0.875 (0.724)	0 (0.231)
F	0 (0.045)	0 (0.067)	0.001 (0.023)	0.545 (0.179)
R-NFC	0.036 (0.303)	0 (0.333)	0.055 (0.150)	0 (0.282)
TGD	0.661 (0.258)	0 (0.333)	0.067 (0.077)	0.364 (0.154)
E	0 (0.015)	0 (0)	0 (0.017)	0 (0.077)

The Bayesian network analysis shows an increase in the probabilities of environmental contamination and toxic gas release compared to the previous data, with environmental contamination increasing by 60% and toxic gas release by 80%. In contrast, the probabilities of near miss, fires and explosions decreased. The results for equipment are in line with the cause data. However, it should be noted that for Structures the probability of near miss, fires and toxic gas dispersion increases, with a decrease in environmental contamination. Additionally, for control & mitigation system the probability of environmental contamination decreases. For the EC&I system, the probability of environmental contamination was approximated to 1, while the probabilities of other scenarios were very low and rounded to zero.

With Bayesian networks, it is possible to predict scenarios following specific events. For example, using factors such as "Pipeline", "Primary Containment System" and "Corrosion", the probability is calculated for different final scenarios, with the probability of environmental contamination being almost 98% as the predicted outcome. Further details on the algorithms applied to BNs and in-depth discussions on the results are available in Vitale et al. (2025b).

5.2 Interaction between H_2 and H_2/CH_4 mixture release consequences and natural events

In previous analyses, two modelling approaches were adopted to assess the consequences of H_2 and H_2/CH_4 mixture atmospheric releases, empirical methods and advanced CFD methods. The empirical modelling aimed to assess the consequences under steady-state conditions, while the CFD focused on evaluating atmospheric dispersion. The latter approach allowed for a more accurate representation of the fluid dynamics and large-scale turbulence associated with H_2 and H_2/CH_4 mixtures. In both cases, the formation of a 50 mm diameter hole at the top of an aboveground pipeline with an external diameter of 500 mm operating at a pressure of 40 atm was assumed to model scenarios. The environmental conditions considered in the analysis included a wind speed of $u_w = 1.5\ \mathrm{m/s}$, atmospheric stability class F, and a relative humidity of 60%.
To complement the findings from the previously developed CFD and empirical models (Capasso et al., 2025), additional simulations were carried out using the PHAST software. These simulations involved releasing H_2/CH_4 mixtures with varying hydrogen content under the same conditions previously adopted. The aim was to conduct a comparative analysis of the results obtained with PHAST software against those derived from both the CFD and empirical approaches, thereby evaluating the consistency, strengths, and limitations of each method in predicting the dispersion dynamics and potential hazard distances associated with high-pressure releases of hydrogen-rich mixtures. The additional input parameters used to carry out the simulations are reported in **Table 5.5.**

Table 5.5 Input parameters for PHAST simulations

Input parameters		
Pipeline lenght		100 m
Distance to break		50 m
Pumped in-flow	Methane	63 $\frac{Kg}{s}$
	90% CH_4 – 10% H_2	57,5 $\frac{Kg}{s}$
	80% CH_4 – 20% H_2	52 $\frac{Kg}{s}$
	Hydrogen	7,7 $\frac{Kg}{s}$

A comparison between the theoretically choked mass flow rates ($Q_{m,chocked}$), using Source model (Crowl, 2002) and the values computed by PHAST **(Table 5.6)** reveals consistent differences across all gas mixtures considered. Specifically, PHAST yields slightly lower mass flow rates than those derived from the empirical model. This discrepancy can be attributed to the different assumptions and modeling approaches adopted in each method. The theoretical choked flow values are typically calculated assuming ideal gas behavior, isentropic flow, and a simplified representation of the release as a perfectly sharp-edged orifice with negligible energy losses. In this context, flow is considered to be choked at the orifice. In contrast, PHAST employs a more comprehensive and realistic modeling framework results in a more conservative estimate of the released mass flow rate, which is generally lower than the idealized theoretical prediction.

Table 5.6 Chocked mass flow rate and PHAST evaluated mass flow rate

Mixture	$Q_{m,chocked}(kg/s)$	$Q_{m,PHAST}(kg/s)$
Methane	13.4	12.1
90% CH_4 – 10% H_2	12.8	11.5
80% CH_4 – 20% H_2	12.2	10.9
Hydrogen	4.7	4.2

5.2.1 CFD vs. PHAST: atmospheric dispersion

By comparing the results obtained from CFD simulations (**Figure 5.20**) with those produced by PHAST, it was observed that the results from PHAST (**Figure 5.21**) are generally in agreement with the trends previously observed in CFD analyses. As the hydrogen content in CH_4/H_2 mixtures increases, both models predict a more significant vertical rise of the plume and an extension of the flammable region downwind, indicating a greater upward thrust due to its low density and high diffusivity.
However, some quantitative discrepancies emerge, particularly concerning the maximum height and downwind extent of the flammable cloud. While both approaches show that these parameters increase with the hydrogen fraction, the absolute values differ; in particular, CFD simulations (**Figure 5.20 right**) tend to estimate lower heights and shorter downwind distances compared to PHAST ones (**Figure 5.21**), as quantitative reported in **Table 5.7**. This discrepancy can be primarily attributed to the transient nature of the CFD simulations, which capture the time-dependent evolution of the release, including detailed turbulence structures and buoyancy-driven flow dynamics. PHAST, on the other hand, typically relies on steady-state or simplified models, which do not fully represent the unsteady behavior of the gas jet, especially in the early stages of the release when momentum and buoyancy forces are most dominant. Despite these differences, the consistency in overall trends between the two models supports the robustness of the physical interpretation. PHAST remains a valuable tool for preliminary assessments, whereas CFD provides deeper insight into the transient and spatial characteristics of gas dispersion, especially for light gases such as hydrogen.

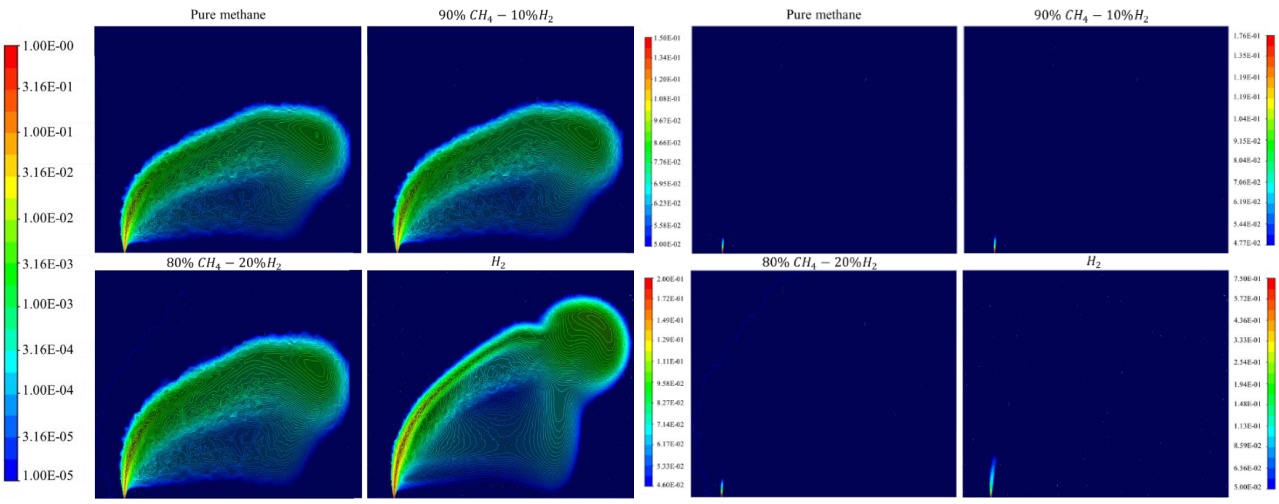

Figure 5.20 Molar fraction profile of the gas released (left) and Molar fraction profile of the gas released within the flammability limits (right) in the plane z-x at y=50 m.

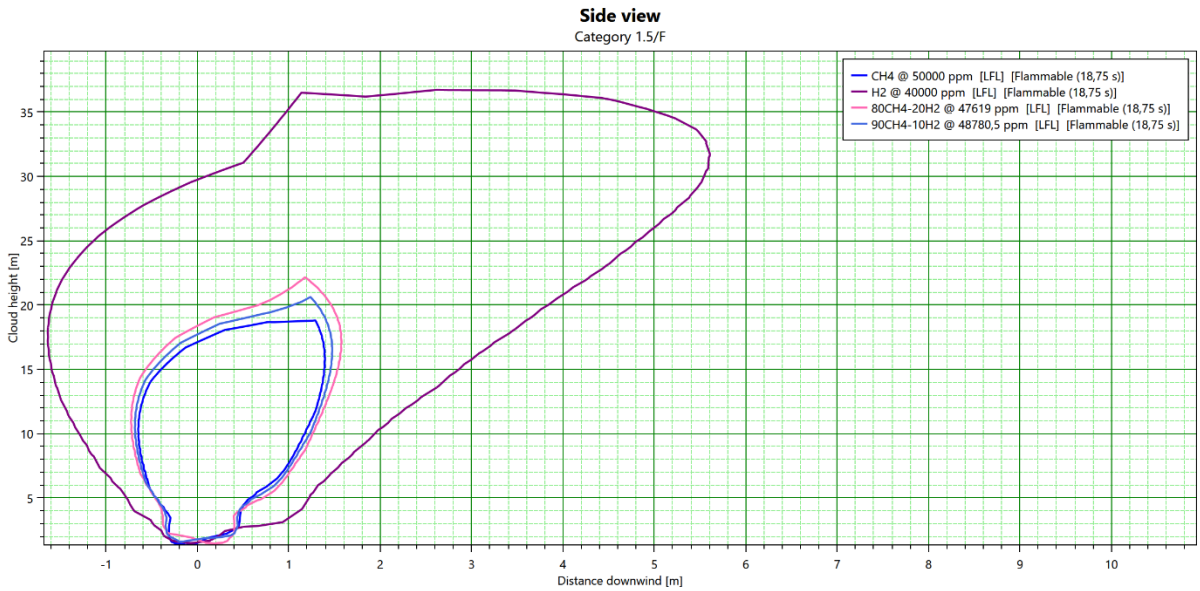

Figure 5.21 Molar fraction profile of the gas released within the flammability limits using PHAST software

Table 5.7 Results obtained from CFD and PHAST simulations, varying the composition of the released gas

Mixture	PHAST		CFD	
	Downwind distance [m]	Height [m]	Downwind distance [m]	Height [m]
Methane	1.4	18.78	0.6	6.6
90% CH_4 – 10% H_2	1.48	20.62	0.7	7.7
80% CH_4 – 20% H_2	1.58	22.2	0.8	7.9
Hydrogen	5.6	36.72	2.8	20

5.2.2 Empirical Point Source Model vs. PHAST: Jet fire consequence

A comparison was carried out between thermal radiation predictions from jet fires using two different approaches: an empirical method based on the Point Source model (Center for Chemical Process Safety (CCPS) 1999), and the PHAST software, which applies the Cone and Miller models depending on the gas type. The objective was to assess the effectiveness of each method in estimating radiative heat flux for CH_4/H_2 mixtures with varying hydrogen content. Both modeling approaches consistently show that increasing the H_2 content the thermal flux received from a receptor increases (**Figure 5.22** and **Figure 5.23**). However, significant differences emerge in the magnitude and spatial distribution of the radiation. The empirical model tends to overestimate heat flux, especially in the near field. This overestimation results from the simplified nature of the model, which does not capture key physical effects such as flame geometry, buoyancy, or wind, making it less suitable for light gases like hydrogen. In contrast, PHAST uses the Cone model for methane and its mixtures, assuming a conical flame and suiting it to conventional hydrocarbons, and the Miller model for hydrogen, which is an extension of the Chamberlain model designed specifically for low-luminosity gases (Miller, 2017). The Miller model represents the flame as a combination of two segments influenced by wind and buoyancy. These models incorporate surface emissive power, jet velocity-dependent radiant fraction, actual flame shape, and atmospheric transmissivity, resulting in more conservative and physically realistic radiation curves. **Table 5.8** shows the predicted flame length for different CH_4/H_2 mixtures. As the hydrogen content increases, both models predict a progressive shortening of the flame. However, the empirical model underestimates flame extent due to its simplified assumptions.

Table 5.9 reports the radiation effect zone radius $R_{e.z.}$ defined as the distance from the flame at which the heat flux drops below a safety threshold. As the hydrogen fraction increases, both models predict a reduction in the hazard distance, though with different magnitudes.

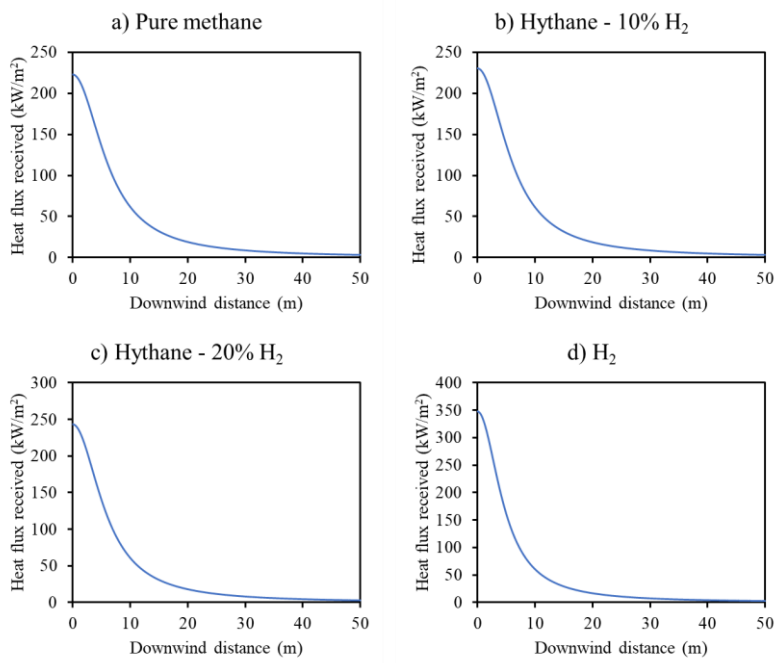

Figure 5.22 Radiation heat flux received, varying the composition of the gas released: pure methane (a), 10% H2 (b), 20% H2 (c), pure hydrogen (d).

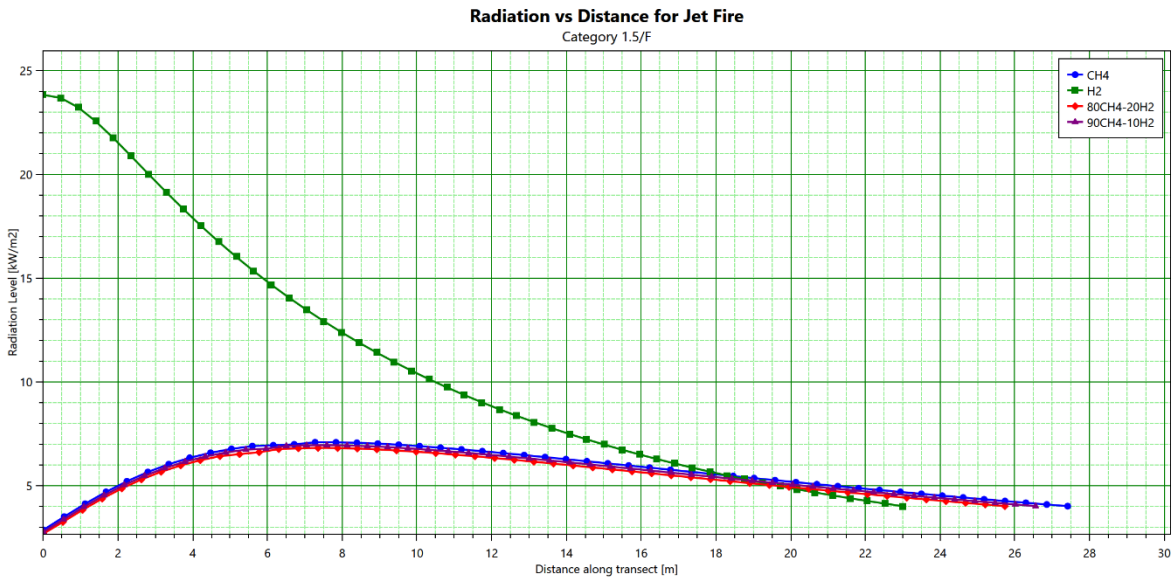

Figure 5.23 Radiation vs. distance for Jet Fire using PHAST software.

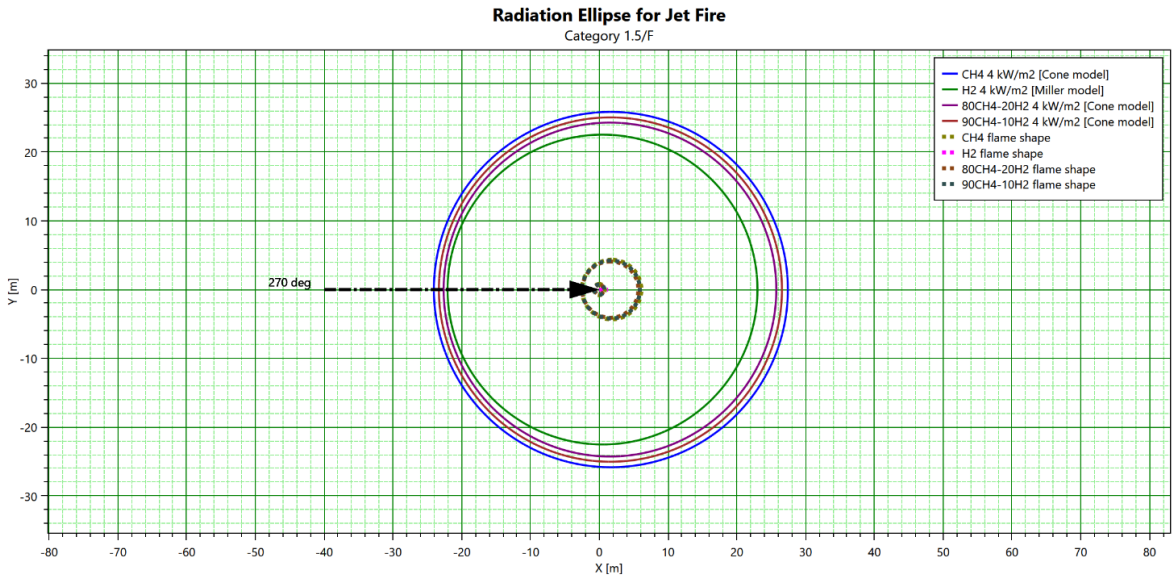

Figure 5.24 Radiation Ellipse for Jet fire using PHAST software.

Table 5.8 Flame Length varying the composition of the released gas.

Mixture	Flame Lenght $_{empirical}$	Flame Lenght $_{PHAST}$
$100\%\ CH_4$	10 m	32 m
$90\%\ CH_4 - 10\% H_2$	9.8 m	31.1 m
$80\%\ CH_4 - 20\% H_2$	9.5 m	30.3 m
$100\%\ H_2$	7.6 m	25.8 m

Table 5.9 Effect Zone Radious varying the composition of the released gas.

Mixture	$R_{e.z.\text{empirical}}$	$R_{e.z.\text{PHAST}}$
$100\%\ CH_4$	44.1	27.4
$90\%\ CH_4 - 10\% H_2$	43.6	26.6
$80\%\ CH_4 - 20\% H_2$	43.1	25.7
$100\%\ H_2$	41.3	23

5.2.3 Assessment of the probability of occurrence of natural events in pipeline ruptures using Fault Tree Analysis (FTA) and Event Tree Analysis (ETA)

In the field of complex industrial systems safety, assessing the probability of occurrence of natural events with the potential to trigger technological failures (NaTech events) has become increasingly central. Particularly, in the context of distribution networks, the interaction between extreme natural events and the structural integrity of pipelines represents a critical area of investigation. Among the most effective tools for analyzing the causes and consequences of failure are Fault Tree Analysis (FTA) and Event Tree Analysis (ETA), complementary methodologies that allow a comprehensive risk assessment from both the perspective of triggering causes and the consequential developments of incident events.
The analysis focused on distribution networks transporting methane and hydrogen, both flammable substances, with hydrogen being susceptible to material embrittlement.

5.2.3.1 Fault Tree Analysis (FTA)

Integrating NaTech scenarios into FTA implies the need to quantify the vulnerability of pipelines to natural events, such as seismic or hydrogeological events. An innovative approach in this regard has been developed through a methodology that segments the network into functional units (between shut-off valves, pumping stations, and pressure regulators) and allows calculating the local probability of failure for each section, based on the event intensity and the specific site hazard.
From a modeling perspective, FTA is based on the use of logic gates (AND/OR) to represent the combination of events. NaTech events are generally modeled as independent causes acting on the structure: for example, an earthquake can cause mechanical failure of a joint or a rigid seismic support, which, when combined with unfavorable operating conditions (high pressure, brittle materials), leads to substance release. The probabilities associated with each event are estimated using historical data, predictive models, or reliability manuals such as OREDA.
Figure 5.25 shows the fault tree, where the analyzed top event is the accidental release of gaseous hydrogen from a buried pipeline. The constructed fault tree identifies multiple intermediate events, including excavation damage, hydrogen embrittlement, structural failure, and, not least, NaTech events such as earthquakes and floods. These elements are treated as primary causes and are evaluated using occurrence frequencies and reliability parameters of individual system components. The probability of occurrence of a seismic event resulting in failure of the rigid support was estimated at 6.69E-06 events/year, while other secondary failures had frequencies in the order of 1E-3 events/year, confirming the rarity but also the high potential impact of NaTech events.

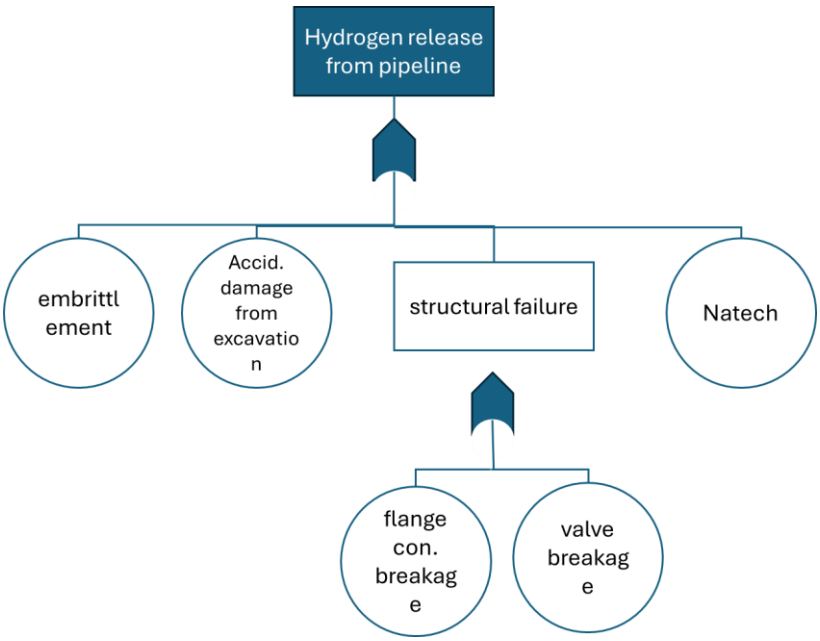

Figure 5.25 Example of event tree for pipelines

It demonstrates how the inclusion of seismic failure probabilities (obtained from probabilistic seismic recurrence models) can significantly influence reliability analysis, especially in high seismicity areas. The results show increases of up to an order of magnitude in the mean frequency of occurrence of the top event (reduced MTTF), with important implications for risk design and management.

5.2.3.2 Event Tree Analysis (ETA)

While FTA allows identifying and quantifying the causes of a failure, Event Tree Analysis (ETA) enables the analysis of the sequence of events that may follow the occurrence of an initiating event. In risk assessment for transport networks, ETA is an essential tool for modeling the various incident trajectories following a pipeline rupture.

For example (see **Figure 5.26**), considering an initial event of pipeline rupture caused by a natural event, ETA develops all possible evolutions, including:

- Failure to ignite the release (controlled release);
- Immediate ignition with jet-fire;
- Formation of an explosive cloud with subsequent delayed ignition (VCE);
- Fire propagation to nearby infrastructure;
- Domino effects on other industrial equipment.

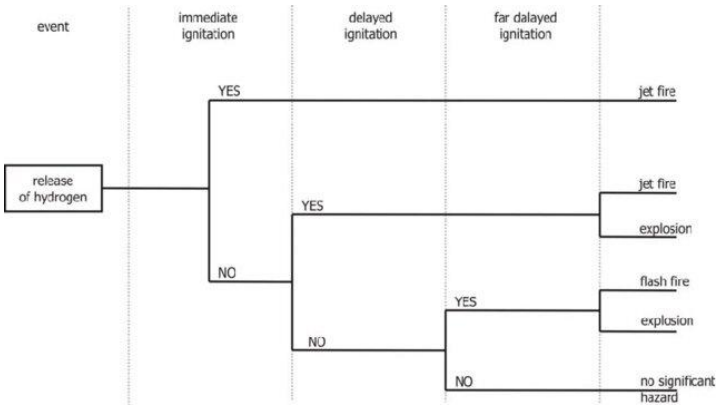

Figure 5.26 ETA hydrogen release

Each branch of the event tree is associated with a conditional probability, which depends on the efficiency of safety systems, environmental conditions, and the operational state of the plant. ETA analysis is based on the definition of "safety barriers" (e.g., rapid isolation systems, ventilation or inerting systems) whose effectiveness is quantified based on reliability data and specific studies.

ETA thus allows estimating the frequency of occurrence of each incident scenario consequent to the initial failure. The combination of FTA (causes) and ETA (consequences) results allows calculating the overall risk ($R = f \times M$), where the frequency f is derived from FTA and the magnitude M from the consequence assessment via ETA. This integrated approach is particularly effective in NaTech risk management, as it allows comparing low-frequency but high-severity scenarios, such as catastrophic explosions or fires.

Overall, the joint adoption of FTA and ETA to integrate the risk from natural events in the reliability assessment of hydrogen distribution networks allows a systematic, logical, and quantitative representation of risk, constituting a fundamental decision-making tool for the design, retrofit, and implementation of mitigation and protection measures. This is all the more necessary in a context where the intensification of extreme events requires increasingly resilient and adaptive risk management."

5.3 Parametric framework for seismic fragility assessment of industrial steel pallet racks

5.3.1 Seismic vulnerability of industrial racks: Literature gap

In recent years, the continuous growth of globalization and e-commerce has greatly increased the need for industrial storage solutions. Among these, standard adjustable steel pallet racks are the most commonly used system in warehouses and logistics centers due to their modularity, versatility, and cost-effectiveness. These structural systems are typically composed of thin-walled cold-formed steel profiles, which are bolted or slotted together to create frame assemblies with multiple pallet levels. Their widespread adoption in Italy and many other countries is largely due to their ease of installation and adaptability to changing operational requirements.
However, pallet racks –especially unbraced configurations– exhibit significant seismic vulnerability. This is mainly due to several interacting features: high live loads even in service conditions, semi-rigid beam-to-column (*btc*) connections, the limited ductility of cold-formed open-section profiles, and the high slenderness of the vertical elements. Under seismic excitation, these characteristics lead to substantial lateral deformability, poor energy dissipation, and sensitivity to local or global instability mechanisms.
In particular, the absence of longitudinal bracing –often omitted to facilitate forklift operations– drastically reduces the lateral stiffness in the down-aisle direction (X), making racks highly flexible and prone to global instability under seismic loads. In contrast, the cross-aisle direction (Y) is typically braced with diagonal and horizontal members, resulting in a significantly stiffer response. This directional asymmetry results in a complex seismic response: while the rack undergoes large deformations and potential instability along the unbraced direction, it is subjected to significant acceleration demands along the braced axis, as the greater stiffness in this direction tends to amplify the seismic input.
The damage observed during recent Italian earthquakes, including the 2012 Emilia-Romagna and 2016 Central Italy events, clearly demonstrated that pallet racks not only pose a risk to worker safety but also play a crucial role in the economic impact of seismic events (Perrone et al., 2019). Their collapse can lead to both direct damage –e.g., loss of goods and equipment– and indirect losses –e.g., long business interruptions (Donà et al. 2019). In several cases, rack failures caused prolonged downtime in entire industrial districts, aggravating the socio-economic consequences of the earthquake and severely affecting the regional supply chains.
The seismic performance of pallet racks has been the subject of several research initiatives at both the component and system level. Some experimental studies have investigated the buckling mechanisms and cyclic behavior of cold-formed profiles under axial and flexural loading (Padilla-Llano et al., 2014, 2016). Others have focused on the rotational response of *btc* connections, whose nonlinear and pinched hysteresis behavior strongly influences the lateral response of racking systems and their dynamics (Bernuzzi and Castiglioni, 2001; Zhao et al., 2018). Large-scale testing campaigns –such as SEISRACKS (Proença et al., 2009) and SEISRACKS2 (Drei et al., 2014)– have further advanced the understanding of rack behavior through full-scale tests and provided data for the development of seismic design guidelines (e.g., CEN, 2016). Previous studies have consistently highlighted the high seismic vulnerability of pallet rack systems. In response, some technological solutions have been proposed to improve their performance, including base isolation systems (Simoncelli et al., 2020), energy-dissipating devices (Shaheen and Rasmussen, 2022), and load-level isolation strategies (Donà et al., 2022; Bernardi et al. 2023).
However, only a few studies have specifically quantified the seismic fragility of these systems, despite its clear importance. Gabbianelli et al. (2020) derived fragility curves for two typical Italian rack types using 2D models and multiple-stripe analysis, while Nuñez et al. (2023) assessed four Chilean archetypes through 3D modeling and incremental dynamic analysis. These contributions, though valuable, underscore the lack of comprehensive fragility assessments for pallet racks and highlight the need for further research.
In response to this gap, the present study introduces a novel methodology for the seismic fragility assessment of industrial pallet racks, applicable to large stocks of storage systems. The approach is based on parametric 3D non-linear finite element modeling and cloud-based analysis, enabling the evaluation of fragility across multiple geometric configurations and ground motion sets. Building on this framework, fragility models were derived for a representative stock of unbraced Italian pallet racks, incorporating multiple engineering demand parameters (EDPs) –total upright strain, inter-level drift, and rotations at beam-to-column and base connections– and conditioned on two intensity measures (IMs): spectral acceleration (S_a) and peak ground acceleration (PGA). As such, they provide a robust and versatile tool for seismic risk estimation and decision support in the context of industrial safety and business continuity.

5.3.2 Parametric analysis framework and selected rack stock

The study focuses on a representative stock of 27 unbraced steel pallet rack configurations, commonly found in the Italian industrial sector. The rack systems are assumed to be designed for gravity loads only, with no consideration for seismic actions in their original design. All racks follow the same longitudinal and transverse plan geometry (**Figure 5.27a**): seven longitudinal bays of 2700 mm and two transverse frames of 1000 mm each, with a 300 mm gap.

The 27 configurations (**Figure 5.27b**) are defined through the systematic combination of three parameters:

- upright cross-section type (U): ranging from slender to thicker cold-formed steel sections (U1, U2, U3);
- load-level height (h): values of 1.0 m, 1.5 m, and 2.0 m;
- total rack height (H): values of 6 m, 9 m, and 12 m.

Each combination defines a unique configuration, with distinct vibration characteristics and load distributions. The number of load levels per rack thus varies depending on the H/h ratio, from 3 to 12 levels. Importantly, the applied pallet loads (**Figure 5.27b**) were calculated based on the static bearing capacity of each transverse frame, which is a function of the upright type and load-level height. This approach ensures comparable compressive stress conditions at the upright bases across the different cases, enabling consistent comparison in fragility analysis.

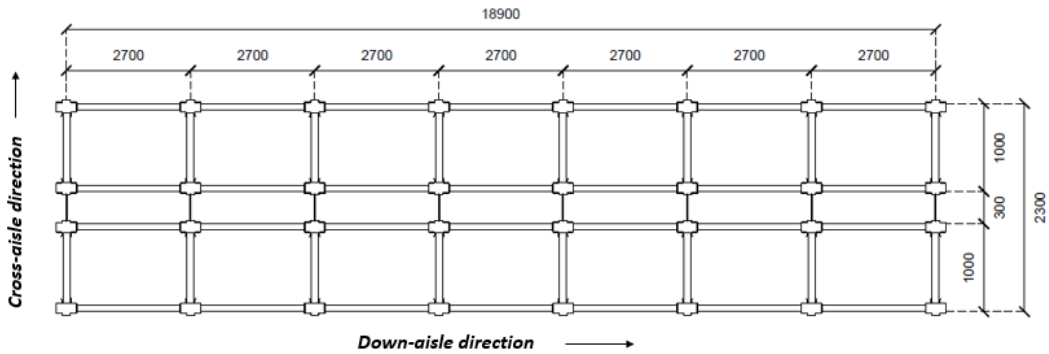

a)

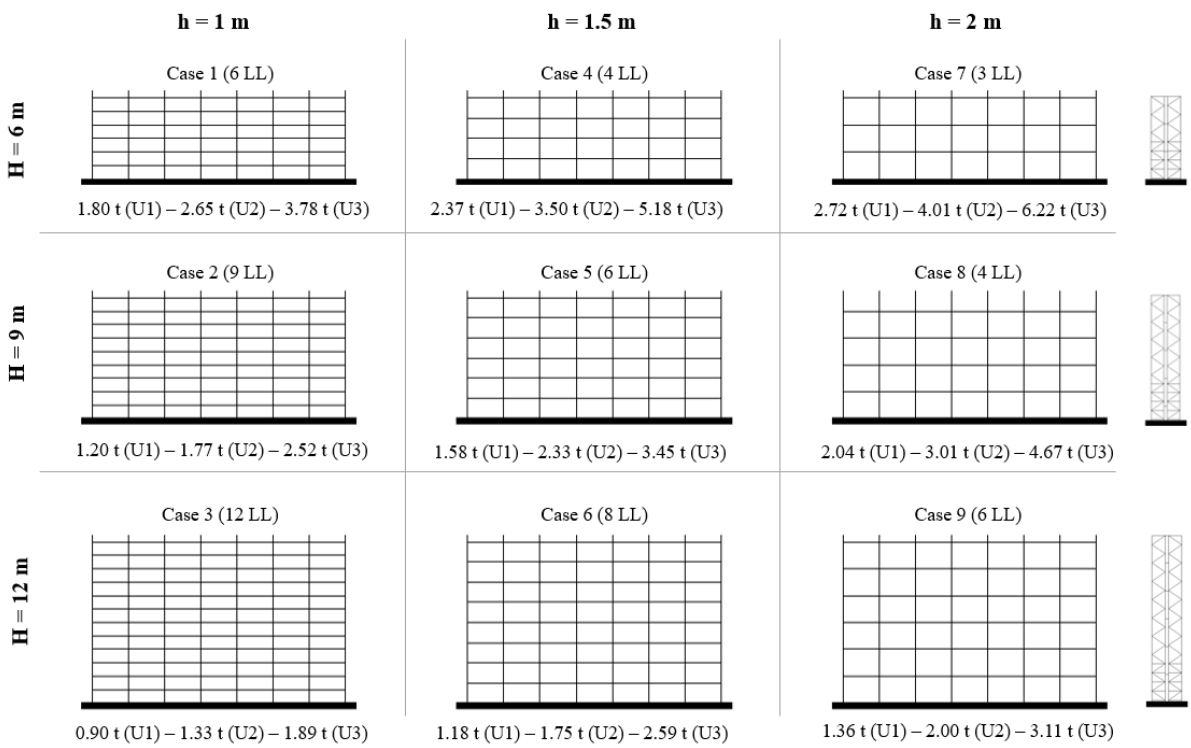

b)

Figure 5.27: a) Common plan layout. b) Rack configurations showing pallet load (in tonnes) per level, span, and frame for each upright type (U1, U2, U3).

For each configuration, the seismic analysis assumes a full-load condition, i.e., all pallet levels are occupied, which is considered the most demanding case –among the load conditions recommended by EN 16681 (CEN, 2016)– for a comprehensive fragility evaluation. Pallet loads are applied to a dummy pyramidal substructure that correctly locates each pallet's center of gravity. A friction contact element beneath the pallets then models sliding in the cross-aisle direction once the friction force –calculated by using a friction coefficient μ_s=0.37 for wood-to-steel contact, as per EN 16681)– is exceeded. **Figure 5.28** shows the 3D FE model of the intermediate rack configuration alongside the cross sections of the main rack elements: pallet beams are Class 3 cold-formed profiles, while uprights and bracing elements fall into Class 4 (CEN, 2005). Accordingly, local and distortional buckling effects in the Class 4 profiles were captured by reducing their stiffness and strength, whereas global buckling was explicitly modeled.

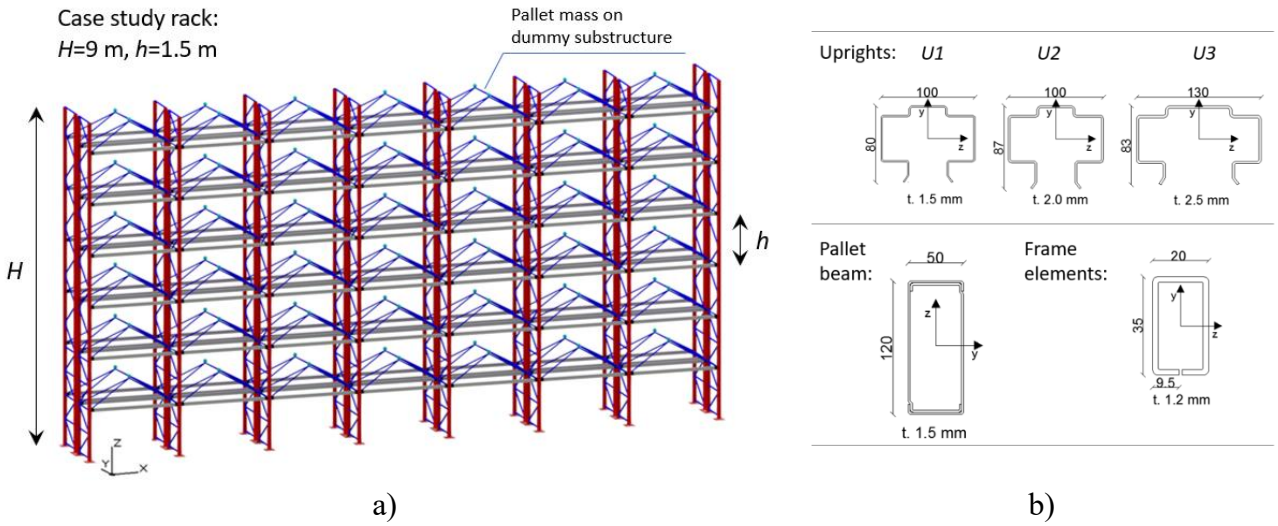

Figure 5.28: a) View of the 3D FE model for the intermediate case study rack. b) Main cross-sections.

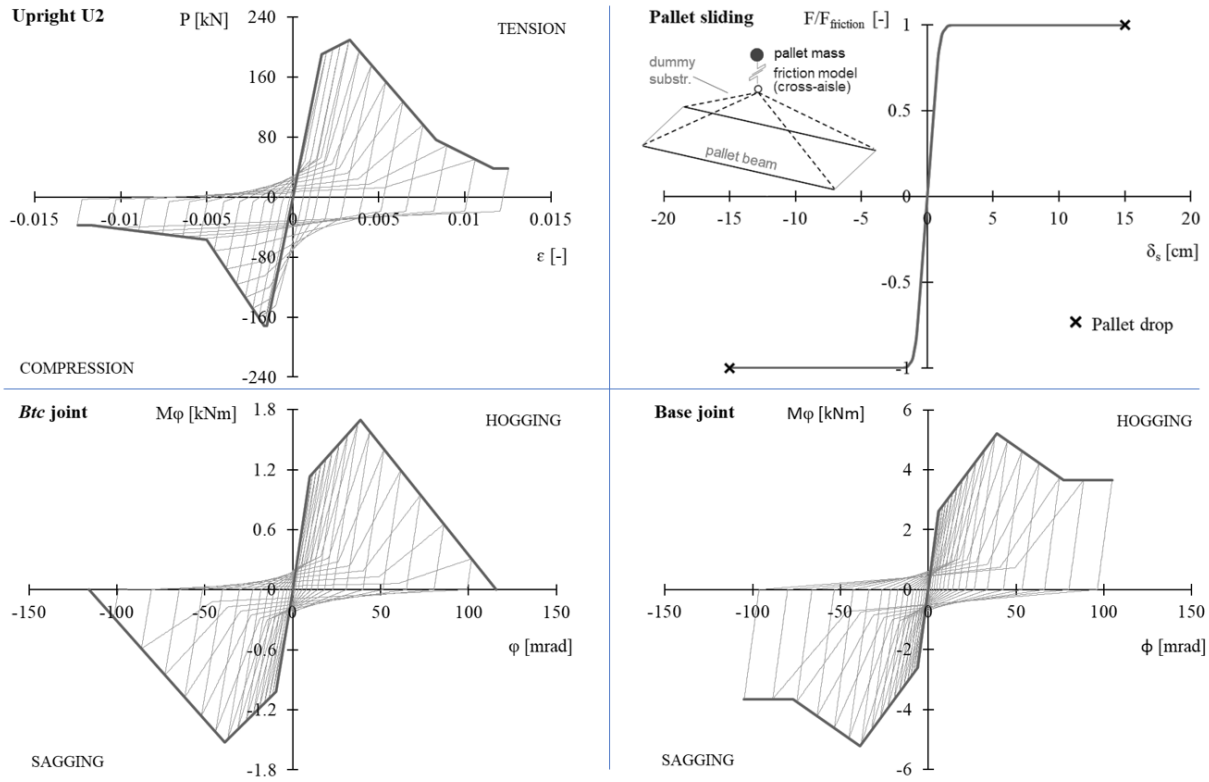

Figure 5.29: Main non-linear hysteretic laws used in the FE rack modelling

A customized parametric modeling framework was developed in MATLAB and OpenSees to automate the generation, analysis, and data extraction of the 3D models. The uprights were modeled using force-based beam-column elements with distributed plasticity, incorporating non-symmetric axial behavior (tension vs. compression) and biaxial flexural response. Regarding the axial behavior, reference was made to the experimental results of Padilla-Llano et al. (2014), while the flexural response was simulated through an elastoplastic model, which is an acceptable approximation –also adopted by other authors (e.g., Gabbianelli et al., 2020)– in favor of greater numerical stability.
Beam-to-column and base connections were represented using zero-length rotational elements with hysteretic response in the longitudinal plane of the rack (rotation around *Y* axis). The hysteretic law and pinching parameters were taken from Gabbianelli et al. (2020), whereas the yield and peak strengths of these connections were defined based on specific test results (Zonta, 2023). Pallet beams, horizontal and diagonal bracing elements, and spacers were modelled as linear elastic components, with their equivalent elastic stiffnesses. **Table 5.10** summarizes the OpenSees elements employed to model the racks and outlines their section behaviors and material laws. The primary constitutive models are then illustrated in **Figure 5.29**.
To account for axial–bending interaction in upright sections modeled with separate response curves, their flexural capacity was scaled down according to the axial compression ratio. Since this ratio varies with load-level height (h), the corresponding flexural capacity reduction also varies: 40% at h = 1.0 m, 35% at h = 1.5 m, and 30% at h = 2.0 m. Furthermore, to capture the loss of frame stiffness due to joint clearances, the diagonal members' cross-sectional properties were reduced according to EN 15512 (CEN, 2020). Further details on the structural models of the pallet racks can be found in Donà et al. (2024).

Table 5.10: OpenSees objects and material laws employed in the pallet rack modelling

Rack elements	OpenSees objects and material laws
Uprights	*Force-Based Beam-Column Elements* Hysteretic asymmetrical axial behaviour via "*uniaxialMaterial Pinching4*" (**Figure 5.29**), accounting for buckling. Elasto-plastic flexural behaviour. Five integration points per element.
Frame bracing elements	*Beam With Hinges Elements* Linear elastic beams with equivalent stiffnesses and end hinges to simulate truss-like behaviour.
Pallet beams/ Spacers	*Elastic Beam Column Elements* Linear elastic beams with equivalent stiffnesses.
Btc and base connections	*Zero-Length Elements* -*Btc*: hysteretic rotational behaviour around *Y* via "*uniaxialMaterial Hysteretic*" (**Figure 5.29**); linear elastic rotational behaviour around *Z*; rotation around *X* equal to that of the beam. -Base: hysteretic rotational behaviour around *Y* via "*uniaxialMaterial Hysteretic*" (**Figure 5.29**); released rotational stiffness around *X*; rotation around *Z* equal to that of the upright.
Mass substructures	*Elastic Beam Column Elements* Linear elastic beams simulating truss behaviour, without affecting modal results.
Pallet-beam contact	*Zero-Length Element* Equivalent friction model (**Figure 5.29**) with penalty stiffness and perfectly plastic behaviour.

To derive the rack fragility models from the time-history (TH) results, a cloud analysis approach was employed. The assessment was carried out using two distinct datasets of 134 unscaled bidirectional ground motion records each, both representative of Italian seismicity (Manfredi et al., 2022): the first characterizing stiff soil conditions, and the second selected to reflect amplifying (soft) soil profiles. For each record, the peak ground acceleration (PGA) values of the two horizontal components (Hc_1 and Hc_2) are shown in **Figure 5.30a.** Two analyses were conducted per ground motion –applying Hc1 in the down-aisle (*X*) and then in the cross-aisle (*Y*) direction– resulting in 268 simulations per rack configuration and per dataset, for a total of 14,472 nonlinear dynamic analyses. **Figure 5.30b** shows the spectral acceleration (S_a) values corresponding to the fundamental periods of the racks in the two main directions ($T_{1,X}$ and $T_{2,Y}$).
Seismic fragility was conditioned to both PGA and S_a as intensity measures (IMs). While PGA is a structure-independent parameter widely used for large-scale risk assessments, S_a –evaluated at the fundamental periods of the rack system– is more effective in capturing the dynamic amplification effects and therefore the actual acceleration demand experienced by the structural system.

Fragility assessment was based on four Engineering Demand Parameters (EDPs) that capture key global and local deformation mechanisms: the normalized global strain of the uprights (ε^*), the down-aisle drift ratio (θ_X), and the maximum rotation of both beam-to-column (φ_{btc}) and base (φ_{base}) connections around the Y-axis. The ε^* parameter, defined in Equation (5.1), combines axial (ε_P) and flexural (χ_Y, χ_Z) demand components normalized by their respective yield thresholds, incorporating a buckling factor for the compressive behavior (χ_P).
Each EDP was linked to three discrete damage states, labeled DS1, DS2, and DS3. DS1 corresponds to the onset of damage, where the system retains predominantly elastic behavior. DS2 represents the initiation of yielding, still ensuring user safety and analogous to a Life Safety limit state. DS3 denotes a severe damage condition in which safety can no longer be guaranteed, and the likelihood of progressive failure –including partial or total collapse– is significant. The threshold values assigned to each damage state for the selected EDPs are reported in **Table 5.11.**

$$\varepsilon^* = \frac{\varepsilon_P}{\left(\varepsilon_{P,y} \cdot \chi_P\right)} + \frac{\chi_Y}{\chi_{Y,y}} + \frac{\chi_Z}{\chi_{Z,y}} \tag{5.1}$$

Table 5.11: Damage state thresholds associated with the adopted EDPs.

EDP	DS1	DS2	DS3
ε^*	[0.8, 1.0 [	[1.0, 1.5 [	[1.5, +∞ [
θ_X / $\theta_{X,y}$	[0.8, 1.0 [	[1.0, 1.5 [	[1.5, +∞ [
φ_{btc} / $\varphi_{btc,y}$	[0.8, 1.0 [	[1.0, 4.0 [	[4.0, +∞ [
φ_{base} / $\varphi_{base,y}$	[0.8, 1.0 [	[1.0, 6.5 [	[6.5, +∞ [
"▪,y" = yield value of specific EDP			

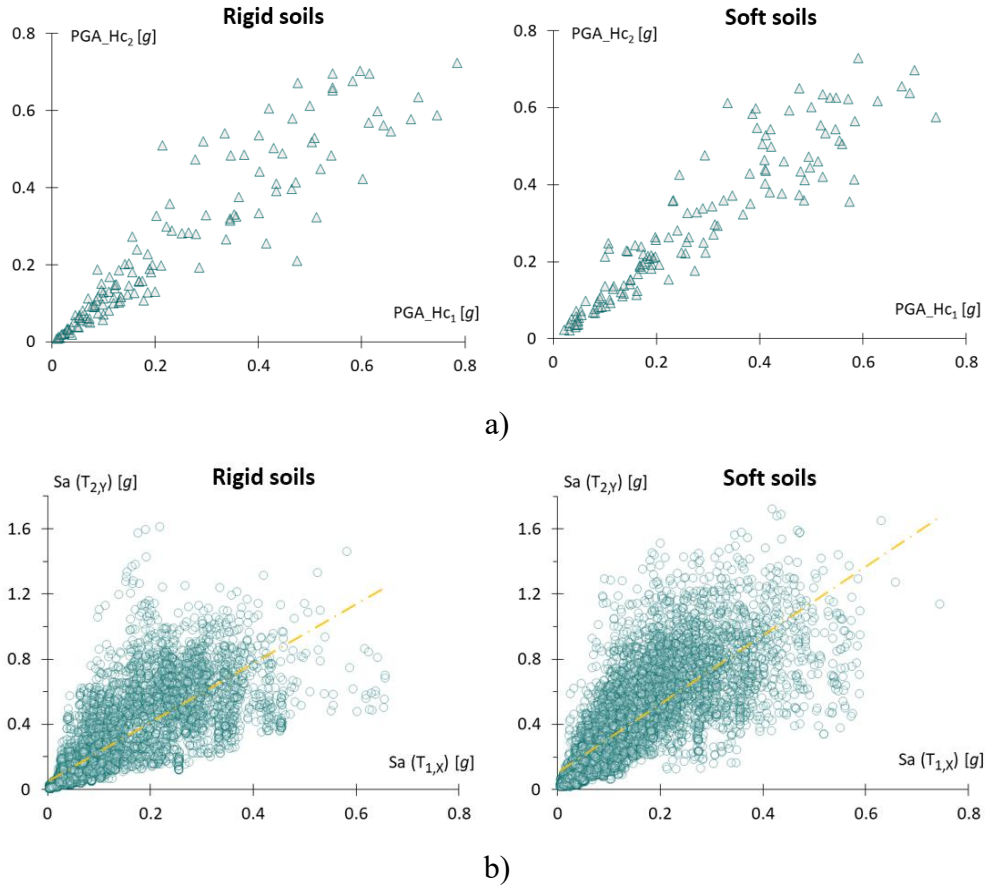

Figure 5.30: Information on ground motion dataset for rigid and soft soils: (a) PGA and (b) S_a values.

The median ($\mu_{DS,i}$) and logarithmic standard deviation ($\beta_{DS,i}$) of the assumed lognormal cumulative distribution function were estimated using the method of moments (see Saler et al., 2021). To enhance the reliability of rack failure probability estimates, non-convergent analyses were also included in the fragility evaluation, as recommended by Jalayer et al. (2017). Indeed, structural collapse was considered to occur under two distinct conditions: (i) the analysis converges and the global strain parameter ε^* meets or exceeds its DS3 threshold; or (ii) the analysis does not converge (*NonC*), which is interpreted as an indication of potential collapse. Based on this dual criterion, the total collapse probability was computed using the total probability theorem (Equation 5.2). A conservative assumption was adopted by setting the conditional probability of collapse given non-convergence (P($D \geq DS3 \mid IM$, *NonC*)) equal to 1, while the probability of non-convergence as a function of seismic intensity (P(*NonC* | *IM*)) was determined through logistic regression, as detailed in Equation 5.3.

$$P\left(D \geq DS_3 \mid IM\right) = P\left(D \geq DS_3 \mid IM,\ Conv\right) \cdot \left(1 - P\left(NonC \mid IM\right)\right) + \\ + P\left(D \geq DS_3 \mid IM,\ NonC\right) \cdot P\left(NonC \mid IM\right) \tag{5.2}$$

$$P\left(NonC \mid IM\right) = \frac{1}{1 + e^{-\left(\alpha_0 + \alpha_1 \cdot \ln\left(IM\right)\right)}} \tag{5.3}$$

5.3.3 Seismic fragility models for pallet racks on rigid and soft soils

Given the use of bidirectional ground motion records, careful consideration was required when evaluating the correlation between EDPs and IMs. The parameters θ_X, φ_{btc}, and φ_{base} represent deformations occurring along the down-aisle (*X*) direction and were therefore correlated with IM values in that same direction. On the other hand, ε^*, being a strain parameter influenced by axial force and biaxial bending, does not have an obvious directional association with a specific IM. However, due to the significantly greater stiffness of the analysed unbraced racks in the cross-aisle direction compared to the down-aisle direction –resulting in higher seismic accelerations and inertial forces along the *Y* axis– ε^* was associated with IM values in the *Y* direction.
For the entire rack stock under rigid soil conditions (Donà et al., 2024; Donà et al., 2025a), **Figures 5.31** and **5.32** present the developed fragility models with respect to the selected EDPs, using PGA and S_a as conditioning IMs, respectively. In addition to DS1, DS2, and DS3, the fragility curves representing the probabilities of non-convergence (*NonC*) and actual collapse (*Collapse*) are also displayed in the fragility model based on ε^*. For comparison, the *Collapse* curve –obtained by analysing ε^*– is also included in the fragility plots of the other EDPs. These fragility plots are accompanied by **Table 5.12**, which reports the corresponding median values (μ) and logarithmic standard deviations (β) of the lognormal distributions. The main considerations on these results are listed below.

- The fragility based on ε^* –characterised by significantly low median PGA values (μ_{PGA})– demonstrates the high seismic vulnerability of these structural systems. The narrow fragility interval between DS2 (μ_{PGA}=0.112 g) and *Collapse* (μ_{PGA}=0.129 g) demonstrates the limited redundancy and ductility capacity of these racks. The close overlap between DS3 (collapse with convergence) and *NonC* (non-convergence) suggests that non-convergence is mainly triggered by excessive upright strain.
- The *Collapse* curve (determined for ε^*) consistently precedes the DS3 curves of the other EDPs (θ_X, φ_{btc}, and φ_{base}), confirming that ε^* governs the collapse mechanism. Among the remaining EDPs, θ_X is the first to reach DS3, making it the most representative indicator of global rack deformation in the down-aisle direction.
- The *Collapse* curve is nearly coincident with DS2 of θ_X, indicating similar probabilities for upright failure and yielding along the X direction. Comparing φ_{btc} and θ_X, φ_{btc} exhibits lower μ_{PGA} values at DS1 and DS2, but higher values at DS3, reflecting a rapid loss of inter-storey stiffness once *btc* joints yield. Fragility for φ_{base} is the lowest: DS1 is reached after DS2 for θ_X and φ_{btc}, and DS3 is never attained, suggesting a hierarchical resistance among rack components.
- For ε^*, the acceleration ranges in PGA and S_a are comparable. For the other EDPs, however, the fragility ranges in S_a are significantly narrower than those in PGA, due to the long vibration periods in the down-aisle direction. Since the *Collapse* curve is derived from the analysis of ε^* –and is therefore associated with IM values in the *Y* direction– it is no longer directly comparable with the fragility curves of θ_X, φ_{btc}, and φ_{base} when conditioned on S_a, although it still serves as a useful reference.

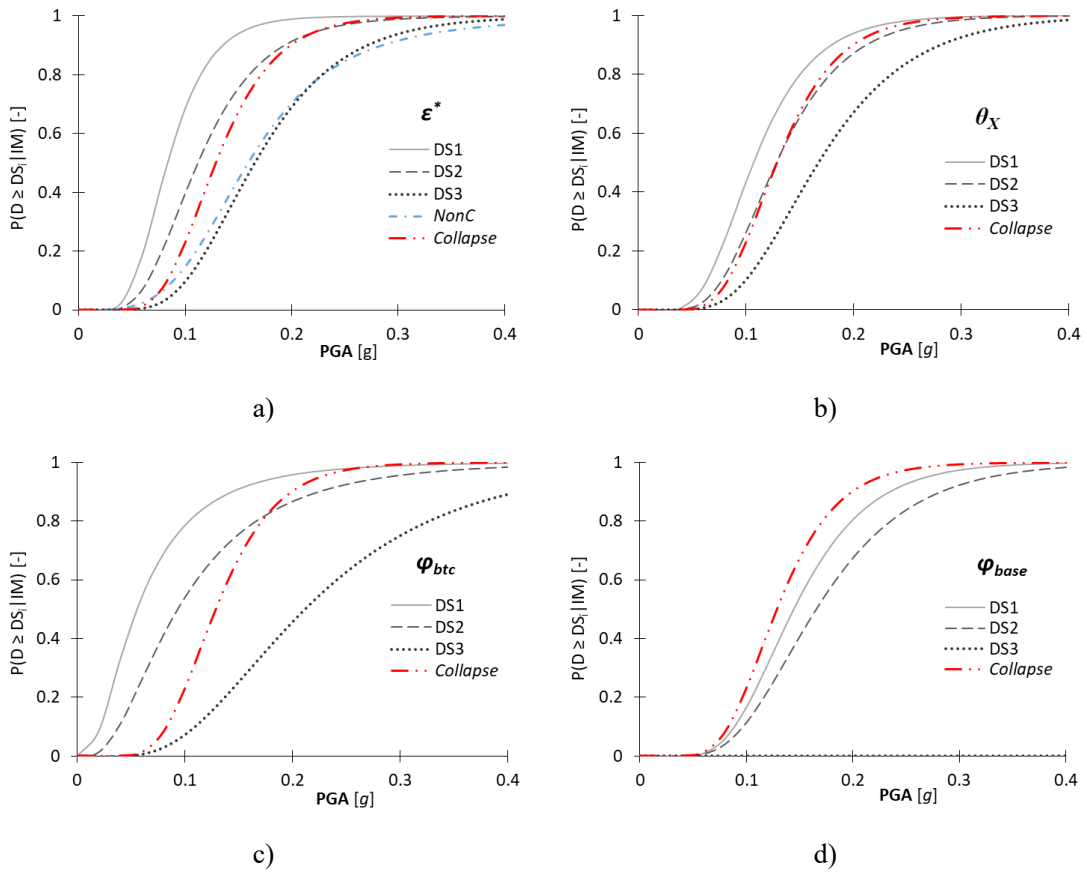

Figure 5.31. Fragility curves of the rack stock on rigid soils in PGA: (a) ε^*, (b) θ_X, (c) φ_{btc}, (d) φ_{base}.

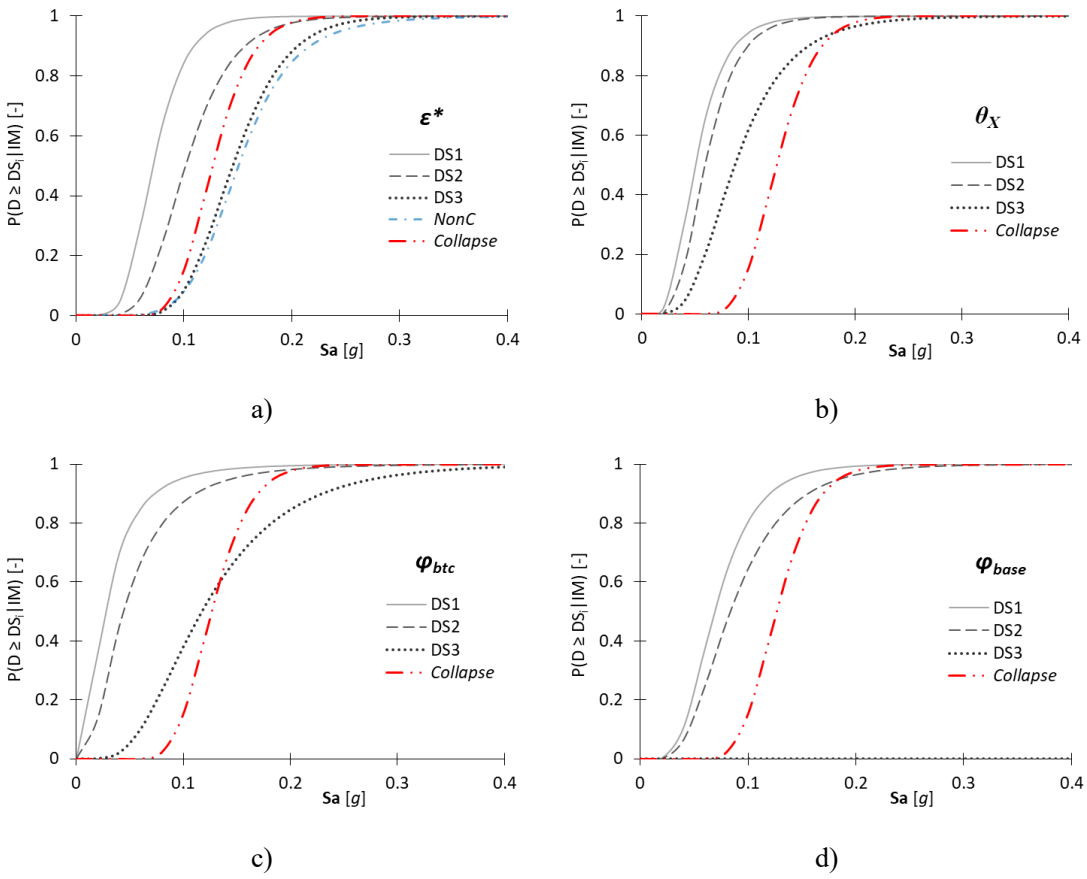

Figure 5.32. Fragility curves of the rack stock on rigid soils in S_a: (a) ε^*, (b) θ_X, (c) φ_{btc}, (d) φ_{base}.

For the same rack stock under soft soil conditions (Donà et al., 2025b), to maintain compactness, only **Table 5.13** is reported, summarising the μ and β values of the associated fragility models. The general considerations that can be drawn are similar to those previously discussed for the fragility estimated under rigid soil conditions. Lastly, **Figure 5.33** compares the median ($\mu_{DS,i}$) and logarithmic standard deviation ($\beta_{DS,i}$) values of the fragility curves based on ε^* across the two soil conditions, offering insight into the influence of local site effects on rack fragility estimates. Regarding this comparison, the main observations are as follows:

- The $\mu_{DS,i}$ values for PGA differ significantly between rigid and soft soils: they are lower for soft soil, indicating higher fragility under amplifying conditions. This difference is reduced when S_a is used as seismic intensity measure. This proves that S_a is a more efficient IM to describe rack fragility. The latter observation is particularly relevant for spatial-scale risk assessments and may warrant further investigation (for instance, investigating alternative intensity measures, such as Housner intensity).
- The $\beta_{DS,i}$ values for PGA are higher for soft soil, which is consistent with the greater variability of seismic demand in amplifying conditions. In contrast, $\beta_{DS,i}$ values for S_a are similar across soil types, confirming the reduced sensitivity of rack fragility to soil condition when using this IM.

Table 5.12. Median values (μ) and logarithmic standard deviations (β) for fragility models on rigid soils.

EDPs	DS1		DS2		*Collapse* (for ε^*) / DS3 (other EDPs)	
IM=PGA	μ_{PGA} (g)	β_{PGA} (-)	μ_{PGA} (g)	β_{PGA} (-)	μ_{PGA} (g)	β_{PGA} (-)
ε^*	0.083	0.378	0.112	0.427	0.129	0.340
φ_{btc}	0.055	0.748	0.093	0.689	0.211	0.517
θx	0.107	0.405	0.128	0.393	0.167	0.405
φ_{base}	0.144	0.380	0.165	0.420	-	-
IM=S_a	μ_{Sa} (g)	β_{Sa} (-)	μ_{Sa} (g)	β_{Sa} (-)	μ_{Sa} (g)	β_{Sa} (-)
ε^*	0.071	0.337	0.101	0.340	0.127	0.228
φ_{btc}	0.027	0.790	0.044	0.726	0.117	0.525
θx	0.050	0.406	0.059	0.406	0.087	0.457
φ_{base}	0.069	0.434	0.083	0.486	-	-

Table 5.13. Median values (μ) and logarithmic standard deviations (β) for fragility models on soft soils.

EDPs	DS1		DS2		*Collapse* (for ε^*) / DS3 (other EDPs)	
IM=PGA	μ_{PGA} (g)	β_{PGA} (-)	μ_{PGA} (g)	β_{PGA} (-)	μ_{PGA} (g)	β_{PGA} (-)
ε^*	0.049	0.412	0.088	0.524	0.097	0.336
φ_{btc}	0.048	0.424	0.083	0.604	0.204	0.313
θx	0.078	0.513	0.104	0.507	0.144	0.437
φ_{base}	0.119	0.458	0.143	0.431	-	-
IM=S_a	μ_{Sa} (g)	β_{Sa} (-)	μ_{Sa} (g)	β_{Sa} (-)	μ_{Sa} (g)	β_{Sa} (-)
ε^*	0.047	0.335	0.087	0.351	0.111	0.231
φ_{btc}	0.020	0.544	0.035	0.672	0.089	0.370
θx	0.033	0.564	0.043	0.546	0.065	0.483
φ_{base}	0.051	0.573	0.060	0.526	-	-

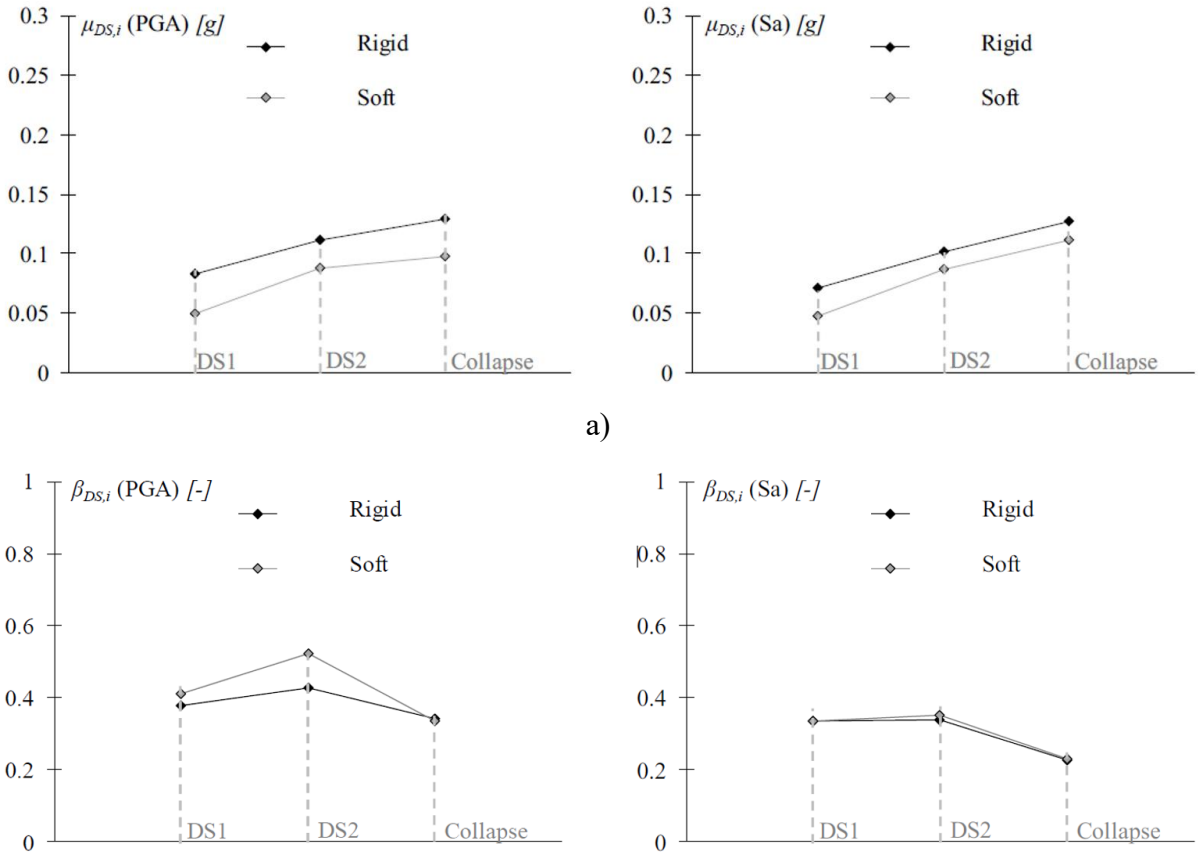

Figure 5.33. Comparison of median ($\mu_{DS,i}$) and logarithmic standard deviation ($\beta_{DS,i}$) values of the fragility curves based on ε^* for different soil conditions.

6. Industrial multi-hazard deployment index

In this section a new multi-hazard indicator will be proposed, derived by improving the multi-risk method proposed by Pilone et al. (2021) for assessing NaTech vulnerability potential. It will be briefly summarized in the following, to discuss the possibility of enhancing it, and then the newly proposed index will be presented. **Figure 6.1** illustrates the theoretical conception of this method from a multi-risk perspective, aligned with the key conceptual elements of the NaTech concept as defined by Krausmann et al. (2017).

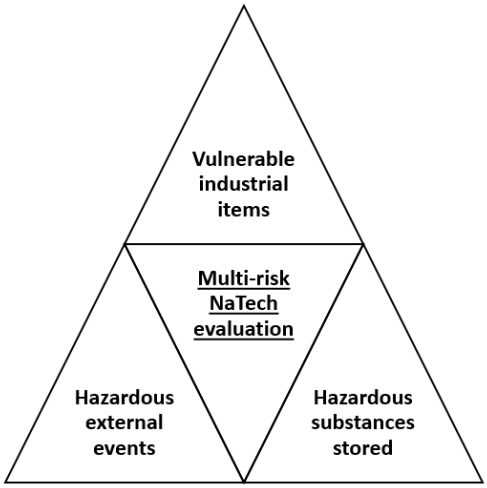

Figure 6.1: Theoretical conception of the multi-risk NaTech vulnerability indicator.

6.1 Multi-risk simplified NaTech indicator for local planners

The Pilone et al. (2021) method is based on a simplified ex-ante indicator designed for local planners, and crosses the ratings given to the exposure of various industrial items (multi-vulnerability) to a set of multiple hazards, with a factor derived from the quantity and hazardousness of the stored dangerous substances.
Once the required data is available, the determination of the simplified NaTech vulnerability indicator consists of three main steps that are subsequently described: Factor A, Factor B, and assessment.

Factor A

Factor A estimates the interaction between a predefined cluster of industrial items categories and a set of hazardous factors that may threaten the plant location. Below are the industrial items and hazards considered by the method to characterize the infrastructure vulnerability in each location.
Industrial items: a) basins for water treatment; b) storage tanks (atmospheric or pressurized); c) underground deposit; d) tall structures (flares, distillation towers, chemins, etc...); e) basins and other process equipment; f) hazardous storage (storage of other hazardous raw materials in warehouses).
Hazards: g) earthquakes; h) floods; i) storms; j) fire; k) obsolescence.
To determine the multi-risk interactions, a table is compiled that contains the six categories of industrial items in the columns and the five categories of hazards in the rows (6×5 matrix). Next, based on the data gathered using the previously mentioned questionnaire, the presence and specific location of each item in the plant layout are verified, while the relevance of hazards is assessed for each case under analysis.
The categories in both columns and rows are turned on or off depending on whether they are present (or not). In consequence, a rating is assigned to each category in a simplified binary way (0 = category not present or not considered; 1 = category considered). Then, the interaction in each cell of the 6×5 interaction matrix is obtained by multiplying the binary ratings of the corresponding industrial item in the column and the hazard of concern in the row. Subsequently, these interactions within the cells of the "6×5 matrix" are totalized column by column, where these column totals are then summed across a final row to calculate the value of total *Factor A*.

Factor B

Factor B, depending on the hazardous substances stored in the plant, is determined by the sub-factors type (B1) and quantity (B2). Firstly, *Factor B1* assigned ratings concerning the classes of hazardous substances considered in the Seveso III Directive (2012/18/EU)[1], which is in line with Regulation (EC) No 1272/2008[2]. Substances that directly impact human health (B1HH) are considered those classified under Section «H» ("health hazards") and Section «P» ("physical hazards"). In contrast, substances with potential environmental impacts (B1Env) were categorized separately and included those listed under Section «E» ("hazardous to the environment"). In addition, the method includes ratings for an extra category denominated "other substances" for substances not mentioned in Annex I of Directive 2012/18/EU. Summing up, from the sub-factor type of substances (B1), two NaTech dimensions must be estimated: one related to the possible harms to human health –NI(HH)–, and the other related to the possible harms to the environment –NI(Env)–. The ratings assigned to the sub-factor substance quantity (B2) are determined by ranges associated with the fulfillment of thresholds declared for any class of substances in Directive 2012/18/EU.

NaTech Indicator assessment

Equation (6.1**Errore. L'origine riferimento non è stata trovata.** proposes the latest refinements in the calculation method to determine the simplified NaTech vulnerability indicator crossing values obtained for *Factor A* and *Factor B*, (Castro Rodriguez et al., 2025a):

$$NI = Factor\ A \times \sum_{j=1}^{m} \frac{1}{n_m} \sum_{i=1}^{n_m} (Factor\ B1_i \times Factor\ B2_i) \qquad (6.1)$$

where,

NI: NaTech vulnerability indicator.

Factor A: final number obtained in a tabular way, from the 6×5 interaction matrix relating industrial items and hazards categories.

*Factor B*1: rating for the type of dangerous substances stored, according to Column 1 of Annex I of Directive 2012/18/EU (Part 1).

*Factor B*2: rating for the quantity of dangerous substances stored in the plant (depending on the thresholds declared for lower tier establishments (LTE) of any category of substances in Column 2 of Annex I of Directive 2012/18/EU).

m: corresponds with index values assigned to each *"j"* section of substance within Annex I of Directive 2012/18/EU (H=1, P=2, E=3, and other substances=4).

n: corresponds to the number of different substances *"i"* detained inside the same *m*-section.

Table 6.1 - Rating of Factors B1 and B2, and thresholds for NI(HH) and NI(Env).

Factor Type (B1)	Dimension	Section	Effect	Rating
B1HH	Human health potential damages	H	Toxic	3
		H	Carcinogenic	2.5
		P	all	2
B1Env	Potential environmental impacts	E	all	3
		Other substances	all	0.5
Factor Quantity (*B2*)	> Seveso lower-tier threshold LTE			1
	> 20% of the threshold for LTE (Sub-threshold Seveso)			0.6
	< 20% of the threshold LTE (Sub-Seveso establishment)			0.2
$NI(HH)_{max} = 26\times(3\times1+2.5\times1+2\times1) = 195$		$NI(Env)_{max} = 26\times(3\times1+0.5\times0.2) = 80.6$		
$NI(HH)$ alert threshold = 27		$NI(Env)$ = alert threshold = 11		

Source: (Pilone et al., 2021).

Summarizing, **Table 6.1** provides the ratings proposed by the original method for *Factor B*1 and *Factor B*2. Additionally, the table also includes the highest values for *NI*(*HH*) and *NI*(*Env*) suggested by Pilone et al. (2021),

[1] Directive 2012/18/EU on the control of major-accident hazards involving dangerous substances, amending and subsequently repealing Council Directive 96/82/EC.

[2] Regulation (EC) No 1272/2008 on classification, labelling and packaging of substances and mixtures, amending and repealing Directives 67/548/EEC and 1999/45/EC, and amending Regulation (EC) No 1907/2006.

and their corresponding alert thresholds, for the simplified case in which the method was originally applied, assuming the presence of only one substance per class.

6.2 Opportunities to enhance the multi-risk simplified NaTech indicator for local planners

The opportunities to enhance the multi-risk NaTech indicator initially introduced by Pilone et al. (2021) are critically discussed in Castro Rodriguez et al. (2025a), and can be summarized in: i) flexibility in integrating relevant natural factors based on the specific hazards associated with the plant location; ii) introduction of a location priority factor to contextualize the multiple hazards of interest including their cascading effects; iii) use of standardized vulnerability categories for industrial items aligned with data from historical NaTech events; iv) evaluation of dynamic vulnerability interactions among industrial components, considering their proximity and functional interdependence; v) development of semi-quantitative multi-risk criteria to assess the interaction between hazards and industrial items; vi) limitations in the classification of the type of substance; vii) shortcomings in rating the quantity of substances stored; viii) multidimensional nature of final NaTech potential assessment.

6.3 Comprehensive evaluation of the NaTech potential in Industrial Critical Infrastructures

Considering the previous opportunities, on the one hand, the Quality Function Deployment (QFD) (Akao, 1972) was tailored to enhance the multi-risk evaluation of multiple hazards and the different vulnerable infrastructural items. On the other hand, the comprehensive evaluation was achieved by integrating an index designed to evaluate the potential for major industrial accidents based on hazardous substance criteria. This index was developed in alignment with the legal requirements of European regulations (Seveso III Directive), extending its scope to include not only major establishments but also the so-called non-Seveso facilities. In this way, the picture of the NaTech definition given by Krausmann et al. (2017) is completed through the analysis of technological accidents contextualized to the natural hazards in the territory and taking also into consideration the hazardous substance criteria (refer to **Figure 6.1**).

6.3.1 The Industrial Critical Infrastructure Multi-Risk Deployment framework (ICI-MRD)

Figure 6.2 illustrates the ICI-MRD framework with the steps to achieve the multi-risk assessment of NaTech vulnerability in ICIs.

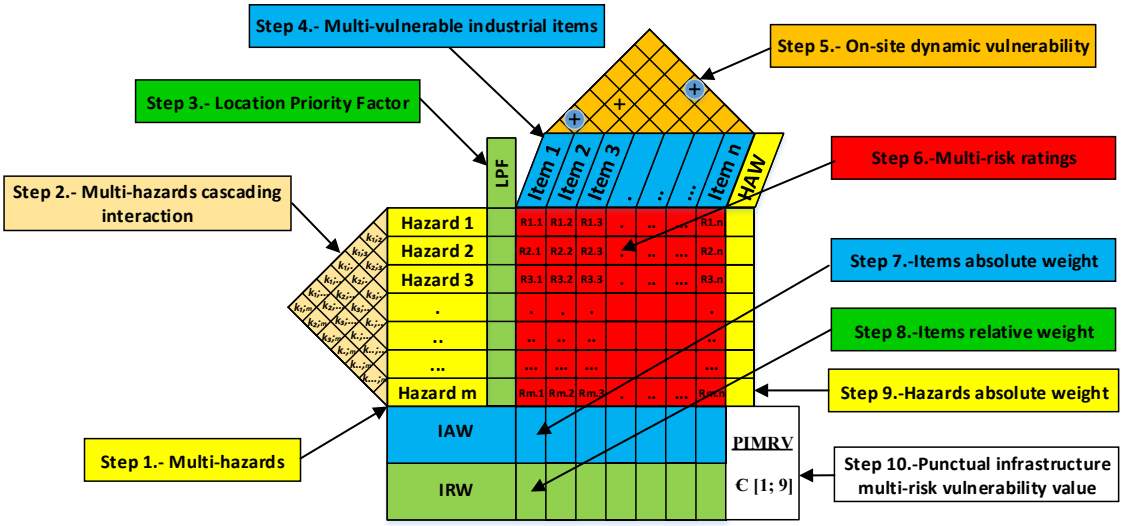

Figure 6.2: Framework Industrial Critical Infrastructure Multi-Risk Deployment (ICI-MRD) numbering the steps for its implementation.

Details about how to implement each step can be found in Castro Rodriguez et al. (2025b). Then, the final output for the ICI-MRD framework applied to a critical energetic infrastructure (thermoelectric plant), is shown in **Figure 6.3**. This output illustrates the multi-risk NaTech evaluation for the potential impacts of four natural hazards -lightning (LN), extreme temperature cold (ETc), extreme temperature hot (ETc), flooding (FL)- on eight industrial items belonging to an energetic critical infrastructure. The categories of industrial items considered were: Storage equipment (SE); Flare stakes (FS); Process equipment (PE); Pipework (PW), Machinery (MC); Electrical equipment and electronic devices (EE); Other hazardous storage (HS); Basins and water treatment elements (BWT).

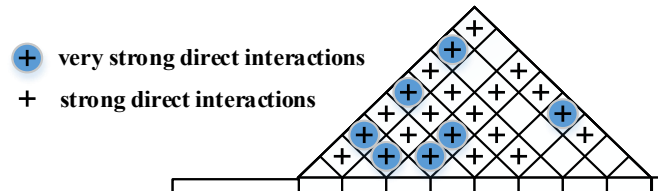

	LPF max	SE	FS	PE	PW	MC	EE	HS	BWT	HAW
1.-LN	0.18	7	1	2	2	2	5	4	2	25
2.-ETh	0.14	5	1	1	1	2	1	5	2	18
3.-ETc	0.17	3	2	2	7	1	3	1	4	23
4.-FL	0.04	8	1	2	3	1	3	1	9	26
IAW		23	5	7	13	6	12	11	17	PIMRV
IRW		2.79	0.70	0.92	1.81	0.85	1.67	1.63	1.60	2.07

Figure 6.3: Output of ICI-MRD framework tested on the energetic critical infrastructure.

Firstly, the punctual infrastructure multi-risk value (PIMRV) determination provides an early warning indicator on potential NaTech, aligned with the function-location approach (refer to deliverable **DV 3.2.b**), which characterizes NaTech vulnerabilities in industrial multi-hazard contexts. This value has implications for the dynamic mapping of critical infrastructures as single points at a primary decision-making level. Although the stakeholders highly value punctual decisions such as PIMRV, the method does not discard the necessity of going deeper with specific analysis.

In the present case, the PIMRV = 2.06 —PIMRV ∈ [1; 9]—falls closer to minor importance than moderate (Castro Rodriguez et al., 2025b), considering the four hazards threatening all the industrial items. However, a detailed analysis may show some criticalities.

For instance, the presence of two triangular matrices can be appreciated, which reflect separately the potential cascading effects. The left triangle shows just the strong interaction between two natural factors ETh→FL. On

the other hand, the roof triangle matrix shows, in general, strong interaction among the items, with implications for domino effects. For example, ASE and PE, according to their position and functions, compromise all the rest of the equipment categories with strong and very strong direct relationships with all the elements. Likewise, the rest of the items, in case of failure, might impact spatially or by function all the process plant.

Moving to the analysis of the IAW (absolute weight of each item category) highlights the multi-vulnerability of each item to the superposed multiple considered hazards (**Figure 6.4**). It can be seen how the bars in yellow accumulate 80 % of the multi-vulnerability of the plant. Just the "atmospheric storage equipment" and the "water treatment basins" account for around 40% of the total weight.

Analogously, **Figure 6.5** shows the multi-risk analysis focusing on each single item but including the location priority factor. It is important to note how the item ranking changes when the vulnerability is contextualized to the specific plant location of the plant through the location priority factor (LPF). For instance, BWT passed from second place to fifth position compared to **Figure 6.4** and **Figure 6.5.**

The conditional probability of NaTech in the power production macro-sector is low for the considered hazards; in consequence, it impacts the LPF and the contextualized items multi-vulnerability. A cautious strategy might be adopted by assigning the highest probability to the factor P(NaTechMS|Hazk). It means calculating the LPF just considering the influence of natural hazards and their potential cascading interactions (Castro Rodriguez et al., 2025b). Moving to the hazards absolute weight (HAW) this column offers the integrated dangerousness of each hazard analyzed concerning all the integrated items (**Figure 6.6**).

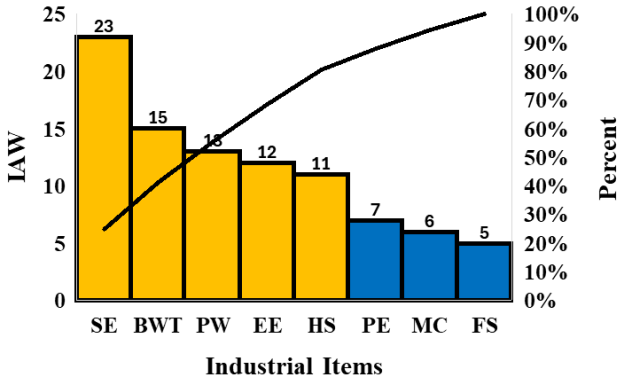

Figure 6.4: Pareto diagram for individual items multi-vulnerability (IAW).

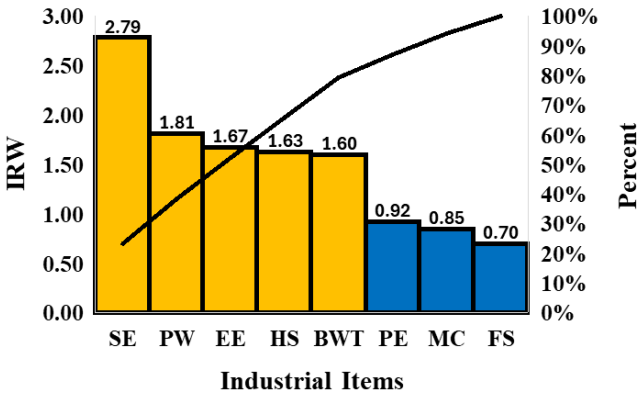

Figure 6.5. Pareto diagram for items individual function-location multi-vulnerability (IRW).

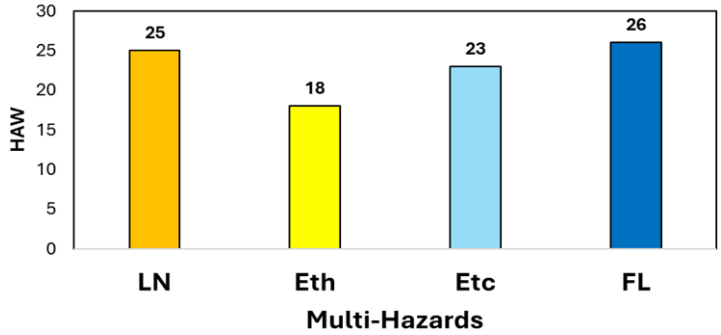

Figure 6.6. Dangerousness of each hazard against the critical infrastructure is a punctual element.

The final *HAW* values are the sum of the contributions of various items (in this case, 8), meaning it depends on the number of items involved. The key aspect of this analysis is that it allows for ranking hazards that overlap within the same industrial context regarding the items analyzed in any case. Differences in the dangerousness of considered hazards can be appreciated, contributing to increasing awareness and having direct implications for achieving resilience by introducing corrective measures according to the importance of the hazard.

6.3.2 Major industrial accident potential based on dangerous substance criteria

Initially, the "type" of hazardous substances (C_s) was classified in the following categories: C_a (health risks), C_b (physical hazards), and C_c (environmental hazards), therefore $s=\langle a, b, c\rangle$. These three categories of hazardous substances align with the Globally Harmonized System (GHS) of classification and labelling of chemicals, which is used by Directive 2012/18/EU. These classifications are directly related to the potential scenarios that the adopted categories can generate (toxic, energetic, spills).

For instance, the C_a dimension may cluster events such as the Seveso dioxin disaster in 1976, the Manfredonia arsenic dispersion in 1976, or the Lubrizol black smoke accident in 2019, all of them with a huge territorial extension of their toxic scenarios and high severity to human health. Moreover, the C_b dimension may include energetic scenarios (fires, explosions) with devasting consequences for both infrastructure and people in the damaged and neighbouring zone. Examples within this category match with those disasters that occurred at Feyzin in 1966, Flixborough in 1974, Dutch State Mines in 1975, Piper Alpha in 1988, Enschede in 2000, Toulouse in 2001, and Buncefield in 2005. Finally, the C_c dimension comprises scenarios like the Sandoz chemical spill in 1986, the dike breakage of Aznalcollar in 1998, the Baia Mare mining accidents in 2000, and the Kolontár red mud disaster in 2010, all of them with very long territorial range of their impacts on the environment.

For accurate classifications, the Seveso III Directive provides clear rules as outlined in Note 4, Note 5, and Note 6 of Annex I, which can also be applied to non-Seveso facilities. In brief, this note states that the hazardous substances (including wastes) potentially located in an establishment shall be provisionally assimilated into the most similar dangerous category or substance listed in Annex I 2012/18/EU. Therefore, if other substances are present, they must be considered in one of the three "C_s" categories.

A current limitation of the Seveso framework is the exclusion of potential synergies or interactions between substances in storage (Jain et al., 2017). Since this research is a first attempt to measure the major accident potential of both Seveso and non-Seveso facilities, the synergy between substances is beyond the scope. However, it represents an opportunity for enhancement in future work.

Moving to the quantity of hazardous substances stored in each facility, the index of compliance is used to calculate the ratio between the amount of hazardous substances stored and the corresponding threshold for each specific substance within each C_s category in line with Note 4 Annex I, of the 2012/18/EU Directive.

$$Q_{Cs} = \sum_{x=1}^{n} \frac{q_{x(s)}}{Q_{Ux(s)}} \tag{6.2}$$

where,

Q_{Cs}: is the total index of compliance for the addition of sub-categories of dangerous substances within each of the three C_s categories.

x: consist of an alphanumeric code to design any different entry within each subcategory in Column 1 of Part 1 or Part 2 of Annex I of 2012/18/EU Directive.

n: refers to the maximum number of "*x*" substances held in any subcategory.

$q_{x(s)}$: is the amount of hazardous substance "*x*" stored in the plant. The categories of substances are in correspondence with the list of substances present in Column 1 of Part 1 or Part 2 of Annex I of 2012/18/EU for substances classified in each C_s category.

$Q_{Ux(s)}$: is the corresponding upper threshold amount (UTE) for any "*x*" that is given in Column 3 of Part 1 or Column 3 of Part 2 of Annex I of 2012/18/EU.

The "*x*" in Eq. (6.2) can be written in the form "*sci*" (subcategory-kind of subcategory-consecutive number for different substances). For example, to differentiate two diverse substances in the dimension C_b (Physical hazards), within the explosive category, sub-categories "*b*", then, $C_{b(x)}=C_{b(sci)} \rightarrow C_{P1b1}$ (for the first substance) and C_{P1b2} (for the second substance). In this way, each substance can be identified in a univocal way.

Moreover, note 6 of Annex I of Seveso III offers criteria for hazardous substances that, due to their properties, rise to more than one C_s classification. For these cases, the lowest threshold quantities (critical) shall be applied for each group of categories (C_a, C_b, C_c) corresponding to the relevant classifications concerned.

Eq. (6.2) calculates a ratio between the stored substances and upper thresholds. Upper-tier establishments exist (UTE) when $Q_{Cs} \geq 1$, while if $Q_{Cs}<0.05$ for each C_s category, the establishment does not have the potential to cause a major accident, based on the consideration that the notification criterion established for the European Commission involves at least 5% of the upper threshold amount (UTE). Therefore, 0.05 represents the cutoff point for Major Accident Potential (MAPP). **Figure 6.7** generalizes the conceptual representation of the framework, including a colored decisional scale for Q_{Cs} *as a function of* $Q_{Ux(s)}$.

From a mathematical perspective, the compliance index Q_{Cs} can theoretically span the range (0; +∞). However, in practical terms, values beyond $Q_{Cs} \geq 2$ are not meaningful, given the evident higher criticality associated with this UTE. Conversely, when a plant falls within the interval [0.05; 1), while it exhibits potential for a major accident, the precise implications of Q_{Cs} within this range are less clear. Notably, this interval includes all lower-tier establishments as well as some other facilities.

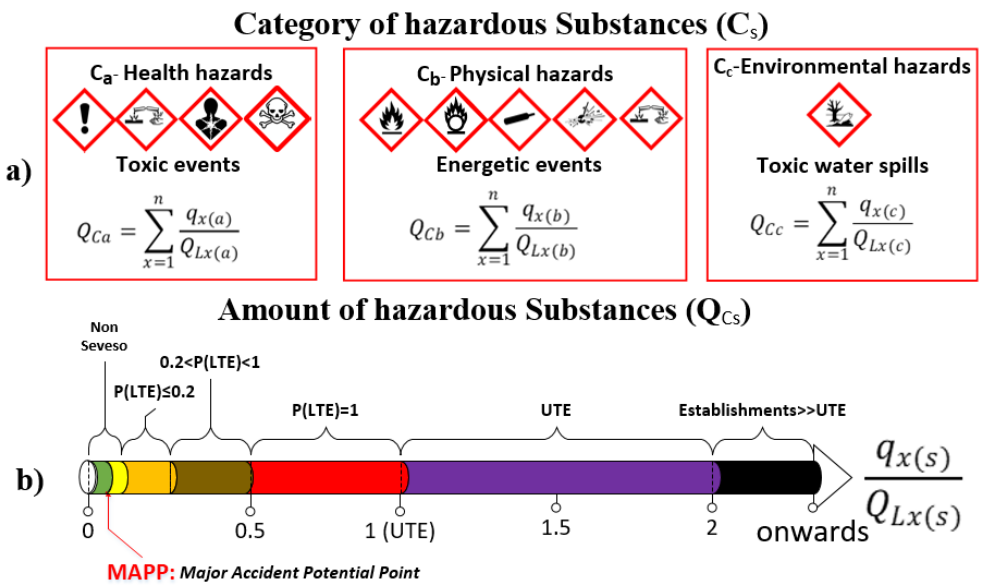

Figure 6.7: a) Framework representation for assessing the potentiality to cause major industrial accidents based on the dangerous substance criteria. *b)* Decisional scale for Q_{Cs} as a function of $Q_{Ux(s)}$.

To address this point, further analyses were conducted using regulatory data for the 69 threshold quantities listed in Columns 2 and 3 of Annex I in Directive 2012/18/EU. Linear relationships between upper and lower-tier thresholds, as well as their respective 5% (UTE) values, were examined. Additionally, the frequency of Q_{Cs} values within five classes in the interval (0; 1) was analyzed to assess the potential of lower-tier establishments and non-Seveso facilities to fall within each class.

For instance, all the plants in the intervals (0; 0.1) are non-Seveso establishments with 100% confidence. However, this interval is split into two groups: the minor risk facilities in the green zone (0; 0.05) with values

that are lower than the **Errore. L'origine riferimento non è stata trovata.**, and facilities in the yellow zone, which are non-Seveso but have the potential to cause a major accident within the range [0.05, 0.1).
Furthermore, in the interval in the orange zone [0.1; 0.25) not only might non-Seveso plants be located with the potential to cause major accidents but also there is a likelihood less than or equal to 20% to find LTE establishments depending on the presence of substances that have lower thresholds in this interval. Similarly, the interval in the brown zone [0.25; 0.5) might encompass non-Seveso plants but here the likelihood of LTE span between 20% and 1. Subsequently, just LTE can be found in the red zone interval [0.5; 1). From the purple zone and onwards (black zone) just UTE can be located [1; 2) and [2; onwards), as previously introduced.
The index of compliance should be calculated separately for each category of C_s (Q_{Ca}, Q_{Cb}, Q_{Cc}). The maximum Q_{Cs} value among Q_{Ca}, Q_{Cb}, and Q_{Cc} will be selected to characterize the highest potential to cause major industrial accidents, based on the dangerousness of the hazardous substance. Attention should still be given to the other categories if they obtain values that fall under color classes holding the potential of major accidents.
Table 6.2 presents the principal features for the hazardous substances stored in the same energetic infrastructure used to implement the ICI-MRD framework. Then, Q_{Ca}, Q_{Cb}, and Q_{Cc} were calculated and are presented in different ways in **Figure 6.8 a** and **b**, along with the reference scale $Q_{S(ref)}$.

Table 6.2 - Characterization of hazardous substances stored in the case study plant.

Hazardous substance	Hazard statements	$Q_{Ux(s)}$	$q_{x(s)}$	Q_{Cs}	C_s critical
Dense Fuel-Oil BTZ	H411, H226, H315	500	20000	40.0000	C_c
Automotive Diesel	H411, H226, H315	50000	100	0.0020	C_b

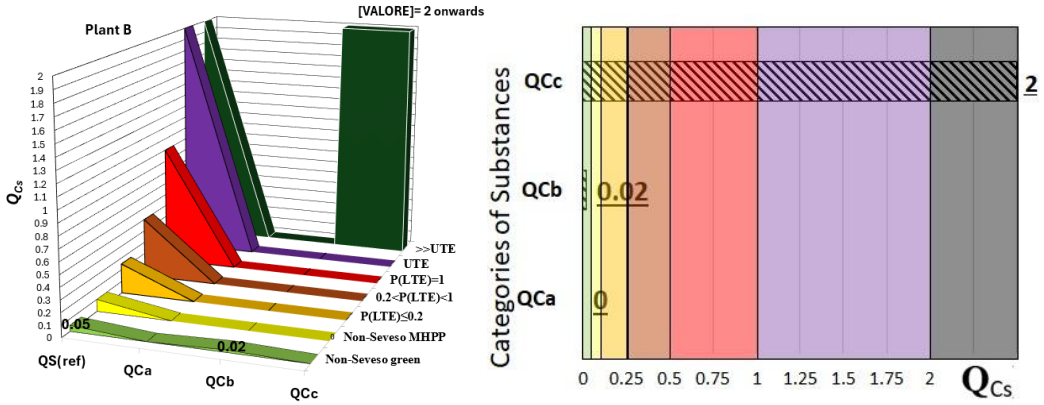

Figure 6.8: Different views for the reference scale of the Index of compliance $Q_{S(ref)}$ including each dimension of substance classification.

While any substances from the health hazards category were present, it can be appreciated how the quantified presence of substances belonging to the category of physical hazards falls under the minor risk facilities, even below the MAPP (0.02) (refer to **Figure 6.7**). On the contrary, the dimension of environmental hazard surpasses the upper bounded value for extremely critical UTE, which aligns with the high quantity of combustible stored in the power production plant for its transformation into energy. In conclusion, the results highlight the catastrophic consequences associated with chronic toxicity to aquatic life with long-lasting effects in case of a major accident involving the dangerous substances stored in this thermoelectric plant.
For the implementation of this index of major industrial accident based on the dangerous substance criteria in a different plant, refer to Castro Rodriguez (2025c).

6.3.3 Multi-risk NaTech decision matrix

As previously described, enhanced *Factor A* should not only provide a single global value reflecting multi-risk interactions between industrial infrastructure and hazards at a given location but also offer intermedium strategic advantages by introducing more sensitive rankings for contextualized industrial items and hazards, in columns and rows respectively, including cascading effects. Meanwhile, improved *Factor B* allows for a more detailed individual assessment of potential major industrial accidents based on hazardous substance criteria.

To integrate these refinements, a decision matrix combining the independent evaluations of both enhanced factors—represented as (A; B) cells—was introduced (refer to **Figure 6.9**). This approach facilitates risk assessment through a categorical decision scale with varying levels of risk tolerance, aligning with established criteria for decision matrices in NaTech research (Krausmann et al., 2011; Suarez-Paba and Cruz, 2022).

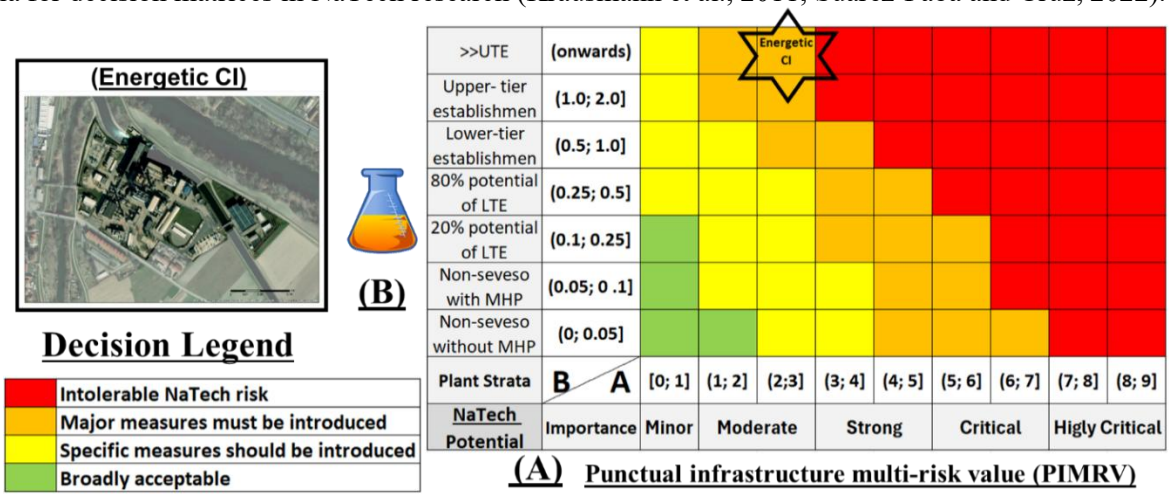

Figure 6.9: Multi-risk NaTech decision matrix.

Therefore, the comprehensive multi-risk NaTech evaluation depends on the global acceptability focus on the localization of the (A; B) cells. It guides the implementation of minor or major intervention strategies, which may be focused on retrofitting infrastructure to mitigate the impact of critical hazards and/or reinforcing safety barriers related to substance storage, including measures to improve inventory management.

In particular, the analyzed case study exhibits an orange code (2.06; 2), indicating that the implementation of strong measures is required. In this case, the decision is primarily influenced by the UTE substance condition (B entrance), as evidenced by the A entry (2.06), which is close to the minor importance level on the horizontal axis. In this regard, strong measures should be oriented to the management and control of the inventory of dangerous substances and internal technical measures in the plant, such as strengthening the safety barriers and redundant systems of contention.

Conversely, for a hypothetical plant registering the pair (A, B) = (7; 0.04), despite their substance condition belonging to non-Seveso without major hazard potential (MHP), the infrastructure factor dictates that the risk level will not be accepted. Therefore, major interventions would be necessary to mitigate the impacts of natural hazards or retrofit the vulnerable items exposed.

7. Potential multi-hazard scenarios for civil infrastructures

7.1 Multi-hazard scenarios approach for water distribution networks

7.1.1 Introduction

Water Distribution Networks (WDN) are critical infrastructures and essential services in modern society, supplying safe and reliable water to households, industries, and critical facilities. As lifeline infrastructures, their uninterrupted operation is crucial.

Natural hazards, exacerbated by climate change, represent an increasing concern for the resilience of critical infrastructures worldwide. Although – as evidenced in DV6.2.4 regarding the WDN – they may demonstrate strong performance under "business as usual" conditions due to effective infrastructure management by operators, the growing frequency and intensity of extreme weather events, floods, ground instabilities, and the existing elevated seismic risk could simultaneously affect multiple components, increasing the likelihood of unforeseen systemic operational failures. A single disruptive event can compromise service continuity.

As mentioned in Section 4.1.1, risks are not isolated. They often emerge in interconnected or cascading forms, where one hazardous event can trigger or amplify others. The interplay between hazards, often assessed independently, gives rise to multi-hazard scenarios – where the impact of one event is amplified or triggered by another – resulting in significantly more severe consequences.

An often-overlooked aspect is interdependency: each infrastructure relies on services provided by other infrastructures. While this potential vulnerability in emergencies has long been recognized, there are usually no systematic processes in place to investigate it in depth and proactively for each specific infrastructure. This can trigger cascading effects and also impair the execution of emergency plans.

This risk is especially pronounced in urban environments, where the close spatial concentration of multiple infrastructures adds geographical interdependences to existing logical and functional ones, and where human factors further link systems. In such contexts, one event may alter the probability, timing, or severity of another, magnifying disruption, hindering emergency response, and extending recovery times.

It must also be acknowledged that operators often lack tools to assess the challenges posed by climate change, as well as detailed knowledge of the current state of the critical infrastructures on which they depend. This lack of situational awareness means they are unaware of additional risks to which they are exposed and cannot accurately evaluate potential mitigation measures. Furthermore, hazards are often considered as independent from one another, when in reality a more reliable assessment should account for the occurrence of multiple, related hazardous events.

Understanding and anticipating these interrelated hazard dynamics is vital for effective WDN risk management. This is one of the purposes of the simulation environment developed within the RETURN framework, fully described in DV6.2.3, which has also been employed for the impact assessment of all possible single failure scenarios, as well as a citywide power blackout, as reported in DV6.2.4, while DV6.2.1 presented a literature review on interdependencies in the domain.

Although already valuable in supporting decision-makers to identify critical vulnerabilities and representing a small step beyond the state of the art, a comprehensive multi-hazard perspective would enable a broader analysis that could form the basis for robust strategies for prevention, preparedness, and mitigation.

This chapter introduces the concept of interrelated man-made and natural disasters in the context of WDN, showing how to set up the analysis and how to use the simulation environment developed in the RETURN framework to gain relevant insights.

7.1.2 Hazard categories, interrelations, and interdependencies in Water Distribution Networks

Water Distribution Networks (WDN) are vulnerable to a broad range of natural hazards, fully analysed in DV6.2.3 along with the modelling approach used to incorporate them into infrastructure behaviour and the selected fragility functions. With the restriction that treatment plants are not considered by our research group, seismic activity can rupture pipelines, damage pumping stations, and impair storage reservoirs. Ground shaking and soil liquefaction may also cause misalignment of pipelines and structural failures. Ruptured pipelines can allow infiltration of polluted groundwater or sewage into the network (O'Rourke and Jeon, 1999; O'Rourke et

al., 2016). Subsidence can damage buried pipelines and associated facilities, again creating pathways for contamination. Floodwaters can damage pumping facilities and cause contamination from surface runoff or sewer overflows. They can also damage industrial storage facilities located near water sources, releasing hazardous substances into the WDN (US EPA, 2014). Although not implemented in the simulation environment, prolonged water scarcity can strain supply capacity, reduce system pressure, and increase the concentration of contaminants.
Man-made hazards include both accidental and intentional threats, localized or widespread. Accidental local failures (e.g., road works) are discussed in DV6.2.1; although problematic from an operational perspective, DV6.2.4 shows that such single failures rarely cause systemic crises and, whenever relevant, will be addressed through targeted mitigation. The same is generally true for intentional local events, as network robustness typically confines the failure locally. Unintentional widespread events, if they do not impair the network, can often be recovered quickly. A different situation arises with cyber-attacks targeting SCADA and other control systems, potentially disrupting operations or altering water quality parameters (Cardenas et al., 2008; Humayed et al., 2017), or with intentional contamination as an act of sabotage. Cyber-attacks could disable all pumping stations, producing effects similar to a power blackout, thus falling under the scenarios already discussed in DV6.2.4. Water quality issues are not addressed in this study and may be considered for future work.
Natural hazards are particularly critical as they can simultaneously affect many components. Hazards rarely act in isolation; they can influence each other through various mechanisms, creating interrelated or cascading effects that amplify their overall impact. For example, an earthquake may cause both structural damage and a chemical spill, or a flood may disable treatment facilities and trigger contamination events.
Interrelations in WDN hazards can be broadly classified as:

- **Sequential**: One hazard follows another, with the first acting as a trigger (Gill & Malamud, 2014).
- **Simultaneous**: Multiple hazards occur at the same time, compounding their effects (Kappes et al., 2012).
- **Compound**: Hazards interact over time, with feedback loops amplifying consequences (Zscheischler et al., 2018).

Interdependency also plays a major role in systemic crises. A critical example is a power outage, which can halt pumping operations and limit water availability for firefighting or cooling critical facilities (U.S. DoE, 2014) as well as lead to loss of communication systems, which in turn can hinder operational coordination and timely public warnings (Pant et al., 2016), especially if it results from earthquakes or floods that have also damaged roads or bridges, delaying repairs and prolonging downtime (AWWA, 2018).

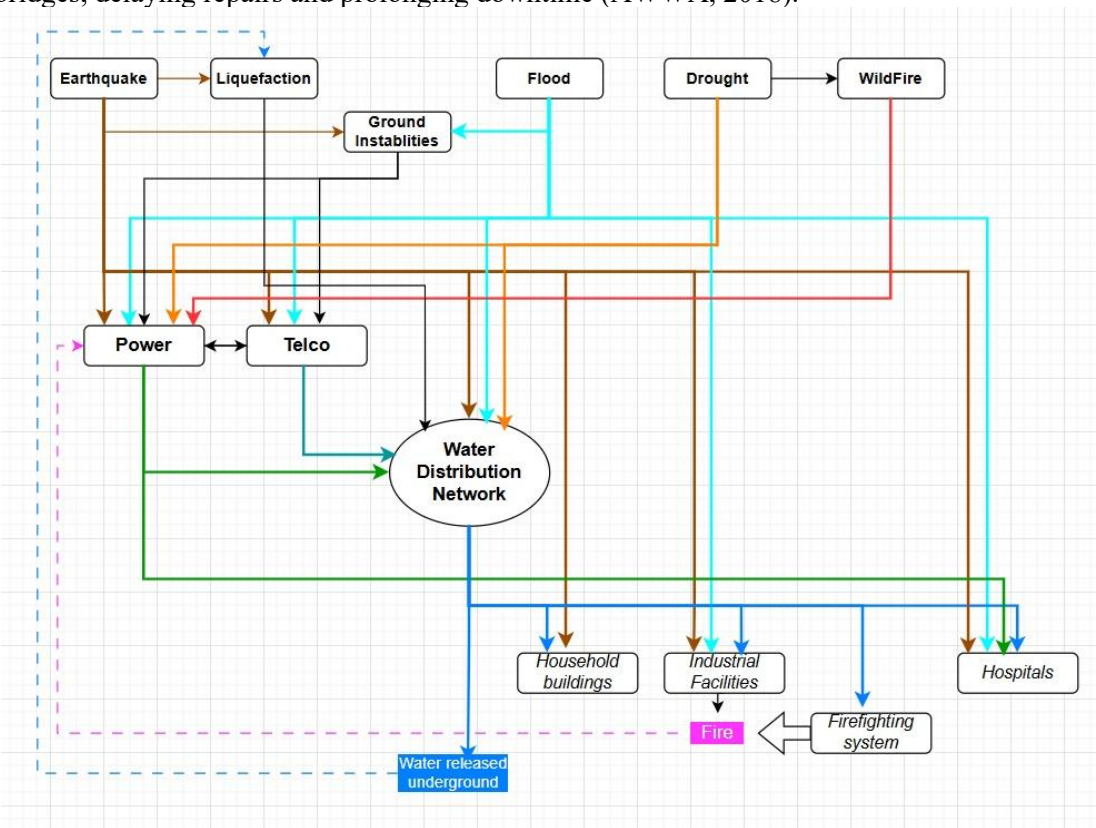

Figure 7.1: Interdependencies between hazards, infrastructures, and the Water Distribution Network (WDN).

Figure 7.1 provides a simplified overview of the main interdependencies between natural hazards, critical infrastructures, and the WDN, as well as potential cascading effects on end users. Natural hazards such as earthquakes, liquefaction, floods, droughts, and wildfires can directly affect the WDN or indirectly impair its operation through impacts on supporting infrastructures such as the power supply and telecommunications systems. These infrastructures are themselves interdependent, and their disruption can further reduce WDN performance. The WDN supplies households, industrial facilities, and hospitals, which can also be directly affected by both natural hazards and failures in power and telecommunications. The figure also highlights secondary effects and feedback loops, such as underground water release contributing to ground instabilities, and the reliance of firefighting systems on WDN functionality, which would be critical to avoid further escalation of a NaTech event. Direct impacts from natural hazards, infrastructure-to-infrastructure dependencies, flows from the WDN to consumers, and feedback mechanisms clearly show how interconnected vulnerabilities can amplify the consequences of multi-hazard events.

7.1.3 Quantitative simulation-based approach for multi-hazard scenarios in WDS

Estimating multi-hazard scenarios for Water Distribution Systems (WDS) requires an integration framework capable of capturing complex interdependencies. We adopted a quantitative approach based on simulation models: the hydraulic model was modified to incorporate the effects of natural hazards and can be coupled with hazard propagation models to estimate system performance under multi-hazard stress. In our case, hazard propagation is addressed by the VS1, VS2, and VS3 teams. To facilitate knowledge exchange, verification, and trust in the analysis results, we interfaced a commercial simulator to run the hydraulic model, as fully described in DV6.2.3.

While DV6.2.4 presented an extensive analysis aimed at identifying weak points in the system and estimating the consequences of failures, the same system can also assess multiple combinations of multi-hazard scenarios, even leveraging previously identified vulnerabilities as worst-case conditions.

Scenarios can be provided as inputs or generated automatically. Given the automated nature of the system, a large number of simulations can be performed. The performance metrics were agreed with the operator but can be easily adjusted, as all parameters from each simulation are recorded in an Excel file. Relevant simulations can be replayed for further manual analysis.

The speed and efficiency of the automated process – each simulation requires only 1-3 minutes depending on complexity, with data outputs of just a few megabytes – allow for a different perspective: considering the "unthinkable" and events that have never occurred before. If an event has already occurred, operators may have gained experience and taken action; history shows, however, that there is always a first time, or that something unforeseen may happen. Moreover, any user can propose a scenario or simulate a past event, then review the crisis evolution step by step, or implement and evaluate the effects of mitigation and prevention measures.

As suggested in **Figure 7.1**, relevant analyses merit a second iteration – manual or automatic, potentially handled by the Knowledge Graph module – to account for second-order or feedback effects. For example, during an earthquake, some end users may be marked as "unserved," but if their building collapsed there is no longer an end user. Similarly, multiple pipe breaks might release enough water to set the stage for liquefaction and further building collapse. In a "business as usual" contingency management, the operator would take actions to isolate the failure, for example closing valves to stop the breakflow, but the preparedness plan needs to take into account the chance the telco system or the power network, mandatory to operate the WDN, may not work being affected by the same natural event.

The simulation environment can also estimate the firefighting system status. This is critical because fires often emerge as the most likely scenario in NaTech incidents (as noted in Section 5.1.1), and are common in cases such as gas pipeline ruptures during earthquakes. It is therefore possible to evaluate the probability of hydrants being unavailable, which could jeopardize emergency plans.

By automatically generating and varying a high number of scenarios, it is possible to shortlist those situations that place the infrastructure or system at risk – similar to pruning an event tree – and then reverse engineer all the sequence of events that could lead to such situations, taking into account probabilities where relevant.

By combining these approaches, WDS operators and planners can better anticipate the range of possible multi-hazard scenarios, assess their likelihood and impacts, and prioritize investments in resilience measures.

8. Conclusions

Potential multi-hazard scenarios for transportation infrastructures

The multi-hazard approach presented in Section 4.1 highlights the importance of an integrated probabilistic analysis for risk assessment in transportation infrastructures, with a specific focus on road and railway tunnels. The combined use of fault tree and event tree analyses within a bow-tie framework enables a structured modelling of initial critical events and cascading progressions, accounting for interactions among fires, seismic events, and structural collapses. The integration of vulnerability models, individual and societal risk indicators, and acceptability criteria based on the ALARP principle provides a robust methodological basis for informed safety-oriented decision-making.

The case study of the San Benedetto tunnel illustrates the relevance of the proposed approach in real-world contexts, emphasizing the need for design and management strategies capable of addressing complex and synergistic events. In a country like Italy, characterized by high seismicity and a dense and vulnerable infrastructure network, the adoption of multi-hazard methodologies is not merely a technical enhancement, but a necessity to ensure infrastructure resilience and user safety.

Regarding the seismic risk assessment for transportation infrastructures (bridges, in particular), a brief description of the main steps that need to be taken into account by risk practitioners is provided. In particular, the section focuses on how to compute the seismic hazard, on the main methods for computing the structural fragility and how to retrieve consequences for a complete risk assessment. Accordingly, the main references are provided

Characterization of industrial vulnerabilities facing NaTech events

A two-phase methodological procedure for improving the identification of industrial vulnerabilities was designed and tested in two cases of studies.

Case 1 focuses on industrial events triggered by natural hazards using as a pilot factor the lightning-triggered NaTech. The data collection covered the source selection, dataset setup, and technical criteria. A lightning-triggered NaTech driven dataset was built encompassing 689 records. Moving to the data analysis phase. It comprises the event overall characterization and modeling. The characterization part showed that 80% of lightning-triggered NaTech caused serious events, mostly in the "chemical and petrochemical" macro-sector during plant operations. The most damaged categories were "storage equipment" and "electric and electronic devices," with fire being the most likely cause. In the Part-2, quantitative modelling techniques were used to raise vulnerability awareness. Using smaller datasets for event tree analysis makes it easy to understand how event routes work, from the first natural element to branches with more specific outcomes. Bayesian network techniques upgrade the event tree model, allowing for the addition of more variables. They provide a robust methodology to analyze complex conditional interactions, providing a significant secondary perspective for unclassifiable data, which is characteristic of open-source industrial accident databases. The calculations from the Bayesian network show that "equipment involved" was the pivotal variable in the model for figuring out the conditional probabilities, with other important factors such as the source of damage, the infrastructural damage state, the final scenario, or the industrial macro-sector.

Case study 2 focuses on industrial events triggered by material degradation. The first phase of data collection involved the development of a dataset, in line with the previous case, consisting of 3,772 incidents within the process industry and caused by material degradation and infrastructure ageing. The analysis confirmed that corrosion is the most widespread failure mechanism in industrial environments, highlighting the need for improved material monitoring and treatment, particularly in the chemical, petrochemical and pipeline sectors. Over 90% of accidents involve loss of containment, which is a major cause of accidents in the process industry. Event tree analysis revealed that for corroded equipment in case of incident there is 50% probability of causing environmental contamination. Due to significant data uncertainty, Bayesian networks were used, to increase

vulnerability awareness. This enhanced data consistency, providing a clearer understanding of the risk factors and their interactions. The analysis revealed an increased probability of environmental contamination and toxic gas dispersion, while the likelihood of fires and explosions decreased.

The procedure, in general, provides novel insights that constitute a significant methodological contribution, which could be applied globally to address the impact of multiple hazardous events on industrial facilities. These findings represent a crucial input that should be linked to the spatial analysis concerning the plant location.

Interaction between H_2 and H_2/CH_4 mixture release consequences and natural events

The comparative analysis of the results obtained with two different tools highlights how the accuracy of consequence predictions for hydrogen-rich gas releases depends strongly on the modeling approach used. Empirical methods, while suitable for fast assessments, tend to overestimate hazard distances due to their simplified assumptions. PHAST improves on this by incorporating more detailed physical models, offering realistic estimates of flame geometry, heat flux, and dispersion behavior. CFD simulations, although more computationally intensive, provide the most accurate depiction of transient and buoyancy-driven effects, particularly relevant for light gases like hydrogen. Overall, while all methods show consistent trends with increasing hydrogen content, the quantitative differences underline the importance of selecting the appropriate model based on the required level of detail and the specific objectives of the safety analysis.

In the context of distribution networks, the interaction between extreme natural events and the structural integrity of pipelines represents a critical area of investigation. Fault Tree Analysis (FTA) and Event Tree Analysis (ETA), complementary methodologies that allow a comprehensive risk assessment from both the perspective of triggering causes and the consequential developments of incident events, are the most effective tools for analysing the causes and consequences of failure.

Parametric framework for seismic fragility assessment of industrial steel pallet racks

This study developed and applied a robust and scalable methodology to quantify the seismic fragility of unbraced industrial pallet racks – non-structural systems whose failure can severely compromise safety, operational continuity, and supply chain resilience in industrial environments. By analysing a comprehensive parametric stock of 27 rack configurations through 3D nonlinear finite element modelling and cloud-based dynamic simulations, the research addressed both structural variability and local soil effects. Fragility models were derived using multiple Engineering Demand Parameters (EDPs) and conditioned on two key seismic intensity measures (IMs): peak ground acceleration (PGA) and spectral acceleration (S_a).

Under full-load conditions, these racks exhibited pronounced seismic vulnerability. The narrow separation between yielding (DS2) and Collapse fragility curves reflects a brittle seismic response governed by low redundancy and limited energy dissipation capacity. Among the EDPs, the global strain in uprights (ε^*) proved to be the most effective in predicting collapse. It consistently governed the onset of failure across configurations and soil types, highlighting its relevance as a synthetic indicator of global instability. Other EDPs, such as down-aisle drift (θ_X) and joint rotations (φ_{btc}, φ_{base}), provided complementary insights into local mechanisms but were less effective in identifying collapse onset. While PGA is commonly used for seismic risk mapping at territorial scale due to its simplicity and structural independence, PGA-based fragility curves showed significant sensitivity to local soil conditions, leading to less reliable fragility estimates. In contrast, S_a-based fragility curves yielded more stable predictions across both rigid and soft soils, making them more suitable for consistent seismic risk evaluation at regional scale.

Overall, the methodology and findings presented in this study provide a solid foundation for performance-based assessment and mitigation of seismic risk in industrial storage facilities. The proposed fragility models are well-suited to support risk-informed decision-making at multiple scales –from individual warehouses to large industrial districts– and can be extended to assess alternative rack typologies or retrofit strategies. As such, they contribute to the development of efficient tools for enhancing the seismic resilience of critical logistics infrastructure.

Industrial multi-hazard deployment index

This work consolidates a comprehensive framework for the multi-risk Natech assessment of critical industrial infrastructures, addressing the complex interactions between natural hazards, vulnerable industrial elements, and major accident potential based on the hazardous substances criteria in line with European regulations.

The framework enables the identification of a bidimensional areas for intervention through a decision matrix that combines infrastructure vulnerability (Factor A) and hazardous substance criteria (Factor B), supporting four levels of decision. The application of this methodology in a case study within the energy sector demonstrates the utility of this methodology to support the preparedness of critical infrastructures and complex systems. This highlights the necessity for targeted risk mitigation strategies, particularly focusing on retrofitting the critical assets, strengthening of safety barriers, and hazardous substance management.
Moreover, the developed methodology offers a flexible structure for adapting to various industrial contexts, supporting decision-makers in designing prevention and protection measures consistent with the principles of resilience promoted by the Sendai Framework and forthcoming European regulations on the resilience of critical entities and interacting with **DV 5.3b**. Ultimately, this research provides valuable insights for regulators, policymakers, and industry stakeholders to improve multi-risk NaTech governance, ensuring more robust and adaptive critical infrastructure systems in the face of evolving multi-hazard scenarios.

Multi-hazard scenarios approach for water distribution networks

Water Distribution Networks (WDN) are critical lifeline infrastructures, exposed to a broad range of natural and man-made hazards whose effects are often interrelated and amplified through cascading impacts and infrastructure interdependencies. The simulation-based quantitative approach developed within the RETURN framework enables large-scale, automated scenario generation and analysis, capturing both direct impacts and complex feedback mechanisms. This capability supports the exploration of “unthinkable” events, reverse-engineering of event sequences, and testing of mitigation strategies under realistic multi-hazard conditions. By providing actionable insights – such as potential loss of firefighting capability, crucial during emergencies – the approach helps operators and planners to identify critical vulnerabilities, prioritize resilience investments, and enhance preparedness for rare but high-consequence scenarios.

9. References

Section 4

Argyroudis, S.A., Mitoulis, S.A., Hofer, L., Zanini, M.A., Tubaldi, E., Frangopol, D.M. (2020). Resilience assessment framework for critical infrastructure in a multi-hazard environment: Case study on transport assets. *Science of the Total Environment* 714, 136854, https://doi.org/10.1016/j.scitotenv.2020.136854.

Badr, A., Li, Z., El-Dakhakhni, W. (2024). Probabilistic dynamic resilience quantification for infrastructure systems in multi-hazard environments, *International Journal of Critical Infrastructure Protection* 46, 100698, https://doi.org/10.1016/j.ijcip.2024.100698.

Baker, J.W. (2015), Efficient analytical fragility function fitting using dynamic structural analysis, *Earthquake Spectra* 31(1), 579-599. https://doi.org/10.1193/021113EQS025M

Baker, J.W., Bradley, B.A., Stafford, P. J. (2021). *Seismic Hazard and Risk Analysis*. Cambridge University Press, Cambridge, England.

Calvi, G.M., Pinho, R., Magenes, G., Bommer, J.J., Restrepo-Vélez, L.F., Crowley, H. (2006). Development of seismic vulnerability assessment methodologies over the past 30 years, *ISET Journal of Earthquake Technology* 43(3), 75–104, https://doi.org/10.63898/BUSY2147

Chen, A., Yang, H., Lo, H.K. Tang, W.H. (2002). Capacity reliability of a road network: An assessment methodology and numerical results, *Transportation Research Part B: Methodological* 36(3), 225-252. https://doi.org/10.1016/S0191-2615(00)00048-5.

Cornell, C. (1968). Engineering seismic risk analysis. *Bulletin of the Seismological Society of America* 58(5), 1583–606, https://doi.org/10.1785/BSSA0580051583

Deng, L., Wang, W., Yu, Y. (2016). State-of-the-Art review on the causes and mechanisms of bridge collapse, *Journal of Performance of Constructed Facilities* 30 (2), 04015005. https://doi.org/10.1061/(ASCE)CF.1943-5509.0000731

Ellingwood, B.R. (2001). Reliability-based condition assessment and life prediction of civil structures, *Reliability Engineering & System Safety* 74(3), 263–274.

Frangopol, D.M., Liu, M. (2007). Maintenance and management of civil infrastructure based on condition, safety, optimization, and life-cycle cost, *Structure and Infrastructure Engineering* 3(1), 29–41. https://doi.org/10.1080/15732470500253164

Grossi P., Kunreuther H., Patel C.C. (2005) *Catastrophe Modelling: A New Approach to Modelling Risk*, Springe + Bussiness Media, Inc. DOI: 10.1007/b100669

Guarascio, M. (2021). "As Low as Reasonably Practicable": How does it work in the rail and road tunnels in Italian rules. Risk acceptability/tolerability criteria. The Gu@larp Model; WIT Press Transactions on The Built Environment: Billerica, MA, USA; Volume 206, p xvii [Published 2022].

Guarascio, M., Lombardi, M., Rossi, G., Sciarra, G. (2007). Risk analysis and acceptability criteria; WIT Transactions on the Built Environment: Billerica, MA, USA, pp. 131.

Hofer, L., Toska, K., Zanini, M.A. (2023). Impact of epistemic and aleatory uncertainties on the seismic Reliability assessment of existing structures, *Structures* 57, 105235. https://doi.org/10.1016/j.istruc.2023.105235

International Organization for Standardization (ISO), 'ISO 31000: Risk management – Guidelines', International Organization for Standardization, Geneva, 2018. [Online]. Available: https://www.iso.org/standard/65694.html

Jalayer, F. (2003). Direct Probabilistic Seismic Analysis: Implementing Non-Linear Dynamic Assessments. Ph.D. Thesis, Dept. of Civil and Environmental Engineering, Stanford University, Stanford, CA.

Kim, S.H., Shinozuka, M. (2004). Development of fragility curves of bridges retrofitted by column jacketing, *Probabilistic Engineering Mechanics* 19(1–2), 105–112. https://doi.org/10.1016/j.probengmech.2003.11.009

Kong, J., Simonovic, S.P., Zhang, C. (2019). Sequential hazards resilience of interdependent infrastructure system: A case study of Greater Toronto area energy infrastructure system, *Risk Analysis* 39, 1141-1168. https://doi.org/10.1111/risa.13222.

Lee, R., Kiremidjian, A.S. (2007). Uncertainty and correlation for loss assessment of spatially distributed systems, *Earthquake Spectra*, 23(4), https://doi.org/10.1193/1.2791001

Legislative Decree of October 5, 2006, No. 264: Implementation of Directive 2004/54/EC on minimum safety requirements for tunnels in the trans-European road network. Normattiva, 2006. Available: https://www.normattiva.it/uri-res/N2Ls?urn:nir:stato:decreto.legislativo:2006-10-05;264

Liu, B., Siu, Y.L., Mitchell, G. (2016). Hazard interaction analysis for multi-hazard risk assessment: A systematic classification based on hazard-forming environment, *Natural Hazards and Earth System Sciences* 16(2), 629-642.

Lombardi, M., Libertà, A.,Berardi, D., Di Benedetto, E., Guarascio, M. (2021). Concepts and operational tools for multihazard risk analysis in road tunnels: the San Benedetto event, Italy. WIT Press Transactions on The Built Environment: Billerica, MA, USA; Volume 206, pp. 229-239 [Published 2022]. DOI:10.2495/safe210191.2021

McGuire, R.K. (1995). Probabilistic seismic hazard analysis and design earthquakes: closing the loop, *Bulletin of the Seismological Society of America* 85(5), 1275-1284 https://doi.org/10.1785/BSSA0850051275

Ouyang, M. (2014). Review on modeling and simulation of interdependent critical infrastructure systems, *Reliability Engineering & System Safety* 121, 43-60. https://doi.org/10.1016/j.ress.2013.06.040.

Porter, K., Kennedy, R., Bachman, R. (2007), Creating fragility functions for performance-based earthquake engineering, *Earthquake Spectra* 23(2), 471–489. https://doi.org/10.1193/1.2720892

Shafei, B., Zareian, F., Lignos, D. G. (2011). A simplified method for collapse capacity assessment of moment-resisting frame and shear wall structural systems, *Engineering Structures* 33(4), 1107–1116. https://doi.org/10.1016/j.engstruct.2010.12.028

Sokolov, V., Wenzel, F. (2010). Influence of spatial correlation of strong ground motion on uncertainty in earthquake loss estimation, *Earthquake Engineering and Structural Dynamics* 20(2), 523–553, https://doi.org/10.1002/eqe.1074

Vamvatsikos, D., Cornell, C.A. (2004). Applied incremental dynamic analysis, *Earthquake Spectra* 20(2), 523–553. https://doi.org/10.1193/1.1737737

Villaverde, R. (2007). Methods to assess the seismic collapse capacity of building structures: State of the art, *Journal of Structural Engineering* 133(1), 57–66.

Wisetjindawat, W., Kermanshah, A., Derrible, S., Asce, A.M., Fujita M. (2017). Stochastic modeling of road system performance during multihazard events: Flash floods and earthquakes, *Journal of Infrastructure System* 23 (4), 04017031. https://doi.org/10.1061/(ASCE)IS.1943-555X.0000391.

Zanini, M.A., Faleschini, F., Pellegrino, C. (2017). Probabilistic seismic risk forecasting of aging bridge networks, *Engineering Structures* 136, 219-232, https://doi.org/10.1016/j.engstruct.2017.01.029

Zanini, M.A., Hofer, L. (2019). Center and Characteristic Seismic Reliability as new indexes for accounting uncertainties in seismic reliability analysis, *Soil Dynamics and Earthquake Engineering* 123, 110-123. https://doi.org/10.1016/j.soildyn.2019.04.8

Zhou, Y., Banerjee, S., Shinozuka, M. (2011). Socio-economic effect of seismic retrofit of bridges for highway transportation networks: a pilot study, *Structure and Infrastructure Engineering* 6 (1–2), 145-157.

Section 5

Bearfield, G., Marsh, W. (2005). Generalising event trees using Bayesian networks with a case study of train derailment, in: Winther, R., Gran, B.A., Dahll, G. (Eds.), *Computer Safety, Reliability, and Security, Lecture Notes in Computer Science*. Springer, Berlin, Heidelberg, pp. 52–66. https://doi.org/10.1007/11563228_5

Bernardi, E., Donà, M., Tan, P., da Porto, F. (2023). Optimal design method of the load-level isolation system for industrial steel racking. *Journal of Constructional Steel Research* 210, 108096. https://doi.org/10.1016/j.jcsr.2023.108096

Bernuzzi, C., Castiglioni, C.A. (2001). Experimental analysis on the cyclic behaviour of beam-to-column joints in steel storage pallet racks. *Thin-Walled Structures* 39(10), 841-859.

British Standards Institution (2017). Protection against lightning Part 1: General principles. BS EN 623051:2011. Implementation of CENELEC corrigendum November 2016.

Candreva, F., Houari, M. (2013). Plant screening for ageing impact in the process industry. *Chemical Engineering Transactions* 31, 253–258. https://doi.org/10.3303/CET1331043

Capasso, E., Di Domenico, A., Portarapillo, M., Di Benedetto, A. (2025). CFD-based risk analysis in Natech scenarios for hythane pipelines. *International Journal of Hydrogen Energy* 137, 665–678. https://doi.org/10.1016/j.ijhydene.2025.05.105

Casal, J. (2008). *Evaluation of the Effects and Consequences of Major Accidents in Industrial Plants.* Industrial safety series. Elsevier Science, Vol. 8.

Casson Moreno, V., Reniers, G., Salzano, E., Cozzani, V. (2018). Analysis of physical and cyber security-related events in the chemical and process industry. *Process Safety and Environmental Protection* 116, 621–631. https://doi.org/10.1016/j.psep.2018.03.026

Castro Rodriguez, D.J., Tufano, C., Vitale, M., Mietkiewicz, J., Baldissone, G., Barresi, A., Demichela, M. (2023). Dataset: NaTech events triggered by lightning within the process industry. Mendeley Data, V1, doi: 10.17632/fff64w3rzn.1, https://data.mendeley.com/datasets/fff64w3rzn/1

Castro Rodriguez, D.J., Mietkiewicz, J., Vitale, M., Baldissone, G., Demichela, M., Barresi, A.A. (2024). NaTech triggered by lightning: Novel insights from past events in the process industry. *Heliyon* 10 (2024), e31610. https://doi.org/10.1016/j.heliyon.2024.e31610

Castro Rodriguez, D.J., Barresi, A.A., Demichela M. (2025). Resilience-based framework for enhancing NaTech risk management in industrial critical infrastructures. *Journal of Environmental Systems and Decisions*. Under review. PREPRINT available at Research Square https://doi.org/10.21203/rs.3.rs-5937501/v1

Cazenave, P., Jimenez, K., Krishnamurthy, R., Shall, Z. (2024). Improvement of ILI sizing accuracy for problematic corrosion profiles: A PRCI/PHMSA project. *Proceedings of the 2024 15th International Pipeline Conference*. Volume 2B: Pipeline and Facilities Integrity. Calgary, Alberta, Canada. September 23–27, 2024. V02BT03A042. ASME. https://doi.org/10.1115/IPC2024-134089

CEN (European Committee for Standardization). (2005). EN 1993-1-1. Eurocode 3: Design of steel structures – Part 1-1: General rules and rules for buildings. Brussels: CEN.

CEN (European Committee for Standardization). (2016). EN 16681. Steel Static Storage Systems – Adjustable Pallet Racking Systems – Principles for seismic design. Brussels: CEN.

CEN (European Committee for Standardization). (2020). EN 15512. Steel Static Storage Systems – Adjustable Pallet Racking Systems – Principles for structural design. Brussels: CEN.

Center for Chemical Process Safety (CCPS). 1999. *Guidelines for Chemical Process Quantitative Risk Analysis*, 2nd Edition.

Cheng, Y., Luo, Y. (2021). Analysis of NaTech risk induced by lightning strikes in floating roof tanks based on the Bayesian network model. *Process Safety Progress* 40, e12164. https://doi.org/10.1002/prs.12164

Crowl, L. (2002). *Chemical Process Safety: Fundamentals with Applications,* 2nd Ed. Pearson

Davis, J.R. (2000). *Corrosion: Understanding the Basics*. ASM International, Chapter 2: Basic Concepts Important to Corrosion. https://doi.org/10.31399/asm.tb.cub.9781627082501

Donà, M., Bizzaro, L., Carturan, F., da Porto, F. (2019). Effects of business recovery strategies on seismic risk and cost-effectiveness of structural retrofitting for business enterprises. *Earthquake Spectra* 35(4), 1795–1819.

Donà, M., Bernardi, E., Zonta, A., Ceresara, M., da Porto, F. (2022). Effectiveness of load-level isolation system for pallet racking systems. *Frontiers in Built Environment* 8, 944026. https://doi.org/10.3389/fbuil.2022.944026

Donà, M., Piredda, G., Zonta, A., Bernardi, E., da Porto, F. (2024). Seismic fragility of unbraced industrial steel pallet racks. *Structural Safety* 110, 102497. https://doi.org/10.1016/j.strusafe.2024.102497

Donà, M., Piredda, G., Zonta, A., Ceresara, M., da Porto F. (2025a). Seismic fragility models for unbraced steel pallet racks, in: Jie Yang, Jiyang Fu, A. Liu, A. Ching-Tai Ng (eds.), *Proc. of 1st International Conference on Engineering Structures (ICES 2024)*, Guangzhou, China, Nov. 8–11, 2024. *Lecture Notes in Civil Engineering*, Vol. 599, 1–11. https://dx.doi.org/10.1007/978-981-96-4698-2_137

Donà, M., Zonta, A., Bernardi, E., Piredda, G., da Porto F. (2025b), Seismic fragility of a stock of unbraced pallet racks considering events on amplifying soils, in: M. Papadrakakis, M. Fragiadakis (eds.), *Proc. of 10th ECCOMAS Thematic Conference on Computational Methods in Structural Dynamics and Earthquake Engineering (COMPDYN 2025)*, Rhodes, Greece, June 15-18, 2025.

Drei, A., Rovere, L., Vayas, I., Jehin, D. et al. (2014). Seismic behaviour of steel storage pallet racking systems (SEISRACKS2): Final report. European Commission, Directorate-General for Research and Innovation. Publications Office. https://data.europa.eu/doi/10.2777/686466.

Fehring, T., Reynolds, T. (2021). *Boiler and Pressure Vessel Safety. Chronicles of Mechanical Engineering in the United States* (Ed. Fehring, TH, and Reynolds, TS.). ASME, 2021. pp. 93-124. https://doi.org/10.1115/1.356056_ch4

Gabbianelli, G., Francesco, C., Nascimbene, R. (2020). Seismic vulnerability assessment of steel storage pallet racks. *Ingegneria Sismica* 37(2), 18-40.

Hansler, R.J., Bellamy, L.J., Akkermans, H.A. (2022). Ageing assets at major hazard chemical sites–The Dutch experience. *Safety Science* 153, 105788. https://doi.org/10.1016/j.ssci.2022.105788

Hao, J., Liu, L., Long, Z., Chu, Y., Zhang, D., Chen, X., Huang, C. (2023). Scenario deduction of NaTech accident based on dynamic Bayesian network: A case study of landslide accident in a liquor storage tank area in Guizhou Province, China. *Journal of Loss Prevention in the Process Industries* 83, 105067. https://doi.org/10.1016/j.jlp.2023.105067

Horrocks, P., Mansfield, D., Parker, K., Thomson, J., Atkinson, T., Worsley, J., Park, B. (2010). Managing ageing plant. HSE, Warrington, UK, Technical Report 823.

Hugin Expert A/S (2023). Hugin software (Version 9.3) [Computer software]. Available from https://www.hugin.com

Jalayer, F., Ebrahimian, H., Miano, A., Manfredi, G., Sezen, H. (2017). Analytical fragility assessment using unscaled ground motion records. *Earthquake Engineering & Structural Dynamics* 46 (15), 2639-63.

Khakzad, N., Van Gelder, P. (2018). Vulnerability of industrial plants to flood-induced NaTechs: A Bayesian network approach. *Reliability Engineering & System Safety* 169, 403–411. https://doi.org/10.1016/j.ress.2017.09.016

Kjærulff, U.B., Madsen, A.L. (2013). *Bayesian networks and influence diagrams: A guide to construction and analysis, information science and statistics*. Springer, New York, NY. https://doi.org/10.1007/978-1-4614-5104-4

Krausmann, E., Renni, E., Campedel, M., Cozzani, V. (2011). Industrial accidents triggered by earthquakes, floods and lightning: lessons learned from a database analysis. *Natural Hazards* 59, 285–300. https://doi.org/10.1007/s11069-011-9754-3

Lauritzen, S.L. (1995). The EM algorithm for graphical association models with missing data. *Computational Statistics & Data Analysis* 19, 191–201. https://doi.org/10.1016/0167-9473(93)E0056-A

Li X., Ma X., Zhang J., Akiyama E., Wang Y., Song X. (2020). Review of hydrogen embrittlement in metals: hydrogen diffusion, hydrogen characterization, hydrogen embrittlement mechanism and prevention, *Acta Metallurgica Sinica* (English Letters) 33, 759–773.

Manfredi, V., Masi, A., Özcebe, A. G., Paolucci, R., Smerzini, C. (2022). Selection and spectral matching of recorded ground motions for seismic fragility analyses. *Bulletin of Earthquake Engineering* 20, 4961–4987. https://doi.org/10.1007/s10518-022-01393-0.

Margaritis, D. (2003). Learning Bayesian network model structure from data (PhD Thesis). School of Computer Science. Carnegie Mellon University, Pittsburgh, PA15213.

Marrazzo, R., Vazzana, F. (2021). The aging challenge of hazardous installations in Italy accidents result of inspections and good practices, in: *Proceedings of the 31st European Safety and Reliability Conference (ESREL)*, 19-23 September 2021, pp 2548–2554. https://doi.org/10.3850/978-981-18-2016-8 444-cd.

Milazzo, M.F., Bragatto, P. (2019). A framework addressing a safe ageing management in complex industrial sites: The Italian experience in «Seveso» establishments. *Journal of Loss Prevention in the Process Industries* 58, 70–81. https://doi.org/10.1016/j.jlp.2019.01.005

Miller, D. (2017). New model for predicting thermal radiation from flares and high pressure jet fires for hydrogen and syngas. *Process Safety Progress* 36(3), 237–251. https://doi.org/10.1002/prs.11867

Misuri, A., Cozzani, V. (2021). A paradigm shift in the assessment of NaTech scenarios in chemical and process facilities. *Process Safety and Environmental Protection* 152, 338–351. https://doi.org/10.1016/j.psep.2021.06.018

Molinari, D., Handmer, J. (2011). A behavioural model for quantifying flood warning effectiveness. *Journal of Flood Risk Management* 4, 23–32. https://doi.org/10.1111/J.1753-318X.2010.01086.X

Moriguchi, N., Ito, L., Tokai, A. (2023). Risk assessment of chemical release accident triggered by landslide using Bayesian network. *Science of the Total Environment* 890, 164321. https://doi.org/10.1016/j.scitotenv.2023.164321

Neath, A.A., Cavanaugh, J.E. (2012). The Bayesian information criterion: Background, derivation, and applications. *WIREs Computational Statistics* 4, 199–203. https://doi.org/10.1002/wics.199

Newhall, C., Hoblitt, R. (2002). Constructing event trees for volcanic crises. *Bulletin of Volcanology* 64, 3–20. https://doi.org/10.1007/s004450100173

Nuñez, E., Aguayo C., Mata, R. (2023). Incremental dynamic analysis of steel storage racks subjected to Chilean earthquakes. *Thin-Walled Structures* 182, 110288.

Padilla-Llano, D.A., Moen, C.D., Eatherton, M.R. (2014). Cyclic axial response and energy dissipation of cold-formed steel framing members. *Thin-walled structures* 78, 95-107.

Padilla-Llano, D.A., Eatherton, M.R., Moen, C.D. (2016). Cyclic flexural response and energy dissipation of cold-formed steel framing members. *Thin-Walled Structures* 98, 518-532.

Perrone, D., Calvi, P. M., Nascimbene, R., Fischer, E.C., Magliulo, G. (2019). Seismic performance of non-structural elements during the 2016 Central Italy earthquake. *Bulletin of Earthquake Engineering* 17(10), 5655-77.

Proença, J., Rosin, I., Calado, L. (2009). Storage racks in seismic areas. European Commission, Directorate-General for Research and Innovation. Publications Office.

Renni, E., Krausmann, E., Cozzani, V. (2010). Industrial accidents triggered by lightning. *Journal of Hazardous Materials* 184, 42–48. https://doi.org/10.1016/j.jhazmat.2010.07.118

Ricci, F., Casson Moreno, V., Cozzani, V. (2021). A comprehensive analysis of the occurrence of NaTech events in the process industry. *Process Safety and Environmental Protection* 147, 703–713. https://doi.org/10.1016/j.psep.2020.12.031

Saler, E., Carpanese, P., Follador, V., da Porto, F. (2021). Derivation of seismic fragility curves of a gravity-load designed RC school building through NLTHA. *Proc. 8th In-ter. Conf. on Computational Methods in Structural Dynamics and Earthquake Engineering*, Athens, Greece.

Shaheen, M.S.A., Rasmussen, K.J.R. (2022). Development of friction damped seismic fuses for steel storage racks. *Journal of Constructional Steel Research* 192, 107216. https://doi.org/10.1016/j.jcsr.2022.107216

Simoncelli, M., Tagliafierro, B., Montuori, R. (2020). Recent development on the seismic devices for steel storage structures. *Thin-Walled Structures* 155, 106827. https://doi.org/10.1016/j.tws.2020.106827

Steck, H., Tresp, V. (2000). Bayesian belief networks for data Mining, in: *Proceedings of the 2nd Workshop on data mining and data warehousing*. Technical University of Munich, Munich, Germany. pp.1-10. URL: https://www.researchgate.net/publication/2376112_Bayesian_Belief_Networks_for_Data_Mining.

Strobl, E.V. (2021). Automated hyperparameter selection for the PC algorithm. *Pattern Recognition Letters* 151, 288–293. https://doi.org/10.1016/j.patrec.2021.09.009

Vílchez, J.A., Espejo, V., Casal, J. (2011). Generic event trees and probabilities for the release of different types of hazardous materials. *Journal of Loss Prevention in the Process Industries* 24(3), 281–287. https://doi.org/10.1016/j.jlp.2011.01.005

Vitale, M., Castro Rodriguez, D. J., Barresi, A., Demichela, M. (2025a). Database of material degradation event within process industry, Mendeley Data, V1, doi: 10.17632/6hd3xky6kb.1. https://data.mendeley.com/datasets/6hd3xky6kb/1

Vitale, M., Shi, H., Castro Rodriguez, D.J., Barresi, A.A, Demichela, M. (2025b). Material degradation: Findings from historical accident analysis in process industries. *Reliability Engineering and System* Safety 226 (part B), 111769. [online 26 September 2025] https://doi.org/10.1016/j.ress.2025.111769.

Vitale, M., Shi, H., Castro Rodriguez, D.J., Barresi, A., Demichela, M. (2024). Ageing in process industry: Identification of material degradation from past accidents analysis. *IFAC-PapersOnLine*, 12th IFAC Symposium on Fault Detection, Supervision and Safety for Technical Processes SAFEPROCESS 2024 58, 568–573. https://doi.org/10.1016/j.ifacol.2024.07.279

Zhao, X., Dai, L., Rasmussen, K. J. (2018). Hysteretic behaviour of steel storage rack beam-to-upright boltless connections. *Journal of Constructional Steel Research* 144, 81-105.

Zonta, A. 2023. Seismic vulnerability of industrial steel pallet racks: Development of fragility curves for existing and retrofitted configurations. Ph.D. Thesis, University of Padova, XXXV cycle

Section 6

Akao, Y. (1972). New product development and quality assurance quality deployment system. *Standardization and Quality Control* 25 (4), 7–14.

Castro Rodriguez, D.J, Barresi, A.A., Demichela M. (2025a). Multi-risk NaTech vulnerability indicator: A step further. *Journal of Loss Prevention in the Process Industries* 95, 105588. https://doi.org/10.1016/j.jlp.2025.105588

Castro Rodriguez, D.J., Barresi, A.A., Demichela, M. (2025b). Critical Infrastructure Multi-Risk Deployment: An innovative framework to support NaTech preparedness in industrial facilities. *Process Safety and Environmental Protection* 202 (part B), 107736. https://doi.org/10.1016/j.psep.2025.107736.

Castro Rodriguez, D.J., Shi, H., Vitale, M., Barresi, A.A., Demichela, M. (2025c). Assessing the major industrial accident potential based on dangerous substance criteria: A framework for Seveso and non-Seveso facilities. *Chemical Engineering Transactions* 136, 409-414. DOI: 10.3303/CET25116069

Jain, P., Pasman, H.J., Waldram, S.P., Rogers, W.J., Mannan, M.S. (2017). Did we learn about risk control since Seveso? Yes, we surely did, but is it enough? A historical brief and problem analysis. *Journal of Loss Prevention in the Process Industries* 49, Part A, 5–17. https://doi.org/10.1016/j.jlp.2016.09.023

Krausmann, E., Cruz, A.M., Salzano, E. (Eds.), (2017). Glossary, in: *NaTech Risk Assessment and Management*. Elsevier, pp. 241–243. https://doi.org/10.1016/B978-0-12-803807-9.00019-X

Krausmann, E., Renni, E., Campedel, M., Cozzani, V. (2011). Industrial accidents triggered by earthquakes, floods and lightning: lessons learned from a database analysis. *Natural Hazards* 59, 285–300. https://doi.org/10.1007/s11069-011-9754-3

Pilone, E., Demichela, M., Camuncoli, G. (2021). A NaTech vulnerability indicator for local planners, in: *Proceedings of the 31st European Safety and Reliability Conference (ESREL 2021)*. Research Publishing, Singapore, pp. 184–191. https://doi.org/10.3850/978-981-18-2016-8 361-cd

Suarez-Paba, M.C., Tzioutzios, D., Cruz, A.M., Krausmann, E., (2020). Toward NaTech resilient industries, in: Yokomatsu, M., Hochrainer-Stigler, S. (eds) *Disaster Risk Reduction and Resilience*. Disaster and Risk Research: GADRI Book Series. Springer, Singapore, 45-64. https://doi.org/10.1007/978-981-15-4320-3_4

Section 7

American Water Works Association (AWWA) (2018). Emergency Preparedness Practices. *AWWA Manual M19*.

Cardenas, A.A., Amin, S., Sastry, S. (2008). Research challenges for the security of control systems. In *3rd USENIX Workshop on Hot Topics in Security (HotSec'08)*.

Gill, J.C., Malamud, B.D. (2014). Reviewing and visualizing the interactions of natural hazards. *Reviews of Geophysics* 52(4), 680–722. https://doi.org/10.1002/2013RG000445

Humayed, A., Lin, J., Li, F., Luo, B. (2017). Cyber-physical systems security – A survey. *IEEE Internet of Things Journal* 4(6), 1802–1831. https://doi.org/10.1109/JIOT.2017.2703172

Kappes, M.S., Keiler, M., von Elverfeldt, K., Glade, T. (2012). Challenges of analyzing multi-hazard risk: A review. *Natural Hazards* 64(2), 1925–1958. https://doi.org/10.1007/s11069-012-0294-2

O'Rourke, T.D., Jeon, S.S. (1999). Factors affecting the earthquake damage of water distribution systems. *Technical Council on Lifeline Earthquake Engineering Monograph* (16), 20–32.

O'Rourke, T.D., Jung, J.K., Argyrou, C. (2016). Underground pipeline response to earthquake-induced ground deformation, *Soil Dynamics and Earthquake Engineering* (91), 272-283, https://doi.org/10.1016/j.soildyn.2016.09.008.

Pant, R., Hall, J.W., Blainey, S. P. (2016). Vulnerability assessment framework for interdependent critical infrastructures: Case-study for Great Britain's transport network. *European Journal of Transport and Infrastructure Research* 16, 174–194. 10.18757/ejtir.2016.16.1.3120

U.S. Department of Energy (DoE) (2014). The Water–Energy nexus: Challenges and opportunities. Available at https://www.energy.gov/articles/water-energy-nexus-challenges-and-opportunities

US Environmental Protection Agency (US EPA) (2014). Flood Resilience: A Basic Guide for Water and Wastewater Utilities. *EPA 817-B-14-006*. https://www.epa.gov/sites/default/files/2015-08/documents/flood_resilience_guide.pdf

Zscheischler, J., Westra, S., van den Hurk, B.J.J.M., et al. (2018). Future climate risk from compound events. *Nature Climate Change* 8, 469–477. https://doi.org/10.1038/s41558-018-0156-3